FUNCTION OF TRANSCRIPTION FACTORS IN THE EVOLUTION AND DEVELOPMENT OF PHARYNGEAL ORGANS

by

LIZHEN CHEN

(Under the Direction of Nancy R. Manley)

ABSTRACT

Diversity of body plan has long been a fascinating topic of study. Changes in the *Hox* genes, especially in the cis-regulatory elements, are believed to contribute to morphological evolution. *Hox* genes encode a family of transcription factors that play conserved roles in patterning the body plan of metazoan embryos. A large number of studies have revealed the functional equivalence between paralogous and orthologous Hox proteins in distant animals. In this thesis study, for the first time the functional equivalence of Hox proteins is tested by expressing a *Hox* gene from an evolutionarily "lower" organism to a "higher" organism by precise gene swapping. Zebrafish Hoxa3a protein expressed from the mouse *Hoxa3* locus complements the mouse *Hoxa3* null mutant phenotype in some tissues, but provides null function in the development of thymus, parathyroid and cranial nerve. Therefore, the mouse Hoxa3 and zebrafish Hoxa3a proteins are functionally distinct despite sharing a highly conserved homeodomain sequence. We further mapped the functional difference to the C-terminal domain of Hoxa3a. Our data suggest that neofunctionalization of Hox proteins might be a key aspect of the evolution of different vertebrate body plans.

Hoxa3 and Foxn1 are two transcription factors that play critical roles in thymus development. In *Hoxa3* knockout mice, which lack the thymus organ, the expression of Foxn1 is never initiated in the pharyngeal region. Foxn1 is both necessary and sufficient for fetal thymic epithelial cells (TECs) differentiation, but its postnatal function is unknown. In this study, a novel allele of *Foxn1*, $Foxn1^{lacZ}$, was shown to down-regulate Foxn1 expression postnatally. We showed that down-regulation of Foxn1 below 50% of normal levels caused degeneration of thymic organization and reduced T cell production, which resembles premature thymus aging. We also showed that specific TEC subsets that express higher Foxn1 levels are most sensitive to its down-regulation, resulting in changes to the postnatal thymic microenvironment and T cell development. These results provide the first functional evidence that *Foxn1* is required to maintain the postnatal thymus in a dosage sensitive manner, and hence provide important information for understanding the molecular mechanism of thymus homeostasis and involution.

INDEX WORDS: evo-devo, *Hox* gene, pharyngeal organs, functional equivalence, thymus, *Foxn1*, postnatal function, thymic epithelial cells, thymic involution

FUNCTION OF TRANSCRIPTION FACTORS IN THE EVOLUTION AND DEVELOPMENT OF PHARYNGEAL ORGANS

by

LIZHEN CHEN

BS., Lanzhou University, China, 2000

A Dissertation Submitted to the Graduate Faculty of The University of Georgia in Partial Fulfillment of the Requirements for the Degree

DOCTOR OF PHILOSOPHY

ATHENS, GEORGIA

2008

FUNCTION OF TRANSCRIPTION FACTORS IN THE EVOLUTION AND DEVELOPMENT OF PHARYNGEAL ORGANS

by

LIZHEN CHEN

Major Professor: Nancy R. Manley

Committee: Brian Condie
James D. Lauderdale
Jeffrey T. Streelman
Richard Meagher

Electronic Version Approved:

Maureen Grasso
Dean of the Graduate School
The University of Georgia
December 2008

ACKNOWLEDGEMENTS

Foremost, I would like to express my deep and sincere gratitude to my supervisor, Dr. Nancy R. Manley. Her wide knowledge and her logical way of thinking have been of great value for me. Her understanding, encouraging and personal guidance have provided a good basis for the present thesis. Without her intellectual and spiritual support, this thesis work would not be possible. And her mentoring will always serve to guide me as I go forth in my scientific endeavors. It's difficult to overstate my appreciation to the other members of my thesis committee: Dr. Brian Condie, Dr. James Lauderdale, Dr. Jeffery Streelman, Dr. Richard Meagher and Dr. Wyatt Anderson for their tremendous help and guidance throughout my graduate study, and for their critiques and suggestions to this thesis work.

I would like to thank the past and present members of Manley Lab, in particular Julie Gordon, Pansy Bond, Jerrod Bryson, Ginny Bain, Kyoko Masuda, Shiyun Xiao, Jennifer Dean and Shana Seamans for their friendship, technical help and collaborations in the past five years. They have become my best friends that I will never forget. I would also like to thank all the graduate students, faculty and staff in Genetics Department for making the department a nice and friendly group.

My deepest gratitude goes to my husband and colleague, Zhijie Liu, who is always there when I need him. Without his love, support, understanding and encouragement, it would be impossible for me to complete my graduate work. Last but certainly not least, I would like to thank my entire family: grandpa, uncles, aunts, cousins, father-in-law and mother-in-law for giving me a loving environment. Particular thanks to my brother, Lilin Chen, and my sister,

Lijun Chen, for being my best mates. Most importantly, I wish to thank my parents, Chunrong Chen and Meirong Yu. They bore me, raised me, taught me, support me, and love me. To them I dedicate this thesis.

TABLE OF CONTENTS

Page

CHAPTER 1

GENERAL INTRODUCTION AND LITERATURE REVIEW

HOX GENES AND DEVELOPMENT

General information of *Hox* genes

Hox genes encode a highly conserved family of transcription factors that are expressed in specific domains of the body along the anterior-posterior (A-P) axis. They confer different identities to body regions by the differential regulation of numerous different down-stream genes. One of the most striking features of *Hox* genes is their organization in clusters on the chromosome and the remarkable colinearity between the cluster arrangement and their expression pattern along the anterior-posterior axis (McGinnis and Krumlauf, 1992). The function of *Hox* genes to specify axial positional information during embryogenesis is conserved in nearly all the bilateral animals that have been studied. Although patterning the A-P axis during embryogenesis is often used to describe the function of Hox genes, it understates the role of *Hox* genes. *Hox* genes are expressed in many adult tissues and organs, and have been found to be key regulators in controlling cellular identity of fully differentiated cells.

The term "Hox" came from "Homeosis", which was first defined by Bateson in 1894 as "certain parts of the body plan displayed morphological features typical of other regions". Initially a Hox gene referred to a gene encoding a protein with a DNA-binding motif, the

homeodomain. At the time, it was a small family with the genes mutated in the homeotic mutants of Drosophila. But it turned out there are numerous proteins that contain a homeodomain but are not involved in homeotic mutations. So the definition of *Hox* genes remains to be the genes involved in the homeotic mutations and their closest relatives.

In 1978, Edward B. Lewis had moved forward the study of *Hox* genes dramatically because of his finding that several homeotic mutants affected segment identity in *Drosophila* (Lewis, 1978). He conceptually divided the *Drosophila* body plan into 8 sections and proposed that the genes involved in the homeotic mutations were master regulators controlling the diversification of segments along the A-P axis. Soon after this remarkable finding, these eight master control genes were discovered in *Drosophila*. These genes were identified to be transcription factors that assigned different cell fates to different segments. Immediately it became important to see whether other animals had a similar set of genes. Thereupon, cloning *Hox* genes from different organisms became a popular activity in the Developmental Biology field in the mid eighties. Remarkably, it was found that the same 8 genes were present all across the animal kingdom, with the protein sequences highly conserved. It was subsequently discovered that mouse and other mammals have four sets of *Hox* genes, unlike *Drosophila* which possesses a single set of *Hox* genes.

Hox proteins and co-factors

Despite of the diversity in protein length, all Hox proteins share two highly conserved domains. One is the DNA binding domain, known as the homeodomain. The homeodomain is about 60 amino acids and comprised of 3 α-helices and an N-terminal arm. All the Hox

homeodomains, including those of vertebrates and invertebrates, possess identical DNA-base contacting residues and show very similar specificity to DNA sequence (Laughon, 1991). The other highly conserve domain is the YPWM motif, which is also known as hexapeptide, at a variable distance (5-50 amino acids) from the N terminal of homeodomain. The YPWM motif is responsible to the interaction between Hox proteins and their co-factors. It is also the minimum requirement for the interaction. Alteration of one or more of the residues in the YPWM motif disrupts the interaction (Knoepfler and Kamps, 1995). The flanking residues, both N-terminal and C-terminal of the YPWM motif, help to stabilize the HOX-co-factor complex. They also contribute to the specificity of the interaction (LaRonde-LeBlanc and Wolberger, 2003).

Although Hox proteins recognize and bind to very similar target DNAs, their biological function in vivo is quite specific. The functional specificity might be mediated by their partner proteins, known as Hox co-factors (Mann and Morata, 2000). Among the cofactors is the PBC family, another homeodomain containing protein family, which includes the *Drosophila* extradenticle (EXD), verterbrate pre-B cell homeobox1 (PBX) and C.elegans CEH-20 (Chang et al., 1995). PBC proteins will selectively form heterodimers with different Hox proteins, and form PBC-HOX-DNA complex. A third homeodomain protein, HTH in flies, MEIS and PREP in vertebrates, is required to localize PBC into nucleus, where the PBC-HOX-DNA complex is formed (Moens and Selleri, 2006). PBC mutants often recapitulate Hox mutant phenotypes. The first identified Hox cofactor was Drosophilar Exd, mutation of which caused homeotic transformation without altering the expression patterns of Hox genes (Peifer and Wieschaus,

1990; Rauskolb et al., 1995). Loss of function of Pbx1 in mouse results in defects in many tissues, the development of which are regulated by Hox genes. In many cases, the defects resemble Hox mutants (Gendron-Maguire et al., 1993; Manley and Capecchi, 1998; Manley et al., 2004; Rijli et al., 1993; Selleri et al., 2001). Another example is zebrafish Pbx4. Zebrafish *pbx4* mutants resemble *Hoxb1* mutants in mouse and *Hoxb1a* morpholino-injected embryos in zebrafish (McClintock et al., 2002; Popperl et al., 1995; Studer et al., 1996). Although mouse and zebrafish *Pbx* mutants phenocopy *Hox* mutants at some degree, many known Hox functions remain unaffected, suggesting that Hox proteins have functions that are independent of Pbx. Indeed, previous studies have described hexapeptide-independent Hox functions (Fischbach et al., 2005; Medina-Martinez and Ramirez-Solis, 2003).

Function of *Hox* genes in development

The function of *Hox* genes to define the body plan of the developing Drosophila was clearly demonstrated by the first two striking mutations: *bithorax* and *antennapedia*. In the *bithorax* mutant fly, the haltere is transformed into part of a wing, whereas in the *antennapedia* mutants, ectopic legs develop from the head to replace antennae. The *bithorax* mutation is a loss-of-function mutation of *Ubx* gene. *Ubx* is expressed in the abdominal segments and the posterior half of the thorax. Loss-of-function of *Ubx* results in the transformation of the third thoracic segment into a second thoracic segment. *Antennepedia* is a gain-of-function mutation of *Antp*. *Antp* promotes the formation of structures of the second and third thoracic segments, such as legs, wings and halteres. *Antp* also inhibits the formation of head structure. So ectopic

expression of *Antp* in the head inhibits the formation of antennae and promotes the formation of legs from the position of antennae (Postlethwait and Schneiderman, 1969).

In *Drosophila*, *Hox* gene mutations usually result in homeotic transformations of the most anterior segment which normally expresses this specific Hox gene, even though this gene may be expressed in multiple segments. Loss-of-function in Hox genes usually result in the development of structures that normally develop in more anterior segments, whereas gain-of-function mutations often result in the development of structures normally associated with more posterior segments. This is due to the overlapping expression pattern of Hox genes and the inhibitory effect on the function of anterior Hox genes by the posterior genes. This effect has been termed 'posterior dominance' or 'posterior prevalence' (Grier et al., 2005). This effect is evolutionary conserved. In vertebrates, mutations of single Hox genes generally cause milder morphological alterations. At least two reasons might account for this. First, duplication of Hox gene clusters resulted in the functional redundancy within the paralogous Hox groups. The other reason is that vertebrate *Hox* genes might regulate more downstream effector genes than *Drosophila* and the regulation is usually quantitative rather than qualitative like in Drosophila.

As transcription factors, Hox proteins regulate target genes expression by either activating or repressing the transcription. An array of diverse gene targets of *Hox* genes has been identified. These targets are involved in numerous cellular processes including patterning, differentiation, cell cycle and apoptosis, cell adhesion and migration. Many targets of *Hox* genes are transcription factors or signaling molecules, putting *Hox* genes at the upstream of many genetic networks(Svingen and Tonissen, 2006).

HOX GENES AND MORPHOLOGICAL EVOLUTION

Evolution of *Hox* genes

Hox genes are present in multiple copies in all bilaterian animals with radically different body plans. Evolution of *Hox* genes has long been studied to understand the nature of diversity of body plans. Plants, fungi and unicellular animals do not have clustered *Hox* genes, although *Hox* genes are present in the genome. Soon after the origins of animals, the primordial *Hox* gene cis-duplicated to form a proto-Hox cluster of two genes (Lappin et al., 2006). More duplication events resulted in multiple *Hox* genes on the cluster. The nematode C.elegans has a single cluster with six *Hox* genes spread widely on one chromosome (Aboobaker and Blaxter, 2003). Amphioxus, a cephalochordate representing the sister group of the vertebrates has a single Hox cluster of 14 genes (Ferrier et al., 2000). This cluster is proposed to be a homology of the ancestral vertebrate Hox cluster, which consisted of 13 *Hox* genes and gived rise to all vertebrate Hox clusters (Lappin et al., 2006). Two trans-duplication events occurred in early vertebrate evolution resulted in four Hox clusters. The two duplications probably happened before and after the lineage divergence of jawless vertebrates, such as lampreys (Escriva et al., 2002; Force et al., 2002; Irvine et al., 2002). Cluster-specific *Hox* gene loss occurred after the duplications with the result that some primordial vertebral *Hox* genes are absent in each of the four clusters. Interestingly, a genome-wild duplication event occurred in the ray-fin lineage, followed by a gene loss of an entire cluster, result in seven Hox clusters in these fish, including zebrafish (Amores et al., 2004).

Conserved Hox gene function during evolution

The function of *Hox* genes to regulate the A-P patterning during development has been evolutionarily conserved among the metazoans. In a wide specturm of animals, mutations in *Hox* genes result in morphological defects that are restricted to specific segmental zones along the A-P axis, and sometimes result in homeotic transformations similar to those that were discovered in *Drosophila*. The colinearity between the A-P expression patterns of *Hox* genes in the body plan and the chromosomal organization of the genes in Hox cluster is also conserved cross phyla. The striking conservation of *Hox* gene function during evolution was further demonstrated by a large number of genetic complementary experiments cross species.

In 1990, McGinnis and co-workers showed that the effects of the ubiquitous expression of *Drosophila Hox* genes could be recaptured by the ubiquitous expression of vertebrate orthologs in *Drosophila* embryos (Malicki et al., 1990; McGinnis et al., 1990). Since this pioneering work, numerous similar studies to express Hox proteins from a large variety of species in *Drosophila* have been done. In many cases, the expression of these proteins is able to complement the loss-of-function of their *Drosophila* counterparts. The functional conservation of *Hox* genes is also reflected by the dramatic functional redundancy of paralogs. For example, *Hoxa11/Hoxd11* double mutant mice show severe defects in limb development and lack kidneys, while the single mutants have mild defects in limb and normal kidneys (Davis et al., 1995). Furthermore, Hoxa11 and Hoxd11 proteins have been shown to be functionally substitute for each other in specifying lumbosacral vertebral identity (Zakany et al., 1996). Another more dramatic example is the essentially complete functional redundancy between

Hoxa3 and Hoxd3, as well as between Hoxa1 and Hoxb1 (Greer et al., 2000; Tvrdik and Capecchi, 2006).

Function of *Hox* genes in morphological evolution

The function of *Hox* genes is highly conserved during evolution. On the other hand, there is abundant correlative evidence that changes in *Hox* gene expression patterns and protein functions contribute to a variety of small or large morphological changes during animal evolution (Carroll et al., 2005). For instance, *Scr* is required for suppression of wings on the prothorax of Drosophila, and the variations in *Scr* expression domains in insects were found correlated with the variations in wing morphology (Rogers et al., 1997). Difference in UBX protein expression patterns has been shown correlated with the evolutionary changes in leg morphology among different *Drosophila* species (Stern, 1998). Another example is the emergence of jaw during vertebrate evolution. The absence of Hox gene expression in the mandibular arch is proposed to be responsible for this innovation (Kuratani, 2004; Takio et al., 2004). These are only a few of the many studies that demonstrate the connections between changes in Hox gene expression pattern and evolutionary changes in body plan. There is also accumulating evidence that changes in Hox proteins function have contributed to morphological diversification during evolution. Studies from two groups showed that, when expressed in flies, crustacean and onychophoran Ubx do not have the ability to repress the enhancer of *Dll* gene, which is repressed by UBX in insects. They further mapped the functional difference into a novel repression domain in the insect UBX protein, and the loss of several putative phosphorylation sites (Galant and Carroll, 2002; Ronshaugen et al., 2002).

FUNCTION OF *HOXA3* IN PHARYNGEAL DEVELOPMENT

The development and evolution of pharyngeal organs

Pharyngeal arches are a series of transient bilateral bulges found on the lateral surface of the embryonic head. Pharyngeal arch is one of the conserved vertebrate-specific features. The pharyngeal arches are separated by pharyngeal pouches, which are transient bilateral endodermal outpocketings. The pouch endoderm contacts the ectoderm and form a narrow slit-like outpocket. Thus pharyngeal arch is covered externally by the ectoderm and internally by the endoderm. Neural crest cells (NCCs) migrate from the midbrain and hindbrain to the pharyngeal arches and form the bulk of the mesenchyme in this region. The pharyngeal pouches therefore separate the neural crest and mesodermal cells of the arches and define the anterior and posterior limits of each arch. The formation and patterning of the pharyngeal apparatus derived from these structures involves interactions of different cell types derived from all embryonic layers: ectoderm, endoderm, mesoderm and neural crest (Graham et al., 2005). NCCs play a critical role in this process by contributing directly to the formation and/or patterning of the structures (Bockman and Kirby, 1984; Dupin et al., 2006; Krumlauf, 1994; Watari et al., 2001). One of the most frequent human microdeletion syndromes, DiGeorge syndrome, is associated with the defects in the development of pharyngeal apparatus (Wurdak et al., 2006).

In mammals, the pouches generate a number of specialized epithelial structures: parathyroid, thymus and ultimobranchial body. The pharyngeal arches give rise to cranial nerves, cartilages, skeletal muscles, and connective and supportive tissues. Although all

vertebrates share a similar bilateral pattern of pharyngeal pouch and arch development, a number of important alterations have occurred to the pharyngeal apparatus during evolution. In fishes and larvae of amphibians, pouch endoderm perforates the mesodermal layer and fuses with cleft ectoderm to form gill slits. But in terrestrial vertebrates and marine mammals, novel pharyngeal organs, thymus and parathyroid are derived from pouch endoderm, and the gill structure is lost. In some fish, such as zebrafish, both gills and thymus will develop from the pharyngeal pouches.

The vertebrate pharyngeal organs have complex developmental origins. In mouse, the third pouch endoderm interacts with arch mesenchyme and forms the common primordia for thymus and parathyroid. Soon after the formation of the primordia, which are surrounded by NCC mesenchyme, they separate from the pouch endoderm and ectoderm, and start to migrate toward the final positions of thymus and parathyroid. During the migration, the thymus domain and parathyroid domain separate and develop into two different organs. The thyroid organ derives from two separate embryological origins, the thyroid diverticulum, which develops and migrates from endodermal epithelium in the floor of pharynx, and the ultimobranchial body, which develops from the fourth pharyngeal pouch and contributes the calcitonin-producing C cells. The ultimobranchial bodies fuse with the thyroid, which becomes a “U” shape double-lobed organ connected with a structure called isthmus (Moseley et al., 1968; Pearse and Carvalheira, 1967; Williams et al., 1989). In fish and birds, these complex migration and fusion events do not occur, and the ultimobranchial bodies stay as separate structures from the thyroid.

Hoxa3 function is required for pharyngeal development

In mouse, *Hoxa3* is expressed in the neural tube with the rostral limit up to the boundary between rhombomere4 and 5 (r4/r5), as well as in the neural crest emanating from r6 and posterior. It is also expressed in the 3rd and 4th pharyngeal pouch endoderm, as well as in the pharyngeal arch mesenchyme that comprises of NCCs from the hindbrain (Manley and Capecchi, 1995). The expression of all the three group3 *Hox* genes in pharyngeal arches shares the same rostral limit of arch3, but *Hoxa3* is the only one that is expressed in pouch endoderm. In 1991, as the first ever knocked out gene, *Hoxa3* was disrupted in mouse with gene targeting (Chisaka and Capecchi, 1991). *Hoxa3* deficient mice exhibit a variety of abnormalities in pharyngeal organs and tissues. Although the *Hoxd3* and *Hoxb3* single mutant does not show any overlapping defects with *Hoxa3*, the absence of the two paralogs exacerbates *Hoxa3* single mutant phenotypes (Greer et al., 2000; Manley and Capecchi, 1995; Manley and Capecchi, 1997; Manley and Capecchi, 1998).

The most consistent phenotype of *Hoxa3* null mutant mouse is the absence of thymus and parathyroid organs, which are derived from the third pharyngeal pouch endoderm. *Pax1* gene expression in the third pouch endoderm is reduced in *Hoxa3* null mutant embryos, while its expression at other pouches remains unchanged. As *Pax1* mutant mice also show thymic hypoplasia, *Hoxa3* might be required to maintain *Pax1* expression in those cells, and at least some of the function of *Hoxa3* in thymus development might be through regulating Pax1 expression (Manley and Capecchi, 1995). Thyroid development is also affected in *Hoxa3* knockout mice. The thyroid isthmus is either deleted or ectopic, and the ultimobranchial

body-derived C cells are reduced in number or ectopically located (Manley and Capecchi, 1995; Manley and Capecchi, 1998).The development of the third arch artery is deficient, causing the absence of the carotid body and malformation of the carotid artery system (Kameda et al., 2002). Many defects are also observed in tissues derived from pharyngeal arches. The throat cartilages are malformed, and the IXth cranial nerve is abnormal (Manley and Capecchi, 1997; Watari et al., 2001). The soft palate, which is derived from the 2nd pharyngeal arch, in these mice is truncated, resulting in the bloated abdomen phenotype in newborn animals (Chisaka and Capecchi, 1991). As *Hoxa3* is not expressed in the second arch, this phenotype suggests that Hoxa3-expressing cells might be required for providing inductive signals to the 2nd arch. Most of the defects observed in Hoxa3 knockout mice are found in tissues derived from or patterned by NCCs. One exception is the tracheal epithelium, a structure derived from the floor of embryonic pharynx, which has been shown to express *Hoxa3* (Gaunt, 1988). The tracheal epithelial lining is disorganized in these mice, no longer a pseudostratified structure like in the wild-type (Manley and Capecchi, 1995).

THE THYMUS, A PHARYNGEAL POUCH DERIVED ORGAN

Physiological function of thymus

The thymus is an organ located in the upper anterior thorax just above the heart and consists of two lobes. For centuries the function of thymus organ remained enigmatic. Although thymus was found to be a lymphocyte-producing organ by 1960s, the prevailing opinion in 1960s was that the thymus was an evolutionary accident with no crucial function (Miller, 2002). The appearance of the thymus in evolution parallels the appearance of lymphocytes expressing

highly diverse antigen receptors based on VDJ recombination (Boehm and Bleul, 2007). No thymus is known in invertebrate or jawless vertebrates. The thymus may have evolved as a derivative of GALT (gut associated lymphoid tissue), a key lymphoid structure in species prior to the emergence of thymus (Rodewald, 2008). It is now clear that the thymus is a primary lymphoid organ with a unique capacity to support the development of T cells. Defects in thymus function or T cell development will cause a variety of diseases from SCID (severe combined immune deficiency) to autoimmunity.

The thymic stroma provides a microenvironment of 3-D matrix network, which is required for T-cell differentiation and repertorie selection (Blackburn and Manley, 2004). The thymic stroma can be broadly divided into two compartments, the cortex and the medulla. It has a complex cellular composition, but the majority of the cells are thymic epithelium cells (TECs). Different TEC subsets play a particular role in thymocyte development. In adults, T cell precursors which have developed from hematopoietic stem cells in the bone marrow migrate into the thymus, where they undergo proliferation, differentiation. They then mature into functional T cells and migrate out of the thymus into periphery. T cell progenitors enter the thymus at the cortico-medullary junction (Thomas M. Schmitt, 2006). At this point, the T cells are double negative (DN) for CD4 and CD8, two different lineage markers. The double negative cells can be further subdivided into four stages (DN1-4) by different expression of CD44 and CD25. With the differentiation process, T cells migrate progressively to subcapsular zone of the outer cortex (DN1 through DN4 stages), and then back through the cortex and into the medulla (double positive through single positive stages). Double positive (DP) T cells must

undergo positive and negative selection before they migrate out of the thymus. Positive selection occurs mainly in cortex with the requirement of cortical TECs (Thomas M. Schmitt, 2006). During positive selection, cells that can recognize self MHC are selected for proliferation and those that do not recognize self MHC die by apoptosis. Cells that survive positive selection migrate further into the cortico-medullary junction. Negative selection occurs mainly in medulla and requires medullary TECs and dendritic cells. T cells that bind self antigen-MHC with high affinity undergo negative selection and die via apoptosis. Only those that bind with low affinity survive, mature into single positive cells (CD4+ T helper cells and CD8+ T cytotoxic cells), and migrate to peripheral lymphoid organs and play their immune function.

Thymus Organogenesis

Thymus organogenesis, like other endoderm-derived organs, can be divided into several consecutive steps: first, formation and pattering of pharyngeal pouches; second, budding and outgrowth of the thymus primordia; third, seperation of the thymus anlage from endoderm; fourth, differentiation and migration to the final position (Blackburn and Manley, 2004; Rodewald, 2008). In mouse, the epithelial compartment of the thymus develops from the third pharyngeal pouches (Blackburn and Manley, 2004; Gordon et al., 2004). Pharyngeal pouches start to form in an anterior-posterior order at E8.5. Pouch formation is required for thymus organogenesis. All of the known mouse mutants with defective third pouch formation lack thymus organ. For example, in *Tbx1* mutant mice, the second, third and fourth pharyngeal pouches are missing. Thymus and parathyroid organs never form in the mutant embryos

(Jerome and Papaioannou, 2001). Soon after the pouch formation (E9.5), the third pouch is patterned into thymus and parathyroid-specific domains. *Gcm2*, a transcription factor required for parathyroid organogenesis, is normally initiated at E9.5 to express in the dorsal/anterior pharyngeal endoderm of the third pouch (Gordon et al., 2001). After the patterning of third pouch into specific organ fates, the thymus and parathyroid rudiment start to bud and outgrow from the third pharyngeal pouch. High level expression of Foxn1 gene, a thymus specific marker, is initiated at E11.25 in the rudiment. By E11.5, the formation of the common primordia is completed, with Gcm2 and Foxn1 expressed in the parathyroid and thymus-specific domains respectively.

Previous studies indicate that a Hoxa3-Pax1/9-Eya1-Six1 regulatory cascade is likely to pattern the third pouch endoderm (Blackburn and Manley, 2004; Rodewald, 2008; Xu et al., 2002; Zou et al., 2006). A Pax-Eya-Six network has been shown to control eye development in Drosophila in a cell-autonomous manner (Pignoni et al., 1997). *Hoxa3, Pax1/9, Eya1* and *Six1* are co-expressed only in the pharyngeal pouch endoderm, though these genes are expressed in multiple cell lineages. Mutations in these genes all result in defects in thymus and parathyroid organogenesis. *Hoxa3* is expressed in the third and fourth arches and pouches, and has been demonstrated by gene knockout to be required for various aspects of thymus and parathyroid organogenesis (Chisaka and Capecchi, 1991; Manley and Capecchi, 1995; Manley and Capecchi, 1998; Su et al., 2001). *Hoxa3* mutation results in the lack of the common primordia without affecting the pouch formation. In *Hoxa3* mutant mice, Pax1/9 expression is down-regulated in the third pouch, while the expression at other pouches remains unchanged

(Manley and Capecchi, 1995). Compared to the transcription factors, the function of signaling molecules in thymus development is supported by less genetic evidence, though the main developmental signaling pathways, Fgfs, Bmps, Wnts and Shh, have been shown involved at some level.

Quickly after the formation of common primordia, the primordia surrounded by NCC mesenchyme separate from the pouch endoderm, and start to migrate toward the final positions of thymus and parathyroid. The Hox-Pax-Eya-Six pathway might also be involved in the separation and migration process, as separation of the rudiments from the pharynx fails in Pax9 mutant embryos (Hetzer-Egger et al., 2002), and is delayed in *Hoxa3*$^{+/-}$*Pax*$^{-/-}$ mutants (Su et al., 2001). During the migration, the thymus domain and parathyroid domain separate and develop into two different organs. At E12.5, lymphocyte progenitor cells start to immigrate into thymus, and TECs start to differentiate with the requirement of Foxn1 expression (Blackburn et al., 1996; Nehls et al., 1996). The keratin expression pattern starts to change, and cortico-medullary organization starts to form (Rodewald, 2008). The interaction between thymocytes and TECs, which is termed as cross-talk, is required for the development of both cell types (Hollander et al., 1995; Klug et al., 1998; van Ewijk et al., 2000; van Ewijk et al., 1994). The overall size of thymus has been found to be controlled, at least partially, by p63, which might function in epithelium stem cells (Candi et al., 2007; Senoo et al., 2007).

In addition to the thoracic thymus, two recent independent studies provide evidence for the existence of a functional cervical thymus in mouse (Dooley et al., 2006; Terszowski et al., 2006). The cervical thymus appears a cortico-medullary structure similar to the thoracic thymus, and is

able to be colonized by T cell progenitors from bone marrow to develop into functional T cells. But the regulation of the cervical thymus organogenesis remains to be further analyzed.

Aging-associated thymic involution

With aging, the function of the immune system declines, associated with increased susceptibility to infection, autoimmune diseases and cancer in elderly individuals (Taub and Longo, 2005). Thymic involution is the most prominent aging-related change in the immune system. It can be observed in mouse and human as progressive reduction of thymus size, loss of thymic epithelial cells, and decrease of T cell output. The thymus architecture, the number and composition of thymic stromal cells and thymocytes change throughout the lifespan. The thymus is fundamental to establishing immunity during early life, but undergoes thymic involution after puberty, when most other organs are robust in functions (Sutherland et al., 2005). In human, a significant reduction of thymic mass starts one year after birth, resulting in a dramatic reduction by puberty (Berzins et al., 2002). In mouse, a reduction in thymus size is visible approximately 6 weeks after birth, though a diminished capacity to promote thymocyte proliferation has been reported as early as two weeks after birth (Aspinall and Andrew, 2000a; Aspinall and Andrew, 2000b).

With progressive involution, the white fat tissue surrounding thymus and within the thymic interlobular space increases with age, while the thymic cortical and medullary regions (which together comprise the thymic epithelial space) decrease. The thymus loses definition between the cortex and medulla. The number of thymocytes is gradually decreased, so that a 24 months old mouse possesses less than 1% of the number of thymocytes at newborn stage (Aspinall,

2003; Taub and Longo, 2005). For a long time, people have believed that the thymus becomes a fatty nonfunctional organ with no capacity to support T cell development post-puberty. But later studies have shown that the function to promote T cell proliferation and differentiation is retained in the involuted thymus, though the capacity is dramatically reduced (Jamieson et al., 1999; Poulin et al., 1999). Although thymocyte number is greatly reduced in aged thymus, there are no significant differences in the percentages of SP and DP T cell subsets between young and aged thymi. However the percentages of particular DN subsets have been reported to be changed significantly in aged thymus (Phillips et al., 2004; Thoman, 1995). The percentage of DN1 cells increases, suggesting a developmental block at the DN1-DN2 transition.

The thymus gene expression profiles have been compared at different stages, trying to identify the genes regulating thymic aging. In thymocytes the mRNA expression level of E2A, a transcriptional regulator required for TCR β rearrangement, decreases with age, whereas expression of LMO2, the negative regulator of E2A activity, increases (Ortman et al., 2002). Growth hormone (GH) is produced by thymocytes and TECs, and has been shown to stimulate thymopoiesis. The introthymic growth hormone protein expression steadily declines with age (Taub and Longo, 2005). TECs produce a number of haematopoietic cytokines, such as IL-7. IL-7 promotes VDJ rearrangement through regulating RAG-1 and RAG-2 genes in thymocytes. IL-7 production has been shown decreased in aged thymus (Andrew and Aspinall, 2001; Andrew and Aspinall, 2002; Ortman et al., 2002). Other cytokines, such as IL-2, IL-9, IL-10, IL-13 and IL-14 decline with age, while LIF, OSM, IL-6 and SCF increase (Taub and Longo, 2005). The expression transcription factor Foxn1, which is critical for thymus organogenesis,

has also been reported reduced in aged thymus (Ortman et al., 2002). Thus, these genes are the potential candidates for therapeutic strategies to rejuvenate the aging thymus.

FOXN1 GENE AND THYMUS DEVELOPMENT

Forkhead transcription factors

Forkhead-box (FOX) proteins are a large family of transcriptional factors. Since the first Fox gene was discovered in Drosophila, more than one hundred of Fox genes have been identified. Members in this family have a conserved 'winged helix' DNA-binding domain, but there is no sequence homology in the transactivation or repression domain. Fox genes are involved in diverse aspects of developmental regulation processes. Members in this family have been shown to play important roles in the regulation of immune system. For example, FOXP3 is required for the development and function of regulatory T cell; members of FOXO subfamily are involved in leukocyte homeostasis; FOXJ1 is involved in suppression of T cell activation and prevention of autoimmunity (Coffer and Burgering, 2004; Jonsson and Peng, 2005); FOXN1 is required for epithelial differentiation, and thus required for thymus organogenesis (Blackburn et al., 1996; Nehls et al., 1996).

Foxn1

Foxn1, which has also been called *Whn* and *Hfh11*, is the gene that is mutated in nude mice (Nehls et al., 1996). The nude mouse was originally reported as a spontaneous mutant with no hair or thymus (Flanagan, 1966; Pantelouris, 1968). In fact, the nude mouse is not hairless, but the hair shaft bends and breaks in the hair canal, and never breakthrough the skin surface (Kopf-Maier et al., 1990). There is also a thymus rudiment in nude mouse, but the rudiment is

not functional to be colonized by T cells. In the original nude allele, there was a single base-pair deletion in exon3, causing a frame shift that results in a truncated protein lacking the DNA-binding and activation domain (Nehls et al., 1994).

The mouse *Foxn1* gene spans about 30kb on chromosome 17. The *Foxn1* gene contains ten exons, eight of which are protein-coding exons. Two alternative non-coding first exons (exon1a and 1b) have been demonstrated using extensive screening of skin cDNA clones. Consistent with two first exons, a reporter assay has revealed the presence of two individual presumptive promoter sequences (Schorpp et al., 1997). Interestingly, tissue-specific alternative first exon usage has been reported. Promoter 1a is active in thymus and skin, but promoter 1b is only used in skin (Kurooka et al., 1996; Schorpp et al., 1997).

Functional domains of the FOXN1 protein have been mapped by using genetic analysis, transfection analysis and DNA-binding assays. The transcriptional activation domain is located at the C-terminal, which comprises of a high number of acidic amino acids and prolines (Brissette et al., 1996; Schuddekopf et al., 1996). The forkhead class DNA binding domain lies on the middle (primary structure) of the protein (Schlake et al., 1997). A previous study has also indicated that the N-terminal domain of Foxn1 protein may have acquired important changes for new protein functions during evolution (Schlake et al., 2000). In this paper, they found that the N-terminal domain of the zebrafish Foxn1-like protein, but not the one of the amphioxus Foxn1-like protein, was able to substitute for the N-terminal domain of mouse Foxn1 protein to activate hair keratin gene expression in cell culture.

Foxn1 expression and regulation

Using RT-PCR, Foxn1 expression in mouse embryos can be detected as early as E9 (Nehls et al., 1994). Foxn1 is expressed specific in epithelial derived cells. Foxn1 expression in primary keratinocytes and cultured hair buds and interfollicular keratinocytes was revealed by Northern blot (Brissette et al., 1996). The detailed expression pattern was later investigated taking advantage of a Foxn1 mutant allele with an IRES-lacZ-neo cassette inserted into exon3) and by *in situ* hybridization (Gordon et al., 2001; Lee et al., 1999; Nehls et al., 1996). In the interfollicular epidermis, Foxn1 is expressed predominantly in the cells of the first suprabasal layer. The most prominent expression in hair follicle is in the proximal part of the outer root sheath and the hair cortex. Foxn1 expression can be detected starting from E11.25 in the thymus primordia, and continues in thymic epithelium lifelong. In addition to the skin and thymus, Foxn1 is expressed in developing nails, teeth, tongue, palate and nasal passages. A transient expression in the developing lens epithelium from E13.5 to E16.5 has also been reported (Meier et al., 1999).

Little is known about upstream regulators of Foxn1 expression. It has been reported that ectopic overexpression of noggin, a BMP signaling antagonist, in the hair follicles and epidermis resulted in a hairless phenotype resembling the nude phenotype. Foxn1 expression in skin is absent in these transgenic mice, indicating that BMP signaling might be required for Foxn1 expression (Kulessa et al., 2000). Wnt glycoproteins, which are expressed in TECs and thymocytes, have also been proposed to regulate Foxn1 expression in thymic epithelia (Balciunaite et al., 2002). Overexpression of beta-catenin (a down stream target of Wnt

glycoproteins) resulted in increased Foxn1 expression in cell culture. As no Wnt mutants have been reported to resemble nude thymus phenotype, the function of Wnt in regulating Foxn1 expression remains to be further investigated. In brief, it is unclear so far how Foxn1 expression is initiated and maintained.

Foxn1 function in thymus development

Foxn1 is the first thymus-specific marker expressed in the thymus rudiment. Its expression in the third pharyngeal pouch can be detected with RT-PCR at E10.5 (Balciunaite et al., 2002), but high level of expression in the thymus primordium can not be detected until E11.25 (Gordon et al., 2001). Analysis of a Foxn1lacZ allele demonstrates that Foxn1 is expressed in most, if not all, TECs both at embryonic stages and in the adult (Nehls et al., 1996). However, another study that used an anti-Foxn1 antibody suggests that not all of the keratin expressing cell express Foxn1 in fetal thymus (E13), and in the adult thymus, even higher percent (80%) of TECs are keratin^{+} but Foxn1^{-} (Itoi et al., 2007). Lineage tracking using a Foxn1cre allele clearly showed that most, if not all, TECs derive from Foxn1 expressing progenitors, or at least have been through a Foxn1 expression stage (Gordon et al., 2007; Liston et al., 2007).

Loss of Foxn1 function causes the absence of all differentiated TEC types, indicating that *Foxn1* is required for the differentiation of all TEC subtypes in a cell-autonomous manner. However, in the *Foxn1* null (nude) mouse, the third pharyngeal pouches are patterned into thymus and parathyroid-specific fate, and the primordium develops from the third pouch. This supports the 'two-step model' that thymus development can be divided into a Foxn1-independent early organogenesis phase and a Foxn1-dependent late phase (Nehls et al., 1996). In addition to

the differentiation of TECs, proliferation of these cells seem to be regulated by Foxn1 as well, since the proliferation of TECs in the rudiment of nude thyus is reduced (Itoi et al., 2001).

Analysis of a hypomorphic allele of Foxn1, in which exon3 is deleted during RNA splicing, showed that Foxn1 is required for both initial and subsequent stages of TEC differentiation (Su et al., 2003). This allele, $Foxn1^{\Delta}$, encodes a Foxn1 protein with a large deletion in the N-terminal domain, but with the DNA-binding, nuclear-localization and activating domains intact. TECs in this mutant develop beyond the block in nude mice, but the development was arrested at a $K5^{+}K8^{+}$ stage. $Foxn1^{\Delta/\Delta}$ thymus is able to be colonized by T cells, though T cell number is greatly reduced and T cell development is delayed. It is so far not clear how the N-terminal domain that is deleted in this mutant is involved in regulating the later stage of TEC development.

As the development of endoderm derived organs share common features, studying the function of other transcription factors in the development and maintenance of other organs will provide important information to understand Foxn1 function. Nkx2.1, which is also called thyroid-specific enhancer binding protein, has been shown to be required for thyroid development. Null mutation of *Nkx2.1* causes thyroid degeneration through apoptosis at E12-13 in mouse, but the initiation of thyroid organogenesis is independent of Nkx2.1 (Kimura et al., 1996). This is similar to Foxn1 function in thymus, which is dispensable for early stage of thymus development but required for later on TEC differentiation. Interestingly, a more recent study has revealed that *Nkx2.1* is also required in maintenance of the normal structure and function of differentiated thyroid (Kusakabe et al., 2006). Conditional knockout of *Nkx2.1* at

later stage resulted in a thyroid phenotype that was also observed in aged control mice. As it is mentioned earlier, Foxn1 expression has been shown to be decreased in aged thymic stroma. It will be of great interest to see whether *Foxn1* play a role in maintenance of postnatal thymus structure and function, and whether Foxn1 function is involved in thymic involution.

REFERENCES

Aboobaker, A. and Blaxter, M. (2003). Hox gene evolution in nematodes: novelty conserved. *Curr Opin Genet Dev* **13**, 593-8.

Amores, A., Suzuki, T., Yan, Y. L., Pomeroy, J., Singer, A., Amemiya, C. and Postlethwait, J. H. (2004). Developmental roles of pufferfish Hox clusters and genome evolution in ray-fin fish. *Genome Res* **14**, 1-10.

Andrew, D. and Aspinall, R. (2001). Il-7 and not stem cell factor reverses both the increase in apoptosis and the decline in thymopoiesis seen in aged mice. *J Immunol* **166**, 1524-30.

Andrew, D. and Aspinall, R. (2002). Age-associated thymic atrophy is linked to a decline in IL-7 production. *Exp Gerontol* **37**, 455-63.

Aspinall, R. (2003). Age-related changes in the function of T cells. *Microsc Res Tech* **62**, 508-13.

Aspinall, R. and Andrew, D. (2000a). Thymic atrophy in the mouse is a soluble problem of the thymic environment. *Vaccine* **18**, 1629-37.

Aspinall, R. and Andrew, D. (2000b). Thymic involution in aging. *J Clin Immunol* **20**, 250-6.

Balciunaite, G., Keller, M. P., Balciunaite, E., Piali, L., Zuklys, S., Mathieu, Y. D., Gill, J., Boyd, R., Sussman, D. J. and Hollander, G. A. (2002). Wnt glycoproteins regulate the expression of FoxN1, the gene defective in nude mice. *Nat Immunol* **3**, 1102-8.

Berzins, S. P., Uldrich, A. P., Sutherland, J. S., Gill, J., Miller, J. F., Godfrey, D. I. and Boyd, R. L. (2002). Thymic regeneration: teaching an old immune system new tricks. *Trends Mol Med* **8**, 469-76.

Blackburn, C. C., Augustine, C. L., Li, R., Harvey, R. P., Malin, M. A., Boyd, R. L., Miller, J. F. and Morahan, G. (1996). The nu gene acts cell-autonomously and is required for differentiation of thymic epithelial progenitors. *Proc Natl Acad Sci U S A* **93**, 5742-6.

Blackburn, C. C. and Manley, N. R. (2004). Developing a new paradigm for thymus organogenesis. *Nat Rev Immunol* **4**, 278-89.

Bockman, D. E. and Kirby, M. L. (1984). Dependence of thymus development on derivatives of the neural crest. *Science* **223**, 498-500.

Boehm, T. and Bleul, C. C. (2007). The evolutionary history of lymphoid organs. *Nat Immunol* **8**, 131-5.

Brissette, J. L., Li, J., Kamimura, J., Lee, D. and Dotto, G. P. (1996). The product of the mouse nude locus, Whn, regulates the balance between epithelial cell growth and differentiation. *Genes Dev* **10**, 2212-21.

Candi, E., Rufini, A., Terrinoni, A., Giamboi-Miraglia, A., Lena, A. M., Mantovani, R., Knight, R. and Melino, G. (2007). DeltaNp63 regulates thymic development through enhanced expression of FgfR2 and Jag2. *Proc Natl Acad Sci U S A* **104**, 11999-2004.

Carroll, S. B., Grenier, J. K. and Weatherbee, S. D. (2005). From DNA To Diversity. In *Blackwell Science*, (ed., pp. 1-258.

Chang, C. P., Shen, W. F., Rozenfeld, S., Lawrence, H. J., Largman, C. and Cleary, M. L. (1995). Pbx proteins display hexapeptide-dependent cooperative DNA binding with a subset of Hox proteins. *Genes Dev* **9**, 663-74.

Chisaka, O. and Capecchi, M. R. (1991). Regionally restricted developmental defects resulting from targeted disruption of the mouse homeobox gene hox-1.5. *Nature* **350**, 473-9.

Coffer, P. J. and Burgering, B. M. (2004). Forkhead-box transcription factors and their role in the immune system. *Nat Rev Immunol* **4**, 889-99.

Davis, A. P., Witte, D. P., Hsieh-Li, H. M., Potter, S. S. and Capecchi, M. R. (1995). Absence of radius and ulna in mice lacking hoxa-11 and hoxd-11. *Nature* **375**, 791-5.

Dooley, J., Erickson, M., Gillard, G. O. and Farr, A. G. (2006). Cervical thymus in the mouse. *J Immunol* **176**, 6484-90.

Dupin, E., Creuzet, S. and Le Douarin, N. M. (2006). The contribution of the neural crest to the vertebrate body. *Adv Exp Med Biol* **589**, 96-119.

Escriva, H., Manzon, L., Youson, J. and Laudet, V. (2002). Analysis of lamprey and hagfish genes reveals a complex history of gene duplications during early vertebrate evolution. *Mol Biol Evol* **19**, 1440-50.

Ferrier, D. E., Minguillon, C., Holland, P. W. and Garcia-Fernandez, J. (2000). The amphioxus Hox cluster: deuterostome posterior flexibility and Hox14. *Evol Dev* **2**, 284-93.

Fischbach, N. A., Rozenfeld, S., Shen, W., Fong, S., Chrobak, D., Ginzinger, D., Kogan, S. C., Radhakrishnan, A., Le Beau, M. M., Largman, C. et al. (2005). HOXB6 overexpression in murine bone marrow immortalizes a myelomonocytic precursor in vitro and causes hematopoietic stem cell expansion and acute myeloid leukemia in vivo. *Blood* **105**, 1456-66.

Flanagan, S. P. (1966). 'Nude', a new hairless gene with pleiotropic effects in the mouse. *Genet Res* **8**, 295-309.

Force, A., Amores, A. and Postlethwait, J. H. (2002). Hox cluster organization in the jawless vertebrate Petromyzon marinus. *J Exp Zool* **294**, 30-46.

Galant, R. and Carroll, S. B. (2002). Evolution of a transcriptional repression domain in an insect Hox protein. *Nature* **415**, 910-3.

Gaunt, S. J. (1988). Mouse homeobox gene transcripts occupy different but overlapping domains in embryonic germ layers and organs: a comparison of Hox-3.1 and Hox-1.5. *Development* **103**, 135-44.

Gendron-Maguire, M., Mallo, M., Zhang, M. and Gridley, T. (1993). Hoxa-2 mutant mice exhibit homeotic transformation of skeletal elements derived from cranial neural crest. *Cell* **75**, 1317-31.

Gordon, J., Bennett, A. R., Blackburn, C. C. and Manley, N. R. (2001). Gcm2 and Foxn1 mark early parathyroid- and thymus-specific domains in the developing third pharyngeal pouch. *Mech Dev* **103**, 141-3.

Gordon, J., Wilson, V. A., Blair, N. F., Sheridan, J., Farley, A., Wilson, L., Manley, N. R. and Blackburn, C. C. (2004). Functional evidence for a single endodermal origin for the thymic epithelium. *Nat Immunol* **5**, 546-53.

Gordon, J., Xiao, S., Hughes, B., 3rd, Su, D. M., Navarre, S. P., Condie, B. G. and Manley, N. R. (2007). Specific expression of lacZ and cre recombinase in fetal thymic epithelial cells by multiplex gene targeting at the Foxn1 locus. *BMC Dev Biol* **7**, 69.

Graham, A., Okabe, M. and Quinlan, R. (2005). The role of the endoderm in the development and evolution of the pharyngeal arches. *J Anat* **207**, 479-87.

Greer, J. M., Puetz, J., Thomas, K. R. and Capecchi, M. R. (2000). Maintenance of functional equivalence during paralogous Hox gene evolution. *Nature* **403**, 661-5.

Grier, D. G., Thompson, A., Kwasniewska, A., McGonigle, G. J., Halliday, H. L. and Lappin, T. R. (2005). The pathophysiology of HOX genes and their role in cancer. *J Pathol* **205**, 154-71.

Hetzer-Egger, C., Schorpp, M., Haas-Assenbaum, A., Balling, R., Peters, H. and Boehm, T. (2002). Thymopoiesis requires Pax9 function in thymic epithelial cells. *Eur J Immunol* **32**, 1175-81.

Hollander, G. A., Wang, B., Nichogiannopoulou, A., Platenburg, P. P., van Ewijk, W., Burakoff, S. J., Gutierrez-Ramos, J. C. and Terhorst, C. (1995). Developmental control point in induction of thymic cortex regulated by a subpopulation of prothymocytes. *Nature* **373**, 350-3.

Irvine, S. Q., Carr, J. L., Bailey, W. J., Kawasaki, K., Shimizu, N., Amemiya, C. T. and Ruddle, F. H. (2002). Genomic analysis of Hox clusters in the sea lamprey Petromyzon marinus. *J Exp Zool* **294**, 47-62.

Itoi, M., Kawamoto, H., Katsura, Y. and Amagai, T. (2001). Two distinct steps of immigration of hematopoietic progenitors into the early thymus anlage. *Int Immunol* **13**, 1203-11.

Itoi, M., Tsukamoto, N. and Amagai, T. (2007). Expression of Dll4 and CCL25 in Foxn1-negative epithelial cells in the post-natal thymus. *Int Immunol* **19**, 127-32.

Jamieson, B. D., Douek, D. C., Killian, S., Hultin, L. E., Scripture-Adams, D. D., Giorgi, J. V., Marelli, D., Koup, R. A. and Zack, J. A. (1999). Generation of functional thymocytes in the human adult. *Immunity* **10**, 569-75.

Jerome, L. A. and Papaioannou, V. E. (2001). DiGeorge syndrome phenotype in mice mutant for the T-box gene, Tbx1. *Nat Genet* **27**, 286-91.

Jonsson, H. and Peng, S. L. (2005). Forkhead transcription factors in immunology. *Cell Mol Life Sci* **62**, 397-409.

Kameda, Y., Nishimaki, T., Takeichi, M. and Chisaka, O. (2002). Homeobox gene hoxa3 is essential for the formation of the carotid body in the mouse embryos. *Dev Biol* **247**, 197-209.
Kimura, S., Hara, Y., Pineau, T., Fernandez-Salguero, P., Fox, C. H., Ward, J. M. and Gonzalez, F. J. (1996). The T/ebp null mouse: thyroid-specific enhancer-binding protein is essential for the organogenesis of the thyroid, lung, ventral forebrain, and pituitary. *Genes Dev* **10**, 60-9.
Klug, D. B., Carter, C., Crouch, E., Roop, D., Conti, C. J. and Richie, E. R. (1998). Interdependence of cortical thymic epithelial cell differentiation and T-lineage commitment. *Proc Natl Acad Sci U S A* **95**, 11822-7.
Knoepfler, P. S. and Kamps, M. P. (1995). The pentapeptide motif of Hox proteins is required for cooperative DNA binding with Pbx1, physically contacts Pbx1, and enhances DNA binding by Pbx1. *Mol Cell Biol* **15**, 5811-9.
Kopf-Maier, P., Mboneko, V. F. and Merker, H. J. (1990). Nude mice are not hairless. A morphological study. *Acta Anat (Basel)* **139**, 178-90.
Krumlauf, R. (1994). Hox genes in vertebrate development. *Cell* **78**, 191-201.
Kulessa, H., Turk, G. and Hogan, B. L. (2000). Inhibition of Bmp signaling affects growth and differentiation in the anagen hair follicle. *EMBO J* **19**, 6664-74.
Kuratani, S. (2004). Evolution of the vertebrate jaw: comparative embryology and molecular developmental biology reveal the factors behind evolutionary novelty. *J Anat* **205**, 335-47.
Kurooka, H., Segre, J. A., Hirano, Y., Nemhauser, J. L., Nishimura, H., Yoneda, K., Lander, E. S. and Honjo, T. (1996). Rescue of the hairless phenotype in nude mice by transgenic insertion of the wild-type Hfh11 genomic locus. *Int Immunol* **8**, 961-6.
Kusakabe, T., Kawaguchi, A., Hoshi, N., Kawaguchi, R., Hoshi, S. and Kimura, S. (2006). Thyroid-specific enhancer-binding protein/NKX2.1 is required for the maintenance of ordered architecture and function of the differentiated thyroid. *Mol Endocrinol* **20**, 1796-809.
Lappin, T. R., Grier, D. G., Thompson, A. and Halliday, H. L. (2006). HOX genes: seductive science, mysterious mechanisms. *Ulster Med J* **75**, 23-31.
LaRonde-LeBlanc, N. A. and Wolberger, C. (2003). Structure of HoxA9 and Pbx1 bound to DNA: Hox hexapeptide and DNA recognition anterior to posterior. *Genes Dev* **17**, 2060-72.
Laughon, A. (1991). DNA binding specificity of homeodomains. *Biochemistry* **30**, 11357-67.
Lee, D., Prowse, D. M. and Brissette, J. L. (1999). Association between mouse nude gene expression and the initiation of epithelial terminal differentiation. *Dev Biol* **208**, 362-74.
Lewis, E. B. (1978). A gene complex controlling segmentation in Drosophila. *Nature* **276**, 565-70.
Liston, A., Farr, A. G., Chen, Z., Benoist, C., Mathis, D., Manley, N. R. and Rudensky, A. Y. (2007). Lack of Foxp3 function and expression in the thymic epithelium. *J Exp Med* **204**, 475-80.
Malicki, J., Schughart, K. and McGinnis, W. (1990). Mouse Hox-2.2 specifies thoracic segmental identity in Drosophila embryos and larvae. *Cell* **63**, 961-7.
Manley, N. R. and Capecchi, M. R. (1995). The role of Hoxa-3 in mouse thymus and thyroid development. *Development* **121**, 1989-2003.

Manley, N. R. and Capecchi, M. R. (1997). Hox group 3 paralogous genes act synergistically in the formation of somitic and neural crest-derived structures. *Dev Biol* **192**, 274-88.
Manley, N. R. and Capecchi, M. R. (1998). Hox group 3 paralogs regulate the development and migration of the thymus, thyroid, and parathyroid glands. *Dev Biol* **195**, 1-15.
Manley, N. R., Selleri, L., Brendolan, A., Gordon, J. and Cleary, M. L. (2004). Abnormalities of caudal pharyngeal pouch development in Pbx1 knockout mice mimic loss of Hox3 paralogs. *Dev Biol* **276**, 301-12.
Mann, R. S. and Morata, G. (2000). The developmental and molecular biology of genes that subdivide the body of Drosophila. *Annu Rev Cell Dev Biol* **16**, 243-71.
McClintock, J. M., Kheirbek, M. A. and Prince, V. E. (2002). Knockdown of duplicated zebrafish hoxb1 genes reveals distinct roles in hindbrain patterning and a novel mechanism of duplicate gene retention. *Development* **129**, 2339-54.
McGinnis, N., Kuziora, M. A. and McGinnis, W. (1990). Human Hox-4.2 and Drosophila deformed encode similar regulatory specificities in Drosophila embryos and larvae. *Cell* **63**, 969-76.
McGinnis, W. and Krumlauf, R. (1992). Homeobox genes and axial patterning. *Cell* **68**, 283-302.
Medina-Martinez, O. and Ramirez-Solis, R. (2003). In vivo mutagenesis of the Hoxb8 hexapeptide domain leads to dominant homeotic transformations that mimic the loss-of-function mutations in genes of the Hoxb cluster. *Dev Biol* **264**, 77-90.
Meier, N., Dear, T. N. and Boehm, T. (1999). Whn and mHa3 are components of the genetic hierarchy controlling hair follicle differentiation. *Mech Dev* **89**, 215-21.
Miller, J. F. (2002). The discovery of thymus function and of thymus-derived lymphocytes. *Immunol Rev* **185**, 7-14.
Moens, C. B. and Selleri, L. (2006). Hox cofactors in vertebrate development. *Dev Biol* **291**, 193-206.
Moseley, J. M., Matthews, E. W., Breed, R. H., Galante, L., Tse, A. and MacIntyre, I. (1968). The ultimobranchial origin of calcitonin. *Lancet* **1**, 108-10.
Nehls, M., Kyewski, B., Messerle, M., Waldschutz, R., Schuddekopf, K., Smith, A. J. and Boehm, T. (1996). Two genetically separable steps in the differentiation of thymic epithelium. *Science* **272**, 886-9.
Nehls, M., Pfeifer, D., Schorpp, M., Hedrich, H. and Boehm, T. (1994). New member of the winged-helix protein family disrupted in mouse and rat nude mutations. *Nature* **372**, 103-7.
Ortman, C. L., Dittmar, K. A., Witte, P. L. and Le, P. T. (2002). Molecular characterization of the mouse involuted thymus: aberrations in expression of transcription regulators in thymocyte and epithelial compartments. *Int Immunol* **14**, 813-22.
Pantelouris, E. M. (1968). Absence of thymus in a mouse mutant. *Nature* **217**, 370-1.
Pearse, A. G. and Carvalheira, A. F. (1967). Cytochemical evidence for an ultimobranchial origin of rodent thyroid C cells. *Nature* **214**, 929-30.
Peifer, M. and Wieschaus, E. (1990). Mutations in the Drosophila gene extradenticle affect the way specific homeo domain proteins regulate segmental identity. *Genes Dev* **4**, 1209-23.

Phillips, J. A., Brondstetter, T. I., English, C. A., Lee, H. E., Virts, E. L. and Thoman, M. L. (2004). IL-7 gene therapy in aging restores early thymopoiesis without reversing involution. *J Immunol* **173**, 4867-74.

Pignoni, F., Hu, B., Zavitz, K. H., Xiao, J., Garrity, P. A. and Zipursky, S. L. (1997). The eye-specification proteins So and Eya form a complex and regulate multiple steps in Drosophila eye development. *Cell* **91**, 881-91.

Popperl, H., Bienz, M., Studer, M., Chan, S. K., Aparicio, S., Brenner, S., Mann, R. S. and Krumlauf, R. (1995). Segmental expression of Hoxb-1 is controlled by a highly conserved autoregulatory loop dependent upon exd/pbx. *Cell* **81**, 1031-42.

Postlethwait, J. H. and Schneiderman, H. A. (1969). A clonal analysis of determination in Antennapedia a homoeotic mutant of Drosophila melanogaster. *Proc Natl Acad Sci U S A* **64**, 176-83.

Poulin, J. F., Viswanathan, M. N., Harris, J. M., Komanduri, K. V., Wieder, E., Ringuette, N., Jenkins, M., McCune, J. M. and Sekaly, R. P. (1999). Direct evidence for thymic function in adult humans. *J Exp Med* **190**, 479-86.

Rauskolb, C., Smith, K. M., Peifer, M. and Wieschaus, E. (1995). extradenticle determines segmental identities throughout Drosophila development. *Development* **121**, 3663-73.

Rijli, F. M., Mark, M., Lakkaraju, S., Dierich, A., Dolle, P. and Chambon, P. (1993). A homeotic transformation is generated in the rostral branchial region of the head by disruption of Hoxa-2, which acts as a selector gene. *Cell* **75**, 1333-49.

Rodewald, H. R. (2008). Thymus organogenesis. *Annu Rev Immunol* **26**, 355-88.

Rogers, B. T., Peterson, M. D. and Kaufman, T. C. (1997). Evolution of the insect body plan as revealed by the Sex combs reduced expression pattern. *Development* **124**, 149-57.

Ronshaugen, M., McGinnis, N. and McGinnis, W. (2002). Hox protein mutation and macroevolution of the insect body plan. *Nature* **415**, 914-7.

Schlake, T., Schorpp, M. and Boehm, T. (2000). Formation of regulator/target gene relationships during evolution. *Gene* **256**, 29-34.

Schlake, T., Schorpp, M., Nehls, M. and Boehm, T. (1997). The nude gene encodes a sequence-specific DNA binding protein with homologs in organisms that lack an anticipatory immune system. *Proc Natl Acad Sci U S A* **94**, 3842-7.

Schorpp, M., Hofmann, M., Dear, T. N. and Boehm, T. (1997). Characterization of mouse and human nude genes. *Immunogenetics* **46**, 509-15.

Schuddekopf, K., Schorpp, M. and Boehm, T. (1996). The whn transcription factor encoded by the nude locus contains an evolutionarily conserved and functionally indispensable activation domain. *Proc Natl Acad Sci U S A* **93**, 9661-4.

Selleri, L., Depew, M. J., Jacobs, Y., Chanda, S. K., Tsang, K. Y., Cheah, K. S., Rubenstein, J. L., O'Gorman, S. and Cleary, M. L. (2001). Requirement for Pbx1 in skeletal patterning and programming chondrocyte proliferation and differentiation. *Development* **128**, 3543-57.

Senoo, M., Pinto, F., Crum, C. P. and McKeon, F. (2007). p63 Is essential for the proliferative potential of stem cells in stratified epithelia. *Cell* **129**, 523-36.

Stern, D. L. (1998). A role of Ultrabithorax in morphological differences between Drosophila species. *Nature* **396**, 463-6.

Studer, M., Lumsden, A., Ariza-McNaughton, L., Bradley, A. and Krumlauf, R. (1996). Altered segmental identity and abnormal migration of motor neurons in mice lacking Hoxb-1. *Nature* **384**, 630-4.

Su, D., Ellis, S., Napier, A., Lee, K. and Manley, N. R. (2001). Hoxa3 and pax1 regulate epithelial cell death and proliferation during thymus and parathyroid organogenesis. *Dev Biol* **236**, 316-29.

Su, D. M., Navarre, S., Oh, W. J., Condie, B. G. and Manley, N. R. (2003). A domain of Foxn1 required for crosstalk-dependent thymic epithelial cell differentiation. *Nat Immunol* **4**, 1128-35.

Sutherland, J. S., Goldberg, G. L., Hammett, M. V., Uldrich, A. P., Berzins, S. P., Heng, T. S., Blazar, B. R., Millar, J. L., Malin, M. A., Chidgey, A. P. et al. (2005). Activation of thymic regeneration in mice and humans following androgen blockade. *J Immunol* **175**, 2741-53.

Svingen, T. and Tonissen, K. F. (2006). Hox transcription factors and their elusive mammalian gene targets. *Heredity* **97**, 88-96.

Takio, Y., Pasqualetti, M., Kuraku, S., Hirano, S., Rijli, F. M. and Kuratani, S. (2004). Evolutionary biology: lamprey Hox genes and the evolution of jaws. *Nature* **429**, 1 p following 262.

Taub, D. D. and Longo, D. L. (2005). Insights into thymic aging and regeneration. *Immunol Rev* **205**, 72-93.

Terszowski, G., Muller, S. M., Bleul, C. C., Blum, C., Schirmbeck, R., Reimann, J., Pasquier, L. D., Amagai, T., Boehm, T. and Rodewald, H. R. (2006). Evidence for a functional second thymus in mice. *Science* **312**, 284-7.

Thoman, M. L. (1995). The pattern of T lymphocyte differentiation is altered during thymic involution. *Mech Ageing Dev* **82**, 155-70.

Thomas M. Schmitt, J. C. Z.-P. (2006). Regulation of Early T-cell Ddevelopment in the Thymus. In *Immunodominance*, (ed. J. A. Frelinger).

Tvrdik, P. and Capecchi, M. R. (2006). Reversal of Hox1 gene subfunctionalization in the mouse. *Dev Cell* **11**, 239-50.

van Ewijk, W., Hollander, G., Terhorst, C. and Wang, B. (2000). Stepwise development of thymic microenvironments in vivo is regulated by thymocyte subsets. *Development* **127**, 1583-91.

van Ewijk, W., Shores, E. W. and Singer, A. (1994). Crosstalk in the mouse thymus. *Immunol Today* **15**, 214-7.

Watari, N., Kameda, Y., Takeichi, M. and Chisaka, O. (2001). Hoxa3 regulates integration of glossopharyngeal nerve precursor cells. *Dev Biol* **240**, 15-31.

Williams, E. D., Toyn, C. E. and Harach, H. R. (1989). The ultimobranchial gland and congenital thyroid abnormalities in man. *J Pathol* **159**, 135-41.

Wurdak, H., Ittner, L. M. and Sommer, L. (2006). DiGeorge syndrome and pharyngeal apparatus development. *Bioessays* **28**, 1078-86.

Xu, P. X., Zheng, W., Laclef, C., Maire, P., Maas, R. L., Peters, H. and Xu, X. (2002). Eya1 is required for the morphogenesis of mammalian thymus, parathyroid and thyroid. *Development* **129**, 3033-44.

Zakany, J., Gerard, M., Favier, B., Potter, S. S. and Duboule, D. (1996). Functional equivalence and rescue among group 11 Hox gene products in vertebral patterning. *Dev Biol* **176**, 325-8.

Zou, D., Silvius, D., Davenport, J., Grifone, R., Maire, P. and Xu, P. X. (2006). Patterning of the third pharyngeal pouch into thymus/parathyroid by Six and Eya1. *Dev Biol* **293**, 499-512.

CHAPTER 2

GENERATION OF EVOLUTIONARY ALLELES SHOWS NON-EQUIVALENT *IN VIVO* FUNCTION FOR MOUSE AND ZEBRAFISH HOXA3 GENES[1]

[1]Lizhen Chen, Brian G. Condie and Nancy R. Manley. To be submit to *PNAS.*

ABSTRACT

Hox genes play evolutionarily conserved roles in specifying axial positional information during embryogenesis. The prevailing paradigm is that divergent *Hox* gene expression patterns drive macroevolution of metazoan body plans, with conservation of Hox protein function across species and among paralogous *Hox* genes within a species supporting a model of functional equivalence. In this report, we show that zebrafish *Hoxa3a* (*zfHoxa3a*) expressed from the mouse *Hoxa3* locus complements the *Hoxa3* null phenotype in some tissues, but has novel or null phenotypes in others despite highly conserved homeodomain and pentapeptide sequences. We further show using an allele encoding a chimeric protein that this functional difference maps to the C-terminal domain of zfHoxa3a. These data suggest that Hoxa3 protein function has diverged significantly since the last common ancestor of mouse and zebrafish, and that the major functional difference between mouse and zebrafish Hoxa3 proteins resides in the C-terminal domain.

INTRODUCTION

Hox genes encode a family of transcriptional factors with conserved functions in patterning the anterior-posterior (A-P) axis during embryogenesis in all bilaterian animals (McGinnis and Krumlauf, 1992). Since the identification of the first *Hox* gene mutation in *Drosophila*, Hox gene mutations in many species have been analyzed. These mutations often cause morphological defects that are restricted to specific segmental zones along the A-P axis. The function of *Hox* genes to specify segmental identity is mediated by the differences in protein sequence, differential spatiotemporal expression patterns, interactions with co-factors and transcriptional regulation of specific target genes (Pearson et al., 2005). The *Hox* clusters evolved from a single *Hox* gene ancestor, which underwent a cis-duplication to generate a cluster of 13 members, and then a trans-duplication of the entire cluster. As a consequence, *Hox* genes from the same group (trans-paralogous genes or paralogs) share more similarity in protein sequence and expression pattern than genes within a cluster. Mice and other mammals have 39 *Hox* genes arranged on four clusters located on 4 different chromosomes, while zebrafish and other teleosts have 48 *Hox* genes over 7 clusters, which resulted from a genome-wild duplication event possessed by the last common ancestor of extant bony fishes(Amores et al., 2004).

After these duplication events, the diverged *Hox* genes play diverse biological functions, as evidenced by their single mutant phenotypes. However, *Hox* genes also show extensive functional overlap. Hox proteins share a highly conserved homeodomain, which recognizes and binds to identical or similar target sequences in *in vitro* DNA binding assays (Desplan et al.,

1988; Hoey and Levine, 1988). There is a large body of evidence showing redundancy and overlapping *in vivo* function of *Hox* genes, particularly for paralogs (Condie and Capecchi, 1994; Davis et al., 1995; Greer et al., 2000; Manley and Capecchi, 1997; Manley and Capecchi, 1998; Tvrdik and Capecchi, 2006). Loss-of-function of *labial* in the specification of the Drosophila tritocerebral neuromere could be restored by any of the other *Hox* gene products in Drosophila, except for Abd-B (Hirth et al., 2001). Genetic complementation study has also shown that chicken *Hoxb1* was able to rescue *Drosophila labial* null mutant (Lutz et al., 1996). A large number of Hox proteins from different species have been expressed in *Drosophila*, and usually play similar functions as their Drosophila orthologues, implying the functional equivalence of *Hox* genes cross phyla.

While the function of *Hox* genes is strikingly conserved during evolution, many studies have shown the correlation between changes in *Hox* expression pattern and variation in morphological pattern (Carroll et al., 2005; Gellon and McGinnis, 1998; Lynch and Wagner, 2008; Pearson et al., 2005; Wray, 2007). For example, the differences in the expression patterns of *Ubx* and *Abd-A* in different crustacean species correlate with the body plans of thoracic limbs and feeding appendages (Averof and Patel, 1997). Another example is that the variations in *Scr* expression patterns in insects were found correlated with the variations in wing morphology (Rogers et al., 1997). In contrast, there are much fewer studies showing that variation in Hox protein functions contributes to the diversity of body plan. Two studies reported changes in UBX protein sequence have been associated with reductions of limb number during the evolution of insects (Galant and Carroll, 2002; Ronshaugen et al., 2002). However in both

studies, changes in UBX protein sequence are concurrent with changes in the expression patterns, consistent with the notion that cis-element evolution is the main driving force of morphological evolution.

The Group3 *Hox* genes are required for patterning of anterior body plan during embryogenesis. *Hox3* genes catch extra attention due to their unique features. First, whereas *Hox* genes play conserved function in embryonic axial patterning, the insect *Hox3* ortholog, *Zen*, is involved in extraembryonic development. Second, class3 Hox proteins possess unusually long C-terminal domain, the function of which remains to be investigated. In addition, *Hoxa3* is the first gene ever knocked out with gene targeting. In mouse, *Hoxa3* is expressed in the neural tube with the rostral limit up to the boundary between rhombomere4 and 5 (r4/r5), as well as in the neural crest emanating from r6 and posterior. It is also expressed in the 3rd and 4th pharyngeal pouch endoderm, as well as in the pharyngeal arch mesenchyme (Manley and Capecchi, 1995). Pharyngeal pouches and arches are transient embryonic structures that give rise to many organs and tissues at the facial and neck region. Neural crest cells (NCCs) migrate from the midbrain and hindbrain to the pharyngeal arches and form the bulk of the mesenchyme in this region. NCCs play a critical role in the development of the pharyngeal organs and tissues by contributing directly to the formation and/or patterning of the diverse skeletal, neural, and organ structures that form in the region (Bockman and Kirby, 1984; Dupin et al., 2006; Krumlauf, 1994; Watari et al., 2001).

Hoxa3 is required for the development of many pharyngeal organs and tissues derived from pharyngeal pouches and arches. Inactivation of mouse *Hoxa3* by gene targeting results in

many defects, including neonatal lethality, pharyngeal organ defects or deletions, disorganization of trachea epithelium, truncation of soft palate, malformation of throat cartilages, defects in the IXth glossopharyngeal nerve and carotid body (Chisaka and Capecchi, 1991; Kameda et al., 2002; Manley and Capecchi, 1995; Manley and Capecchi, 1997; Watari et al., 2001). In addition, mutation in *Hoxa3* exacerbates the defects of single or compound mutants of Group3 *Hox* paralogs, showing that Hoxa3 functions synergistically with *Hoxb3* and *Hoxd3* (Condie and Capecchi, 1994; Manley and Capecchi, 1997; Manley and Capecchi, 1998).

The striking functional redundancy of *Hox3* paralogs was further demonstrated by the Hoxa3-Hoxd3 swapping experiment (Greer et al., 2000). By swapping the protein coding regions of these two genes, they showed that the proteins are functionally equivalent, in spite of the distinct biological functions and different protein sequences. Similarly, HoxA1 and HoxB1 were found functionally interchangeable by gene swapping. Another example of functional equivalence between Hox paralogs is that HoxA11 and HoxD11 have been shown to be functionally substitutable to each other in specifying lumbosacral vertebral identity (Zakany et al., 1996). These and other similar studies support the functional equivalence model, which proposes that *Hox*-encoded proteins are functionally equivalent, and that the overall quantity of Hox proteins may be more important than the specific Hox proteins present (Duboule, 1995; Duboule, 2000).

In this study we tested whether the zebrafish Hoxa3a protein can substitute for mouse Hoxa3, by generating the *Hoxa3^{zf}* allele in which the *zfHoxa3a* coding sequence precisely replaced the mouse *Hoxa3* coding sequence, leaving all regulatory elements intact. Protein

sequence alignments showed that the murine and zebrafish Hoxa3 protein sequences have identical homeodomain and pentapeptide sequences, and were about as similar overall as the mouse Hoxa3 and Hoxd3 paralogs, which have been shown to have similar function. Consistent with this similarity, the zebrafish gene expressed from mouse *Hoxa3* locus complemented some defects seen in the mouse *Hoxa3* null mutant, showing that the proteins share conserved biological functions. However, the *Hoxa3*^{zf} allele provided null function in the development of the IXth cranial nerve, thymus and parathyroid, and generated a novel pharyngeal skeleton phenotype. Using a second mouse strain in which only the C terminal half of the protein is from zebrafish, we show that these functional differences map to the unusually long C terminal domain. These data provide evidence that the zebrafish Hoxa3a and mouse Hoxa3 proteins have functionally diverged since their last common ancestor, due to changes outside the homeodomain.

RESULTS

Protein sequence alignment

We compared the protein sequences of zebrafish Hoxa3a, mouse Hoxa3 and mouse Hoxd3 (Fig. 2.1A). The overall identity between zfHoxa3a and muHoxa3 (59%) is slightly higher than that between muHoxa3 and muHoxa3 (52%). At the N-terminal of the proteins, there is a block of amino acid sequence that present in muHoxA3 but absent in muHoxd3, and a even larger block is absent in zfHoxa3a. MuHoxa3 and zfHoxa3a share identical DNA-binding homeodomain sequence, whereas the homeodomain of muHoxd3 is one amino acid different. All three proteins have large C-terminal domains which are only seen in class3 Hox proteins.

The C-terminal domains of the three proteins share relatively higher homology than the N-terminal.

Expression of zebrafish Hoxa3a protein from mouse Hoxa3 locus

We generated a new *Hoxa3* allele (*Hoxa3^{zf}*) that encodes the zebrafish Hoxa3a protein from the endogenous moue *Hoxa3* locus, replacing the mouse *Hoxa3* protein coding domains with zebrafish *Hoxa3a* protein coding domains using gene targeting, using a similar strategy as previously used for the mouse Hoxa3-Hoxd3 swap (Fig. 2.1B-D) (Greer et al., 2000). All sequences outside the protein coding domains, including 5' to the ATG, the intron between the two coding exons, and 3' to the TGA stop codon, were from the mouse *Hoxa3* locus. The *Hoxa3^{zf}* allele was expressed correctly, with the same spatial and temporal pattern as the endogenous Hoxa3 mRNA (Fig. 2.1E-H). The expression level from the wild-type and *Hoxa3^{zf}* alleles was also equivalent (Fig. 2.1I). Analysis of the zebrafish Hoxa3a protein, which is tagged with HA, showed that the protein was present and had the correct anterior limit in the hindbrain (Fig. 2.1J-K).

***Hoxa3^{zf}* allele complements *Hoxa3^{null}* phenotype in some tissues**

We then tested whether zebrafish Hoxa3a protein was able to complement *Hoxa3* null mutant phenotypes. *Hoxa3* null mutant mouse is deficient in the development of thyroid. The ultimobranchial body derived C-cells failed to mix with the thyroid diverticulum derived follicular cells, and the ventral thyroid isthmus structure was either absent or ectopic (Manley and Capecchi, 1995). *Hoxa3$^{zf/zf}$* and *Hoxa3$^{zf/null}$* mice, however, has normal thyroid organ as

wild-type. The calcitonin-producing cells were mixed with the follicular cells in thyroid (Fig. 2.2E-H), and a normal isthmus structure was present (Fig. 2.2A-D).

Another defect in *Hoxa3* null mutant was found in trachea epithelia (Manley and Capecchi, 1995). In wild-type mouse, the trachea epithelium is pseudostratified and comprised of organized columnar epithelial cells which all rest on the basement membrane (Fig. 2.2I). But in the null mutant, trachea epithelium is poorly organized with cells piling on top of each other, resulting in a thicker epithelium layer and sometimes a convoluted surface (Manley and Capecchi, 1995) (Fig. 2.2J). In all the $Hoxa3^{zf/zf}$ and $Hoxa3^{zf/null}$ animals examined, this abnormal epithelial lining phenotype was completely rescued by zebrafish HoxA3A protein (Fig. 2.2K-L).

It was previously reported that most of the $Hoxa3^{null/null}$ animals that found alive at newborn had a bloated abdomen, and the soft palate was truncated (Chisaka and Capecchi, 1991) (Fig.2.3B, F). Unlike the normal soft palate, which facilitates air passage to enter the trachea, the truncated one might cause the animal to breathe the air into both trachea and esophagus. But due to neonatal lethality (see below), not all of the $Hoxa3^{null/null}$ newborns can live long enough to develop a bloated abdomen. In all $Hoxa3^{zf/zf}$ newborns analyzed, the soft palate is normal, and the bloated abdomen phenotype was never found in these mice (Fig. 2.3C, G; Table 2.1). Interestingly, $Hoxa3^{zf/null}$ animals had a very high penetrance of bloated abdomen phenotype (Fig. 2.3D; Table 2.1). Truncated soft palate was observed in all the $Hoxa3^{zf/null}$ animals (Fig. 2.3H), but the soft palate phenotype is not as severe as $Hoxa3^{null/null}$ (Fig. 2.3F). This suggests that the development of soft palate is sensitive to *Hoxa3* dosage.

zfHoxa3a and msHoxa3 proteins are functionally distinct

Although zebrafish Hoxa3a can substitute for mouse Hoxa3 for the normal development of some tissues, it provided null function in some other aspects. Neonatal lethality phenotype associated with *Hoxa3* null mutant was not complemented by the *Hoxa3*^{zf} allele (Chisaka and Capecchi, 1991). *Hoxa3*$^{zf/zf}$ mice could not survive more than one day after birth and no *Hoxa3*$^{zf/zf}$ adult mice were ever recovered (Table 2.2). The defect of the glossopharyngeal (IX) nerve, which is derived from Hoxa3-expressing neural crest cells (Watari et al., 2001), was not rescued in *Hoxa3*$^{zf/zf}$ embryos. In the majority of *Hoxa3* null mutants, the IX nerve was either truncated or fused to the vagus (X) nerve (Manley and Capecchi, 1997; Watari et al., 2001). Similar defect was observed in *Hoxa3*$^{zf/zf}$ embryos: 20% of the examined embryos had truncated glossopharyngeal nerve that was not connected to hindbrain, and about 70% of them showed a fusion between the IX and X nerves (Fig. 2.4, Table 2.3), suggesting that *Hoxa3*^{zf} allele functions as a null allele in the development of the IX cranial nerve.

One of the most consistent phenotypes of the null mutant is the absence of thymus and parathyroid organs. In wild-type embryos, the common primordia of thymus and parathyroid start to develop from the 3rd pharyngeal pouches at E11.0-E11.5 (Cordier and Haumont, 1980). Foxn1 is a transcription factor that can be served as a thymus-specific marker (Gordon et al., 2001). It is expressed in the thymus primordium starting at E11.25, and required for the initiation of the differentiation of thymic epithelial cells (Nehls et al., 1996). When we examined *Hoxa3*$^{zf/zf}$ animals, no thymus or parathyroid was ever detected at the normal location or any other ectopic locations (Fig. 2.5A-F and data not shown). Whole-mount in situ

hybridization of Foxn1 showed that expression of Foxn1was absent from the third pharyngeal pouch at E11.5 in both the *Hoxa3*$^{null/null}$ and *Hoxa3*$^{zf/zf}$ embryos (Fig. 2.5G-I). Gcm2, a transcription factor starting to be expressed at E9.5 at the 3rd pharyngeal pouches, is required for parathyroid organogenesis (Gunther et al., 2000; Liu et al., 2007). Expression of Gcm2 was greatly reduced from the 3rd pouch in both mutant embryos at E10.5 (Fig. 2.5J-L). We also examined the expression of Pax1, which is expressed in the endoderm of pouch one through four, in *Hoxa3*$^{zf/zf}$ embryos. Like the null mutant, the *Hoxa3*$^{zf/zf}$ embryos had reduced Pax1 expression at the third pharyngeal pouches at E10.5, while the expression at other pouches was not affected (Manley and Capecchi, 1995) (Fig. 2.5M-O). Taken together, *Hoxa3*$^{zf/zf}$ and *Hoxa3*$^{null/null}$ embryos showed the same phenotypes on the organogenesis of thymus and parathyroid, indicating that zebrafish Hoxa3a provides null function in the development of these two organs.

Hoxa3^{zf} provides a novel function in mouse hyoid bone development

Hoxa3 null mutant is also characterized with malformed hyoid bone. The lesser horn and greater horn of hyoid born are derived from the second and third pharyngeal arches respectively. In *Hoxa3*$^{null/null}$ mouse, the lesser horn of the hyoid bone is absent or greatly reduced and the greater horn is malformed and fused to the thyroid cartilage (Condie and Capecchi, 1994; Manley and Capecchi, 1997) (Fig. 2.6B). *Hoxa3*$^{zf/zf}$ mouse has the same greater horn as *Hoxa3*$^{null/null}$, but has a lesser horn different from either wildtype or null mutant. The lesser horn is restored in *Hoxa3*$^{zf/zf}$ mice, but it is in an abnormal shape (Fig. 2.6D-E), showing that *Hoxa3*^{zf} allele provides a novel function in the development of mouse hyoid bone. Interestingly, the

restored hyoid lesser horn was in a shape similar to the hyoid opercle bone in zebrafish (Fig. 2.6G). But the origin of the opercle bone in zebrafish is currently not clear, so it is not sure whether this structure is homolog to the mouse hyoid bone. This neomorphic phenotype also confirmed that *Hoxa3*^{zf} allele function beyond a hypomorphic *Hoxa3* allele. When we examined *Hoxa3*$^{+/zf}$ animals, we observed a normal hyoid phenotype (Fig. 2.6C), showing that the wildtype allele is dominant to *Hoxa3*^{zf} allele when they are both present.

Synergistic interaction between *zfHoxa3* and *Hoxd3*

Previous studies have demonstrated synergistic interactions of the *Hox* group3 paralogous genes in patterning multiple structures within the throat region (Condie and Capecchi, 1994; Manley and Capecchi, 1997). Single mutant of *Hoxa3* and *Hoxd3* show no obvious overlap in the phenotype in spite of the conserved protein sequence and expression pattern (Chisaka and Capecchi, 1991; Condie and Capecchi, 1993). *Hoxa3* single mutant have defects in pharyngeal tissues and organs derived from the pharyngeal pouches and arches. *Hoxd3* single mutant show defects in axial skeleton derived from somatic mesoderm. However double mutant of *Hoxa3* and *Hoxd3* showed more severe defect in the axial skeleton and throat cartilage than the single mutants, revealing dosage-dependent interaction between these genes. We then asked whether zebrafish *Hoxa3a* expressed from mouse *Hoxa3* locus interacts with mouse *Hoxd3*. Figure 2.7 shows cervical vertebrae of newborn animals of different genotypes. The anterior arch of atlas in *Hoxa3*$^{+/+}$*;Hoxd3*$^{-/-}$ was deleted and the atlas was fused to the exoccipital. *Hoxa3*$^{+/-}$*;Hoxd3*$^{-/-}$ had a more severe defect, with only a small piece of atlas remained and the axis remodeled toward a more posterior vertebra. *Hoxa3*$^{-/-}$*;Hoxd3*$^{-/-}$ had the most severe phenotype with the

entire atlas deleted. The range of the phenotypes in different genotypes indicates dosage-sensitive function for Hoxa3 to pattern the cervical vertebrae. *Hoxa3*$^{zf/zf}$*;Hoxd3*$^{-/-}$ showed the same phenotype as *Hoxa3*$^{-/-}$*;Hoxd3*$^{-/-}$, suggesting that *Hoxa3*^{zf} allele might function as a null allele in the development of cervical vertebrae. However *Hoxa3*$^{+/zf}$*;Hoxd3*$^{-/-}$ mice did not show the same phenotype as *Hoxa3*$^{+/-}$*;Hoxd3*$^{-/-}$; instead, they had a similar phenotype as *Hoxa3*$^{+/+}$*;Hoxd3*$^{-/-}$, with the atlas fused to the exoccipital, suggesting that zebrafish *Hoxa3a* gene has a function intermediate between the null and wild type alleles of mouse *Hoxa3* to interact with *Hoxd3* gene in patterning the cervical vertebrae.

Zebrafish Hoxa3a failed to complement the loss of Hoxa3 in neural crest cells

The role of Hoxa3 in NCC development was investigated by disrupting Hoxa3 in NCCs with crossing *Wnt1cre;Hoxa3*$^{+/null}$ mice with *Hoxa3*$^{fx/fx}$ mice. Like *Hoxa3*$^{null/null}$, *Wnt1cre;Hoxa3*$^{fx/null}$ embryos survive until newborn. But different from the null mutant, thymus and parathyroid organs were detected in these embryos, though they were ectopically located (Fig. 2.8B, E). When we examined *Wnt1cre;Hoxa3*$^{fx/zf}$ animals, we observed neonatal lethality phenotype as well (data not shown). Thymus was formed in these mice but appeared as two lateral lobes located anterior to the normal position. The overall size and organization of these lobes was similar to wild-type thymus, with recognizable medullary and cortical regions (Fig. 2.8C). Parathyroid was also found ectopically located but normal in morphology (Fig. 2.8F). Thyroid organ in these mice appeared normal, with normal location, size and isthmus structure (Fig. 2.8G-I and data not shown). Cranial nerve phenotype in these embryos was also checked. It looked similar to Hoxa3 null mutant (Fig. 2.8J-L and data not shown). Overall,

Wnt1cre;Hoxa3$^{fx/zf}$ mimics *Wnt1cre;Hoxa3*$^{fx/null}$ in all the phenotypes we examined, showing that *Hoxa3*^{zf} allele provides null function in NCCs.

Major functional difference resides in the C-terminal domain

We show that zebrafish Hoxa3a protein fails to rescue many of the null mutant phenotypes in mouse, indicating distinct protein functions. Using another Hoxa3 allele, we were able to ask which domain, the N-terminal or C-terminal, is more important for the functional difference. *Hoxa3*^{mz} allele that encodes a protein with mouse N-terminal and zebrafish C-terminal domains was generated as a byproduct of *Hoxa3*^{zf} allele (Fig. 2.1B). We then compared *Hoxa3*$^{mz/mz}$ to *Hoxa3*$^{zf/zf}$, *Hoxa3*$^{null/null}$ and wild-type. *Hoxa3*$^{mz/mz}$ mice died at or right after birth. The bloated abdomen and truncated soft palate, however, were not found in those newborn mice (Fig. 2.9G-H and Table 2.1). *Hoxa3*$^{mz/mz}$ mice have normal thyroid isthmus structure and normal trachea epithelium organization (Fig. 2.9A-F), but lack thymus or parathyroid organs (Fig. 2.9I-L). They showed the same defect in the greater horn of hyoid born as *Hoxa3*$^{zf/zf}$ and *Hoxa3*$^{null/null}$. But the lesser horn was in a shape different from either *Hoxa3*$^{null/null}$ or *Hoxa3*$^{zf/zf}$. Interestingly, there is an extra cartilage structure connecting the hyoid bone to the skull, which is not seen in either *Hoxa3*$^{zf/zf}$ or *Hoxa3*$^{null/null}$ (Fig. 2.9M). When there is only one copy of mz allele, *Hoxa3*$^{mz/null}$ appeared the same to *Hoxa3*$^{mz/mz}$ (Fig. 2.9), the overall phenotypes of which are the same as *Hoxa3*$^{zf/zf}$. Thus, the new chimera protein plays a role similar to zebrafish HoxA3a in the development of the structures that are affected in *Hoxa3*$^{null/null}$ mutant. The difference in the protein sequence of the N-terminal domain, therefore, doesn't contribute to the

functional divergence between the two proteins, which resides in the C-terminal domain of the protein instead.

DISCUSSION

Evolution of *Hox* genes and its contribution to the morphological diversity has long been a fascinating subject to biologists. Cross-species functional tests have provided valuable information in understanding the evolution of *Hox* genes. To our knowledge, this is the first cross-species study with a very precise gene replacement approach, in which the expression of the orthologous Hox gene is controlled by the regulatory machinery of the host species. We tested whether zebrafish *Hoxa3a* is functionally equivalent to mouse Hoxa3 when they are expressed in the same naturally selected biological context. Our data show that these two proteins play non-equivalent in vivo functions, suggesting that Hoxa3 protein function has evolved significantly since the divergence of mouse and zebrafish, and that this essential functional difference between mouse and zebrafish HoxA3 proteins maps to the C-terminal domain.

Non-equivalent function between mouse and zebrafish Hoxa3 proteins

In this study we showed that zebrafish Hoxa3a protein was capable to substitute for mouse Hoxa3 protein in the development of thyroid, trachea and soft palate, but not thymus, parathyroid, cranial nerve or carotid body. Thus these two proteins are functionally distinct. This non-equivalent function was not predicted by the functional equivalence model. The widely accepted functional equivalence model states that the function of Hox protein is

equivalent between paralogs and orthologs. Indeed, there is a large body of evidence showing the functional equivalence between Hox proteins. According to the functional equivalence model, we would predict that zebrafish Hoxa3a expressed from the mouse Hoxa3 locus would be able to functionally replace mouse Hoxa3. However, the expression of zebrafish Hoxa3a in mouse, when controlled by mouse Hoxa3 cis-regulatory machinery, failed to complement the loss of mouse Hoxa3. This result is also not consistent with the prevailing model of morphological evolution via cis-regulatory changes (Carroll et al., 2005).

Although the non-equivalence in Hox protein function revealed in this study was not predicted by the prevailing models, it is not individual. There are quite a few studies showing non-equivalent protein function between Hox proteins (Lynch and Wagner, 2008). It's generally believed that modulation in Hox genes, especially in cis-regulatory elements, contributes to morphological changes (Averof and Patel, 1997; Pearson et al., 2005; Stern, 1998). Actually there is also accumulating evidence showing that changes in Hox protein sequences have also contribute to the diversity of body plan (Galant and Carroll, 2002; Hsia and McGinnis, 2003; Lynch and Wagner, 2008; Ronshaugen et al., 2002).

Previous genetic complementary studies cross species reveal a high degree of functional equivalence between Hox orthologs. However, in most cases, these experiments were done by expressing a vertebrate *Hox* gene in Drosophila. Therefore we can't distinguish these two possible scenarios for the evolution of Hox proteins: Hox proteins evolve novel functions and maintain their ancestral function, or protein function was established in the ancestral Hox protein and remains unchanged during evolution. Thus, expressing Hox genes from

evolutionarily more ancestral organisms in mouse become indispensable. The failure of zebrafish Hoxa3a to substitute for mouse Hoxa3 suggests that mouse Hox gene has added novel functions onto the more ancestral protein function, or zebrafish Hox gene has lost some of the ancestral function since the divergence of mouse and zebrafish.

Hox protein function and morphological evolution

As many previous studies have shown functional equivalence between orthologous and paralogous Hox proteins, it is not surprising that our data revealed conserved protein function between mouse and zebrafish Hoxa3 proteins in the development of thyroid, trachea and soft palate. But it is important to note that the ultimobranchial bodies stay as separate structures from the thyroid and there is no trachea or soft palate structure in zebrafish. This might reflect the conserved ancestral function at cellular level. This is consistent with the previous studies showing that the Hox gene expression pattern required for novel body plan was present before the evolution of the novel body plan. For instance, it is generally believed that the absence of Hox expression at the mandibular arch is responsible for the evolution of jaw. Hox-free state of the mandibular arch was proposed to predate the emergence of gnathostomes (Kuratani, 2004).

On the other hand, out data also indicate diverged protein function between mouse and zebrafish Hoxa3 proteins. Zebrafish Hoxa3a protein is not able to substitute for mouse Hoxa3 in the development of thymus, parathyroid, cranial nerve or carotid body, though zebrafish shows similar anatomy with mouse in many of those tissues. In zebrafish, thymus develops from the pharyngeal pouches like in mouse. Expression of the groupI pax genes (Pax1/9) in pharyngeal pouch is conserved from urochordates to vertebrates (Hetzer-Egger et al., 2002;

Holland et al., 1995; Nornes et al., 1996; Ogasawara et al., 2000; Ogasawara et al., 1999; Wallin et al., 1996; Zou et al., 2006). *Pax1/9* genes have been identified as gill-specific molecular markers, and their expression in hemichordates gills has been proposed to be molecular evidence for organ-level homology between hemichordates and chordates (Ogasawara et al., 1999). In mouse, down-regulation of Pax1/9 is companied with transient fusion between pouch endoderm and cleft ectoderm (data not shown), and the failure of thymus and parathyroid organogenesis (Manley and Capecchi, 1995), suggesting that high level of Pax1/9 expression at the 3rd pharyngeal pouch in mouse might be required to prevent the fusion between cleft and pouch and then promote the development of thymus and parathyroid. It has been suggested that Pax1/9 function downstream of Hoxa3 (Manley and Capecchi, 1995; Su et al., 2001). Since Hoxa3 expression in pouch endoderm seems correlated with the existence of thymus in higher vertebrates, we propose that *Hoxa3* play a role in the evolution of pharyngeal organs, and that the role might be mediated by regulating Pax1/9 expression. Our study suggests that function of HoxA3 protein might have diverged significantly since the last common ancestor of mouse and zebrafish, and thus, changes in protein function might then facilitate the emergence of novel pharyngeal organs, such as thymus and parathyroid.

Failure in phenotypic complement is not caused by insufficient expression

We have generated the *Hoxa3^{zf}* allele, which expresses zebrafish Hoxa3a gene from the endogenous mouse Hoxa3 locus. And we showed that zebrafish Hoxa3a gene was expressed in the same pattern and at the same level as the mouse Hoxa3 gene. The results that zebrafish Hoxa3a was able to substitute for mouse Hoxa3 at least in some of the pharyngeal tissues

confirm the correct expression of zebrafish Hoxa3a. However, the fish protein showed a range of different capacities in replacing the mouse protein:

Thyroid defects found in *Hoxa3* null mutant, including the deletion of isthmus and failure of fusion of ultimobranchial body to thyroid, are completely rescued by zebrafish Hoxa3a. Disorganized trachea epithelial lining phenotype seen in *Hoxa3* null mutant is also entirely complemented in $Hoxa3^{zf/zf}$ animals. And a single copy of $Hoxa3^{zf}$ allele is sufficient to complement both of the thyroid and trachea deficiency. Therefore, $Hoxa3^{zf}$ allele functions equivalently to a wild-type allele in these two organs (zf = +).

Zebrafish HoxA3a is also found capable to substitute for mouse HoxA3 protein in the development of soft palate. In Hoxa3 deficient mouse, the soft palate is truncated, resulting in a bloated abdomen. The truncated soft palate and bloated abdomen was never found in $Hoxa3^{zf/zf}$ mice or any of $Hoxa3^{+/+}$, $Hoxa3^{+/null}$ and $Hoxa3^{+/zf}$ animals. Strikingly, $Hoxa3^{zf/null}$ mimics $Hoxa3^{null/null}$ in soft palate and bloated abdomen phenotype, whereas $Hoxa3^{+/null}$ displayed a normal phenotype essentially the same to $Hoxa3^{+/+}$, suggesting that $Hoxa3^{zf}$ might function as a hypomorphic *Hoxa3* allele in the development of soft palate and that there might be a dosage threshold below which Hoxa3 is not sufficient to support a normal soft palate development.

When we analyzed the function of zfHoxa3a in the development of skeleton, we found another pattern. $Hoxa3^{zf/zf}$ and $Hoxa3^{zf/null}$ have a unique hyoid lesser horn structure which differs from either $Hoxa3^{+/+}$ or $Hoxa3^{null/null}$, showing that $Hoxa3^{zf}$ allele functions as a neomorphic allele. But $Hoxa3^{+/zf}$ shows a wild-type phenotype, so it seems that the $Hoxa3^{zf}$ allele is recessive when present with a wild-type allele. ZfHoxa3a function in cervical vertebrae

was further tested at *Hoxd3* deficient background. *Hoxa3*$^{zf/zf}$*;Hoxd3*$^{-/-}$ showed the same phenotype as *Hoxa3*$^{-/-}$*;Hoxd3*$^{-/-}$, suggesting that *Hoxa3*^{zf} allele might function as a null allele. However *Hoxa3*$^{+/zf}$*;Hoxd3*$^{-/-}$ mice did not show the same phenotype as *Hoxa3*$^{+/-}$*;Hoxd3*$^{-/-}$, in stead, they had a similar phenotype as *Hoxa3*$^{+/+}$*;Hoxd3*$^{-/-}$. This indicates that *Hoxa3*^{zf} allele function more than a null allele. Collectively, two copies of *Hoxa3*^{zf} allele together work not as well as only one copy of wild-type, but one *Hoxa3*^{zf} allele and one wild-type allele together work better than only one copy of wild-type. Thus *Hoxa3*^{zf} allele works better than null but not as well as even 50% of + (- < zf < 50%+).

Hoxa3$^{zf/zf}$ mimics *Hoxa3*$^{null/null}$ in all the examined aspects of the development of thymus and parathyroid, showing that zfHoxA3a provides null function (zf = -).

Overall, zfHoxa3a complements the absence of mouse Hoxa3 in different tissues at a degree ranging from 0 to 100%. This argues against the possibility that insufficient expression of zfHoxA3a caused functional distinction. Otherwise, we would see the same degree of partial rescue in all the different tissues, and always see more several phnotypes in *Hoxa3*$^{zf/null}$ than *Hoxa3*$^{zf/zf}$. In addition, our data has shown the same expression pattern and expression level between *Hoxa3*^{zf} and *Hoxa3*$^{+}$ alleles.

Quantity versus Quality

The difference in the single mutant phenotype of *Hoxa3* and *Hoxd3* reveals the different biological functions (qualities) for these two genes. On the other hand, Greer et al have demonstrated that Hoxa3 and Hoxd3 protein are functionally equivalent by swapping the protein coding sequences of *Hoxa3* and *Hoxd3* (Greer et al., 2000). Hoxd3 protein expressed

from the *Hoxa3* locus complements the *Hoxa3* mutant phenotypes completely. In reverse, HoxA3 protein from Hoxd3 locus compensates the endogenous deficiency of *Hoxd3*. This study implies that the overall quantity, rather than the quality of group3 *Hox* genes is critical for the normal gene function.

Skeleton analysis shows that $Hoxa3^{+/-};Hoxd3^{-/-}$ have a more severe phenotype than $Hoxa3^{+/+};Hoxd3^{-/-}$. But on the $Hoxd3^{+/+}$ background, $Hoxa3^{+/+}$ and $Hoxa3^{+/-}$ do not show any obvious difference in phenotype (Chisaka and Capecchi, 1991; Condie and Capecchi, 1994; Manley and Capecchi, 1995). Moreover, while Hoxa3+/- mice exhibit no phenotypic defects, $Hoxa3^{+/-};Hoxb3^{-/-};Hoxd3^{-/-}$ mouse has ectopic thymus and parathyroid (Manley and Capecchi, 1998). Thus, when there is no functional *Hoxb3* or *Hoxd3*, quantity of *Hoxa3* gene matters. Interestingly, $Hoxb3^{+/-};Hoxd3^{-/-}$ had the same vertebrae phenotype as $Hoxa3^{+/-};Hoxd3^{-/-}$, though single mutant of *Hoxb3* had a very mile phenotype compare to *Hoxa3*. It has also been shown that mutations in *Hoxb3* or *Hoxd3* exacerbate the throat cartilage phenotype in Hoxa3 mutant (Manley and Capecchi, 1997). These results suggest that the overall quantity of *Hox3* genes is more critical than the quality at some functional context.

In this study, we have shown that on $Hoxd3^{-/-}$ background, one wild-type allele and one $Hoxa3^{zf}$ allele together function equivalently as two wild-type alleles, and more than only one wild-type allele, in determining cervical vertebrae identity. This again supports the notion that quantitiative modulations in Hox gene expression are critical for the qualitative readout of Hox gene products (Duboule, 2000; Duboule and Morata, 1994; Zakany et al., 1996). On the other hand, we have also shown that zebrafish Hoxa3a failed to complement NCC-specific loss of

Hoxa3. Thus, even with the presence of Hoxb3 and Hoxd3, the quality of Hoxa3 appears dominant to the quantity for the proper gene function.

The C-terminal domain of Hoxa3 protein

A large number of studies have shown that paralogous and orthologous Hox proteins are functionally equivalent, whereas swaps of the 60 amino acid homeodomain from different mouse paralogous *Hox* groups reveal different functions between non-paralogous Hox proteins (Zhao and Potter, 2001; Zhao and Potter, 2002). Thus it has been proposed that Hox protein function largely resides in the homeodomain. Compatible with this view, extreme functional equivalence has been discovered between mouse Hoxa3 and Hoxd3 (Greer et al., 2000), which share highly conserved homeodomain with only one amino acid difference in the sequence. However, although zebrafish Hoxa3a has identical homeodomain as mouse Hoxa3, the function of zebrafish Hoxa3a is non-equilavent to its mouse ortholog, indicating that the functional difference resides outside the homeodomain.

The emergence of HoxA, B, C and D clusters occurred before the divergence of lobe fin (mouse) and ray fin (zebrafish) lineages (Amores et al., 2004). Thus, compared to mouse Hoxd3, zebrafish Hoxa3a is closer to mouse Hoxa3 phylogenetically. Consistent with this notion, compared to mouse Hoxd3, zebrafish Hoxa3a shows a higher overall protein sequence identity to mouse Hoxa3. But this close phylogenetical relationship and the high level of overall identity do not correlate to the level of functional similarity, suggesting that the protein sequence at some particular regions might be crucial for Hox protein function.

Our data show the chimera Hoxa3 protein plays almost identical function as zebrafish Hoxa3a protein. Both proteins are functionally distinct to mouse Hoxa3, though they are able to substitute for mouse Hoxa3 for normal development of some tissues. This implies that the chimera protein can be expressed from the endogenous locus and folded into a stable protein structure. Otherwise, we would observe null mutant phenotype in *Hoxa3*$^{mz/mz}$ animals. Despite of the poorly conserved amino acid sequences of the N-terminal domain (Fig. 2.1A), the in vivo function of this domain are highly conserved. And the homeodomains of mouse and zebrafish Hoxa3 proteins are completely identical. Then the domain responsible to the functional divergence has been narrowed down to the C-terminal domain. Interestingly, group3 Hox proteins have larger C-terminal domains compare to all the other Hox proteins. And this large C-terminal domain unique to group3 Hox proteins appears highly conserved cross species. Therefore this domain might be very important for the functional evolution of Hox3 proteins. The regions that are conserved between mouse Hoxa3 and Hoxd3 proteins, but diverged in zebrafish Hoxa3a protein, might be the most important for the functional divergence.

EXPERIMENTAL PROCEDURES

Gene Targeting

Mouse Hoxa3^{zf} allele was generated by homologous recombination in Bl6 ES cells. Details on the targeting vector construction, southern blot screening and genotyping with PCR can be found in the Supplemental Data. Genomic DNA containing the Hoxb3 locus was obtained by BAC recombination followed by digestion with NotI. The Hoxa3 locus was targeted with

vectors based on the 12kb NotI fragment of Bl6 genomic DNA. The targeting vector was linearized and electroporated into Bl6 ES cells. Clones were screened with southern Blot with 5' and 3' franking probes and an internal probe. ES cell electroporation and injection was performed in the Mouse ES cell Core Laboratories of Medical College of Georgia.

In situ Hybridization

Whole-mount in situ hybridizations were performed essentially as previously described (Manley and Capecchi, 1995). E10.5 and E11.5 mouse embryos were fixed in 4% PFA overnight then dehydrated in gradient methanol and stored at -20℃ until use. The roof plate of E10.5 embryos was opened to reduce background, and E11.5 mouse embryos were hemisected to help penetration. Digoxigenin-labelled RNA probes were used at 0.25-0.5 ug/ml. Probes for mouse *Hoxa3* and *Pax1* (Manley and Capecchi, 1995), *Foxn1* and *Gcm2* (Gordon et al., 2001) have been described. Probe for Zebrafish *Hoxa3a* was full-length cDNA fragment. Signal is detected using 1:5000 alkaline phosphatase-conjugated anti-dig antibody Fab fragments (Roche) and color reaction was carried out in BM-purple substrate (Roche) over time periods from 2 hours to 7 hours. The embryos were photographed with a Leica MZ125 dissection scope and a Q imaging digital camera. Embryos stained in whole mount were processed for sectioning by standard paraffin embedding and then cut into10 μm sections and counterstained with Nuclear Fast Red. Sections were photographed with a Zeiss microscope with Optronics digital camera.

Histology and Immunohistochemistry

Newborn animals were killed by CO_2 asphyxiation and the skin was removed. Newborns or embryos were fixed in 4% PFA, dehydrated in gradient ethanol, embedded in paraffin, and then

cut into 10 μm sections. Paraffin sections were either stained with hematoxylin and eosin or used for immunohistochemistry.

Calcitonin staining

Anti-calcitonin staining was performed essentially as described previously (Manley and Capecchi, 1995), the sections were de-waxed, rehydrated and treated with 3%H_2O_2 in PBST before blocked in 10% goat serum/PBST for 30 minutes at room temperature. The sections were then incubated with 1:200 anti-calcitonin (AnaSpec Inc. San Jose CA 95131) in PBST for 1 hour at room temperature or overnight at 4℃. After washing, Goat anti Rabbit IgG-HRP (Santa Cruz Biotechnology) was diluted 1:1000 in PBST and incubated for 30 minutes at room temperature followed by wash in PBST. Color reaction was developed by incubating in 0.6 mg/ml diaminobenzidine and 0.06% H_2O_2 in PBS for 10-15 minutes at room temperature. Sections were then counter-stained with Nuclear Fast Red and then dehydrated and mounted with Cytoseal 280 mounting medium (Richard-Allan Scientific). Imaging was done on a Zeiss microscope with Optronics digital camera.

Neurofilament Staining

Whole-mount neurofilament staining was performed as described previously (Manley and Capecchi, 1997). E11.5 mouse embryos were fixed in methanol:DMSO (4:1) overnight followed by incubation in methanol:DMSO:30% H_2O_2 (4:1:1) for 4-6 hours at room temperature. The embryos were then stored in methanol at -20℃ for upwards of a month until use. The embryos were dehydrated with a gradient methanol in PBST (0.5% triton X-100 in PBS), then blocked in PBSTMD (2% skim milk powder, 1% DMSO in PBST) for 2 hours at

room temperature. The embryos were then incubated in PBSTMD:neurofilament monoclonal antibody 2H3 cell supernatant (Developmental Studies Hybridoma Bank) (4:1) overnight at 4°C. After 5 times of 1 hour wash in PBSTMD, the embryos were incubated in goat anti-mouse antibody (Sata Cruz Biotechnology, 1:100 diluted in PBSTMD) for 3 days at 4°C. Color reaction was performed by incubating with 1mg/ml diaminobenzidine in PBS for 1 hour, followed by incubation in 0.03% H_2O_2/PBS for 1-2 minutes. The embryos were then dehydrated in methanol and cleared in BABB buffer (1:2 benzyl benzoate:benzyl alcohol). Imaging was done on a Leica MZ125 dissection scope with a Q imaging digital camera.

Skeleton Preparation

Zebrafish embryo skeleton preparation was performed as previously described (Kimmel et al., 1998). Skeleton preparation on mice was performed as follow. Newborn mice were killed by CO2 asphyxiation. The skin and the internal organs up to the diaphragm were removed. The newborn mice were then fixed in 95% ethanol for 5 days, soaked in acetone for 2 days, then stained in the staining solution (0.015g alcian blue 8GX, 0.005g alizarin red S, 5ml acetic acid, 75ml 95% ethanol, 20ml water) at 37°C for 10 days. The staining solution was then replaced with pure water and then with the trypsin solution (30% saturated sodium borate, 1% trypsin). The samples were cleared in the trypsin solution at 37°C for 4-6 hours and then in gradient glycerol/1% KOH. Skeletons were photographed with a Leica MZ125 dissection scope and a Q imaging digital camera.

REFERENCES

Amores, A., Suzuki, T., Yan, Y. L., Pomeroy, J., Singer, A., Amemiya, C. and Postlethwait, J. H. (2004). Developmental roles of pufferfish Hox clusters and genome evolution in ray-fin fish. *Genome Res* **14**, 1-10.

Averof, M. and Patel, N. H. (1997). Crustacean appendage evolution associated with changes in Hox gene expression. *Nature* **388**, 682-6.

Bockman, D. E. and Kirby, M. L. (1984). Dependence of thymus development on derivatives of the neural crest. *Science* **223**, 498-500.

Carroll, S. B., Grenier, J. K. and Weatherbee, S. D. (2005). From DNA To Diversity. In *Blackwell Science*, (ed., pp. 1-258.

Chisaka, O. and Capecchi, M. R. (1991). Regionally restricted developmental defects resulting from targeted disruption of the mouse homeobox gene hox-1.5. *Nature* **350**, 473-9.

Condie, B. G. and Capecchi, M. R. (1993). Mice homozygous for a targeted disruption of Hoxd-3 (Hox-4.1) exhibit anterior transformations of the first and second cervical vertebrae, the atlas and the axis. *Development* **119**, 579-95.

Condie, B. G. and Capecchi, M. R. (1994). Mice with targeted disruptions in the paralogous genes hoxa-3 and hoxd-3 reveal synergistic interactions. *Nature* **370**, 304-7.

Cordier, A. C. and Haumont, S. M. (1980). Development of thymus, parathyroids, and ultimo-branchial bodies in NMRI and nude mice. *Am J Anat* **157**, 227-63.

Davis, A. P., Witte, D. P., Hsieh-Li, H. M., Potter, S. S. and Capecchi, M. R. (1995). Absence of radius and ulna in mice lacking hoxa-11 and hoxd-11. *Nature* **375**, 791-5.

Desplan, C., Theis, J. and O'Farrell, P. H. (1988). The sequence specificity of homeodomain-DNA interaction. *Cell* **54**, 1081-90.

Duboule, D. (1995). Vertebrate Hox genes and proliferation: an alternative pathway to homeosis? *Curr Opin Genet Dev* **5**, 525-8.

Duboule, D. (2000). Developmental genetics. A Hox by any other name. *Nature* **403**, 607, 609-10.

Duboule, D. and Morata, G. (1994). Colinearity and functional hierarchy among genes of the homeotic complexes. *Trends Genet* **10**, 358-64.

Dupin, E., Creuzet, S. and Le Douarin, N. M. (2006). The contribution of the neural crest to the vertebrate body. *Adv Exp Med Biol* **589**, 96-119.

Galant, R. and Carroll, S. B. (2002). Evolution of a transcriptional repression domain in an insect Hox protein. *Nature* **415**, 910-3.

Gellon, G. and McGinnis, W. (1998). Shaping animal body plans in development and evolution by modulation of Hox expression patterns. *Bioessays* **20**, 116-25.

Gordon, J., Bennett, A. R., Blackburn, C. C. and Manley, N. R. (2001). Gcm2 and Foxn1 mark early parathyroid- and thymus-specific domains in the developing third pharyngeal pouch. *Mech Dev* **103**, 141-3.

Greer, J. M., Puetz, J., Thomas, K. R. and Capecchi, M. R. (2000). Maintenance of functional equivalence during paralogous Hox gene evolution. *Nature* **403**, 661-5.

Gunther, T., Chen, Z. F., Kim, J., Priemel, M., Rueger, J. M., Amling, M., Moseley, J. M., Martin, T. J., Anderson, D. J. and Karsenty, G. (2000). Genetic ablation of parathyroid glands reveals another source of parathyroid hormone. *Nature* **406**, 199-203.

Hetzer-Egger, C., Schorpp, M., Haas-Assenbaum, A., Balling, R., Peters, H. and Boehm, T. (2002). Thymopoiesis requires Pax9 function in thymic epithelial cells. *Eur J Immunol* **32**, 1175-81.

Hirth, F., Loop, T., Egger, B., Miller, D. F., Kaufman, T. C. and Reichert, H. (2001). Functional equivalence of Hox gene products in the specification of the tritocerebrum during embryonic brain development of Drosophila. *Development* **128**, 4781-8.

Hoey, T. and Levine, M. (1988). Divergent homeo box proteins recognize similar DNA sequences in Drosophila. *Nature* **332**, 858-61.

Holland, N. D., Holland, L. Z. and Kozmik, Z. (1995). An amphioxus Pax gene, AmphiPax-1, expressed in embryonic endoderm, but not in mesoderm: implications for the evolution of class I paired box genes. *Mol Mar Biol Biotechnol* **4**, 206-14.

Hsia, C. C. and McGinnis, W. (2003). Evolution of transcription factor function. *Curr Opin Genet Dev* **13**, 199-206.

Kameda, Y., Nishimaki, T., Takeichi, M. and Chisaka, O. (2002). Homeobox gene hoxa3 is essential for the formation of the carotid body in the mouse embryos. *Dev Biol* **247**, 197-209.

Kimmel, C. B., Miller, C. T., Kruze, G., Ullmann, B., BreMiller, R. A., Larison, K. D. and Snyder, H. C. (1998). The shaping of pharyngeal cartilages during early development of the zebrafish. *Dev Biol* **203**, 245-63.

Krumlauf, R. (1994). Hox genes in vertebrate development. *Cell* **78**, 191-201.

Kuratani, S. (2004). Evolution of the vertebrate jaw: comparative embryology and molecular developmental biology reveal the factors behind evolutionary novelty. *J Anat* **205**, 335-47.

Liu, Z., Yu, S. and Manley, N. R. (2007). Gcm2 is required for the differentiation and survival of parathyroid precursor cells in the parathyroid/thymus primordia. *Dev Biol* **305**, 333-46.

Lutz, B., Lu, H. C., Eichele, G., Miller, D. and Kaufman, T. C. (1996). Rescue of Drosophila labial null mutant by the chicken ortholog Hoxb-1 demonstrates that the function of Hox genes is phylogenetically conserved. *Genes Dev* **10**, 176-84.

Lynch, V. J. and Wagner, G. P. (2008). Resurrecting the role of transcription factor change in developmental evolution. *Evolution* **62**, 2131-54.

Manley, N. R. and Capecchi, M. R. (1995). The role of Hoxa-3 in mouse thymus and thyroid development. *Development* **121**, 1989-2003.

Manley, N. R. and Capecchi, M. R. (1997). Hox group 3 paralogous genes act synergistically in the formation of somitic and neural crest-derived structures. *Dev Biol* **192**, 274-88.

Manley, N. R. and Capecchi, M. R. (1998). Hox group 3 paralogs regulate the development and migration of the thymus, thyroid, and parathyroid glands. *Dev Biol* **195**, 1-15.

McGinnis, W. and Krumlauf, R. (1992). Homeobox genes and axial patterning. *Cell* **68**, 283-302.

Nehls, M., Kyewski, B., Messerle, M., Waldschutz, R., Schuddekopf, K., Smith, A. J. and Boehm, T. (1996). Two genetically separable steps in the differentiation of thymic epithelium. *Science* **272**, 886-9.

Nornes, S., Mikkola, I., Krauss, S., Delghandi, M., Perander, M. and Johansen, T. (1996). Zebrafish Pax9 encodes two proteins with distinct C-terminal transactivating domains of different potency negatively regulated by adjacent N-terminal sequences. *J Biol Chem* **271**, 26914-23.

Ogasawara, M., Shigetani, Y., Hirano, S., Satoh, N. and Kuratani, S. (2000). Pax1/Pax9-Related genes in an agnathan vertebrate, Lampetra japonica: expression pattern of LjPax9 implies sequential evolutionary events toward the gnathostome body plan. *Dev Biol* **223**, 399-410.

Ogasawara, M., Wada, H., Peters, H. and Satoh, N. (1999). Developmental expression of Pax1/9 genes in urochordate and hemichordate gills: insight into function and evolution of the pharyngeal epithelium. *Development* **126**, 2539-50.

Pearson, J. C., Lemons, D. and McGinnis, W. (2005). Modulating Hox gene functions during animal body patterning. *Nat Rev Genet* **6**, 893-904.

Rogers, B. T., Peterson, M. D. and Kaufman, T. C. (1997). Evolution of the insect body plan as revealed by the Sex combs reduced expression pattern. *Development* **124**, 149-57.

Ronshaugen, M., McGinnis, N. and McGinnis, W. (2002). Hox protein mutation and macroevolution of the insect body plan. *Nature* **415**, 914-7.

Stern, D. L. (1998). A role of Ultrabithorax in morphological differences between Drosophila species. *Nature* **396**, 463-6.

Su, D., Ellis, S., Napier, A., Lee, K. and Manley, N. R. (2001). Hoxa3 and pax1 regulate epithelial cell death and proliferation during thymus and parathyroid organogenesis. *Dev Biol* **236**, 316-29.

Tvrdik, P. and Capecchi, M. R. (2006). Reversal of Hox1 gene subfunctionalization in the mouse. *Dev Cell* **11**, 239-50.

Wallin, J., Eibel, H., Neubuser, A., Wilting, J., Koseki, H. and Balling, R. (1996). Pax1 is expressed during development of the thymus epithelium and is required for normal T-cell maturation. *Development* **122**, 23-30.

Watari, N., Kameda, Y., Takeichi, M. and Chisaka, O. (2001). Hoxa3 regulates integration of glossopharyngeal nerve precursor cells. *Dev Biol* **240**, 15-31.

Wray, G. A. (2007). The evolutionary significance of cis-regulatory mutations. *Nat Rev Genet* **8**, 206-16.

Zakany, J., Gerard, M., Favier, B., Potter, S. S. and Duboule, D. (1996). Functional equivalence and rescue among group 11 Hox gene products in vertebral patterning. *Dev Biol* **176**, 325-8.

Zhao, Y. and Potter, S. S. (2001). Functional specificity of the Hoxa13 homeobox. *Development* **128**, 3197-207.

Zhao, Y. and Potter, S. S. (2002). Functional comparison of the Hoxa 4, Hoxa 10, and Hoxa 11 homeoboxes. *Dev Biol* **244**, 21-36.

Zou, D., Silvius, D., Davenport, J., Grifone, R., Maire, P. and Xu, P. X. (2006). Patterning of the third pharyngeal pouch into thymus/parathyroid by Six and Eya1. *Dev Biol* **293**, 499-512.

Table 2.1. Rescue of bloated abdomen and truncated soft palate phenotype by *Hoxa3*^{zf} and *Hoxa3*^{mz} alleles.

Genotype	Bloated abdomen (%)	Truncated soft palate (%)
Hoxa3$^{+/+}$	0 (0/20)	0 (0/3)
Hoxa3$^{+/-}$	0 (0/10)	0 (0/3)
Hoxa3$^{+/zf}$	0 (0/22)	0 (0/3)
Hoxa3$^{-/-}$	75 (6/8)	100 (5/5)
Hoxa3$^{zf/zf}$	0 (0/15)	0 (0/3)
Hoxa3$^{zf/-}$	83 (5/6)	100 (3/3)
Hoxa3$^{mz/mz}$	0 (0/6)	0 (0/3)
Hoxa3$^{mz/-}$	0 (0/5)	0 (0/3)

Newborn animals of different genotypes were checked for the bloated abdomen and the soft palate phenotype. Percentages of the phenotypes were indicated (number of animals showing the phenotype per total number of individuals examined)

Talbe 2.2. Neonatal lethality of *Hoxa3*$^{zf/zf}$

Parental genotypes	*Hoxa3*$^{+/zf}$ X *Hoxa3*$^{+/zf}$		
Possible genotypes of progeny	+/+	+/*zf*	*zf*/*zf*
Number of progeny observed at P0	22	47	20/26*
Number of progeny observed at P1	22	47	0

*Most of *Hoxa3*$^{zf/zf}$ animals were found alive (20/26) at newborn, but never survived more than one day after birth

Table 2.3. Summary of embryonic neurofilament analysis

	Hoxa3$^{+/+}$	*Hoxa3*$^{zf/zf}$
Unconnected[a]	0	14% (2)[c]
Unconnected/Fused[b]	0	7% (1)
Fused/fused	0	21% (3)
Fused/normal	20% (3)	43% (6)
Normal/normal	80% (12)	14% (2)
Total number affected	20% (3)	86% (12)
Total number unaffected	80% (12)	14% (2)
Total number analyzed	15	14

[a]The IXth cranial nerve was unconnected to the hindbrain, including both unilateral and bilateral phenotyeps.

[b]IXth nerve on one side and IXth nerve fused to Xth nerve on the other side.

[c]Percentage of total (number observed)

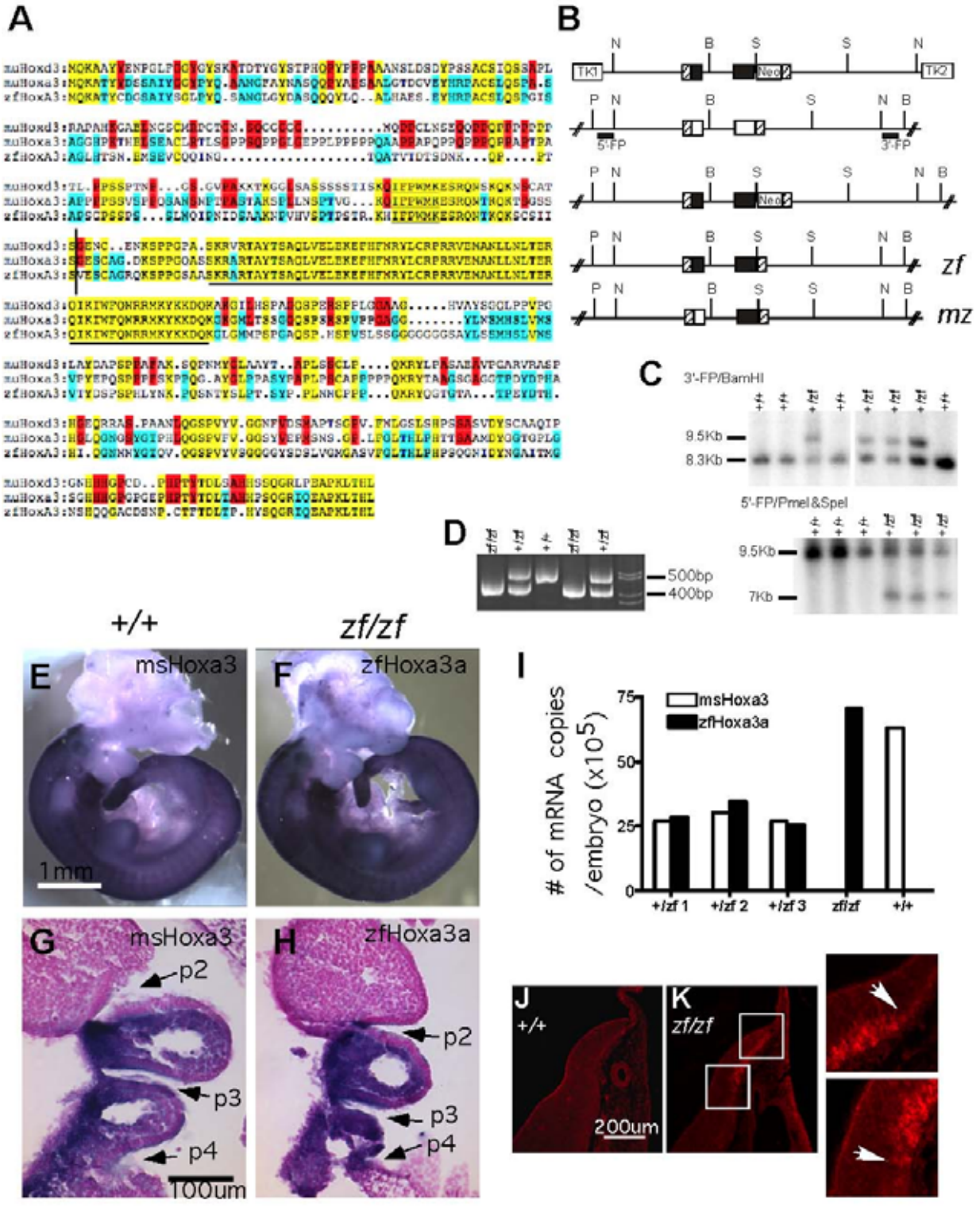
A
B
TK1
Neo
TK2
5'FP
3'FP
zf
mz
C
3'-FP/BamHI
9.5Kb
8.3Kb
5'-FP/PmeI&SpeI
9.5Kb
7Kb
D
500bp
400bp
+/+
zf/zf
E
msHoxa3
1mm
F
zfHoxa3a
G
msHoxa3
p2
p3
p4
100um
H
zfHoxa3a
p2
p3
p4
I
# of mRNA copies /embryo (x10^5)
msHoxa3
zfHoxa3a
+/zf 1
+/zf 2
+/zf 3
zf/zf
+/+
J
+/+
200um
K
zf/zf

Fig. 2.1

Fig. 2.1. Protein sequence alignment, gene targeting strategy and expression of zebrafish Hoxa3a in mouse. (**A**) Amino acid sequence alignment of zebrafish Hoxa3a, mouse Hoxa3 and mouse Hoxd3. Yellow blocks highlight the identical amino acids among the three proteins. Red blocks highlight the identity between mouse Hoxa3 and mouse Hoxd3, which is 52%. Cyan blocks show the 59% identity between mouse Hoxa3 and zebrafish Hoxa3a. The hexapeptide motifs are underlined. The homeodomains are underscored with solid black bar. The vertical line indicates the splice junctions. (**B**) Map of targeting vector (top), wild-type mouse Hoxa3 genomic locus and targeted locus before and after the deletion of neomycin with cre recombinase. *Hoxa3*^{zf} (*zf*) allele comprises of zebrafish Hoxa3a protein coding exons and mouse introns and UTRs. *Hoxa3*^{mz} (*mz*) allele comprises of mouse protein coding exon1 and zebrafish protein coding exon2. Horizontal thin lines represent non-coding genomic DNA at mouse Hoxa3 locus, boxes with heavy diagonal lines represent 5' or 3' UTR of mouse Hoxa3, boxes in black represent coding exons of zebrafish Hoxa3a, open boxes represent coding exons of mouse Hoxa3. Black bars under the horizontal line identify the 5' and 3' franking probes for southern blot. P, PmeI; N, NotI; B, BamHI; S, SpeI. (**C**) Southern blot analysis of the implicated mosue genotypes. Genomic DNA was digested with the PmeI and SpeI and probed with 5'-franking probe, or digested with BamHI and probed with 3'-franking probe. (**D**) Genotyping with PCR. (**E-F**) Whole-mount in situ hybridization analysis on E10.5 +/+ (**E**) and *zf/zf* (**F**) embryos with probes specific to mouse Hoxa3 or zebrafish Hoxa3a. Zebrafish Hoxa3a mRNA is expressed in mouse in the same pattern. Scale bar: 1mm. (**G-H**) The embryos analyzed with whole-mount in situ hybridization were cut into 10μm coronal sections. Cranial is up. Zebrafish

Hoxa3a and mouse Hoxa3 are expressed in the third and fourth pharyngeal pouch endoderm, as well as the arch mesenchyme. Scale bar: 100um. (**I**) Absolute quantitative real-time PCR analysis on total cDNA of E10.5 embryos showing that *Hoxa3*^{zf} allele is expressed at the same level as the wild-type allele. In heterozygous (*+/zf*) embryos, the two Hoxa3 alleles produce similar amount of mRNA. cDNA from wild-type or homozygous littermate embryos were analyzed as controls. In the wild-type embryo, mouse Hoxa3 expression level is roughly two fold of that in *+/zf* embryos, and there is no PCR amplification from zf allele. There is no mouse Hoxa3 PCR amplification in *zf/zf* embryo, but the expression level of zebrafish Hoxa3a is similar to mouse Hoxa3 in +/+ embryo. (**J**-**K**) Immunostaining with anti-HA antibody on cronal sections of E10.5 +/+ (J) and zf/zf (K). Higher magnification views of the boxes in (K) are on the right to show the anterior and posterior expression boundaries.

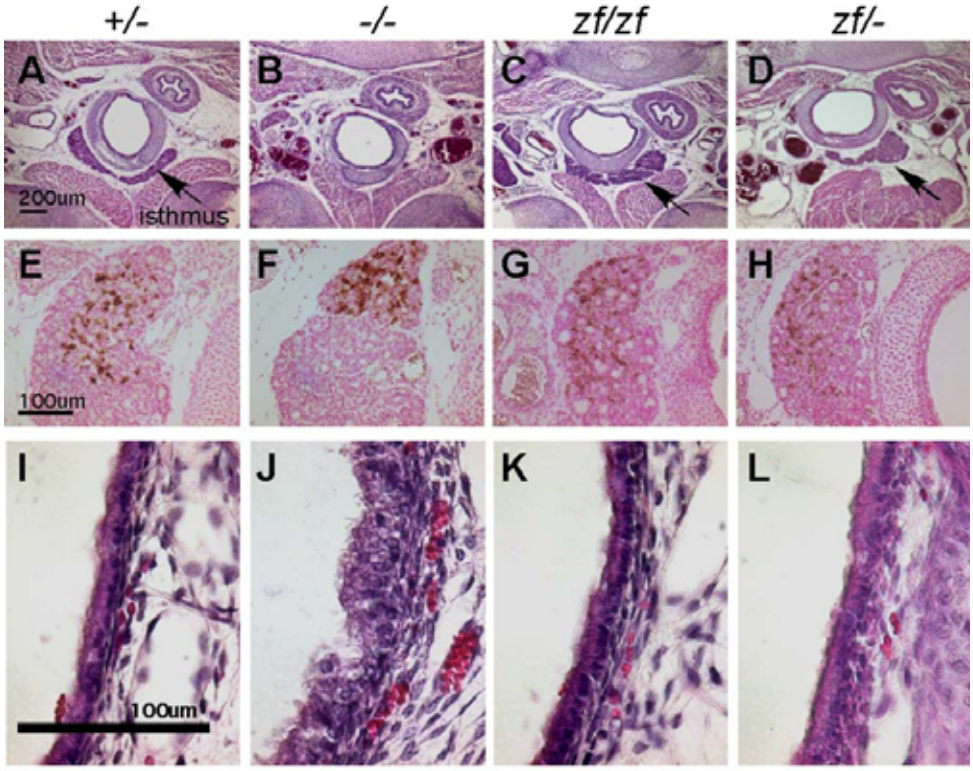

Fig. 2.2

Fig. 2.2. ZfHoxA3a expressed from mouse Hoxa3 locus complement thyroid and trachea defects. (**A-D**) 10 μm transverse paraffin sections of newborn animals were stained with hematoxylin and eosin. Thyroid isthmus structure (arrow) is deleted in *Hoxa3*$^{null/null}$ (-/-) mouse, but restored in *Hoxa3*$^{zf/zf}$ (*zf/zf*) and *Hoxa3*$^{zf/null}$ (*zf/-*). Scale bar: 200 um. es, esophagus; tr, trachea; th, thymus. (**E-H**) Transverse sections of newborn mice were stained with anti-calcitonin antibody. Calcitonin-positive cells are shown in brown. In wild-type thyroid, calcitonin-positive C cells are dispersed throughout the lobe. But in Hoxa3 null mutant, C cells usually stay dorsal to the thyroid follicular cells. In *Hoxa3*$^{zf/zf}$ (*zf/zf*) and *hoxa3*$^{zf/null}$ (*zf/-*) animals, calcitonin-positive cells are embedded within the thyroid lobe, showing a normal distribution. Scale bar: 100 μm. (**I-L**) Transverse sections were stained with hematoxylin and eosin. In the heterozygous control, tracheal epithelial cells are columnar cells resting on the basement. The epithelial layer is disorganized in Hoxa3 null (-/-) mutant, with the cells losing the polarity and forming multiple cell layers. *Hoxa3*$^{zf/zf}$ (*zf/zf*) and *Hoxa3*$^{zf/null}$ (*zf/-*) have normal trachea epithelium lining. Scale bar: 100μm.

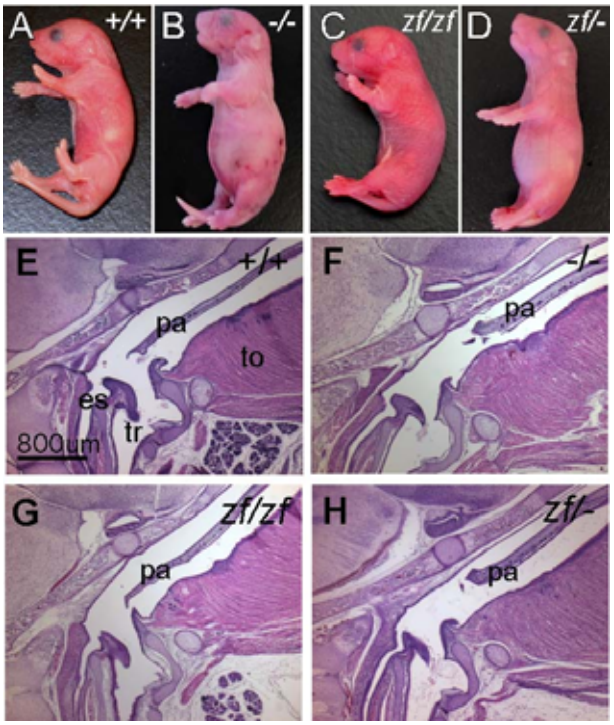

Fig. 2.3

Fig. 2.3. Bloated abdomen and soft palate defect is rescued.

(**A-D**) New born animals of implicated genotypes. *Hoxa3*$^{null/null}$ (-/-) animals are characterized by a bloated abdomen, which is never seen in *Hoxa3*$^{zf/zf}$ mice. However, with only one copy of *Hoxa3*^{zf} allele, the *Hoxa3*$^{zf/null}$ (*zf*/-) mutant mimics *Hoxa3*$^{null/null}$ in the bloated abdomen phenotype. (**E-H**) Sagital paraffin sections of new born animals were stained with hematoxylin and eosin. The posterior palate (velum) is shortened in *Hoxa3*$^{null/null}$ (-/-) and *Hoxa3*$^{zf/null}$ (*zf*/-) animals. Truncated soft palate was correlated with the bloated abdomen phenotype. tr: trachea; es, esophagus; pa, soft palate; to, tongue. Anterior is up, dorsal is to the left. Scale bar: 800μm.

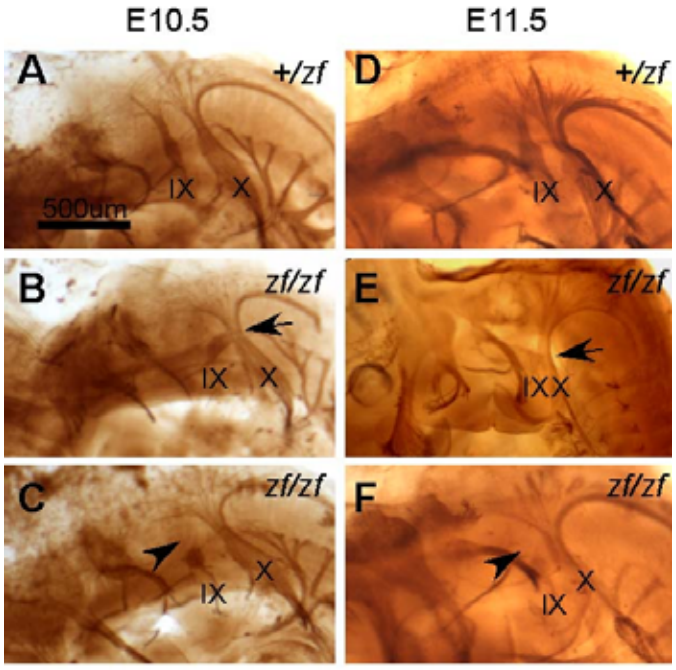
E10.5
E11.5
A
+/zf
500um
IX
X
D
+/zf
IX
X
B
zf/zf
IX
X
E
zf/zf
IXX
C
zf/zf
IX
X
F
zf/zf
IX
X

Fig. 2.4

Fig. 2.4. Cranial nerve defect in Hoxa3 zf/zf embryos.

Lateral vies of cleared E10.5 (**A-C**) and E11.5 (**D-F**) embryos stained in whole-mount with the 2H3 anti-neurofilament antibody. Dorsal is up, anterior is to the left. (A, D) in control embryo, the IX cranial nerve is connected to hindbrain. In Hoxa3zf/zf embryos, the IX cranial nerve is either fused (arrow) to the X cranial ganglia (B, E) or partially deleted (arrow head), not connected to the hind brain (C, F). Scale bar: 500um.

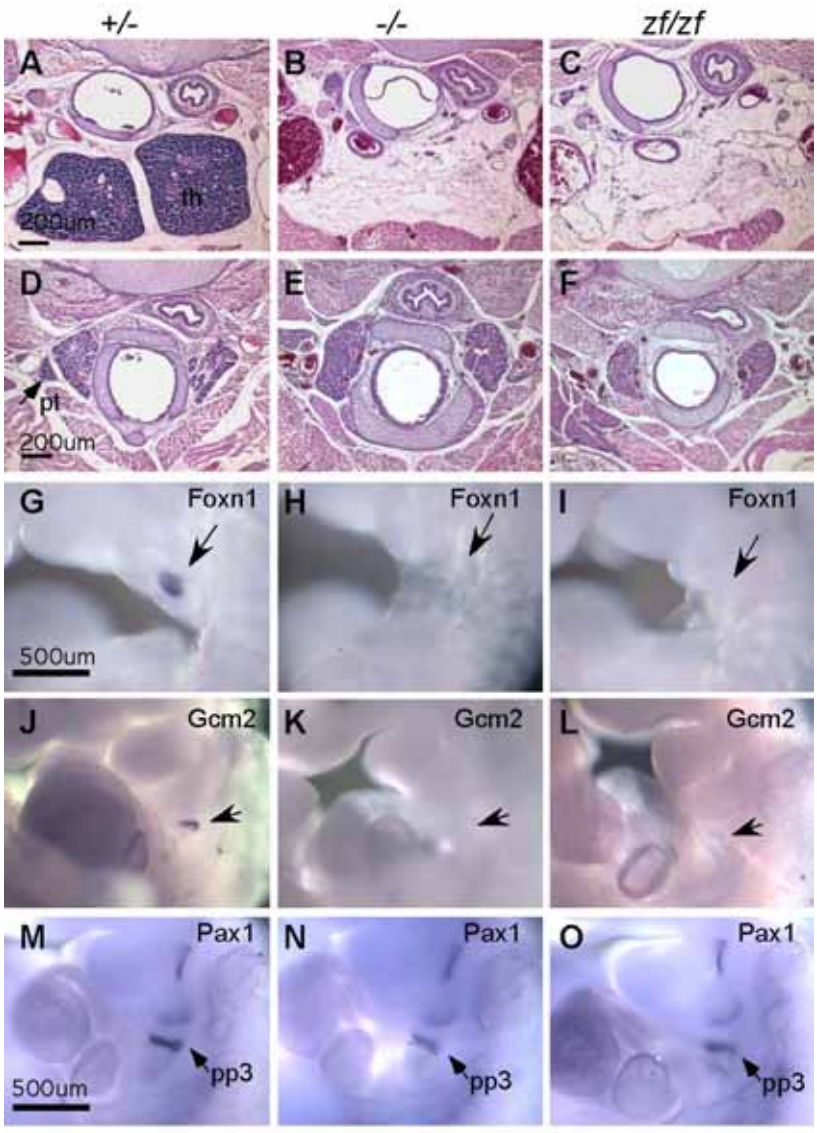
+/-
-/-
zf/zf
A
B
C
th
200um
D
E
F
pt
200um
G
Foxn1
H
Foxn1
I
Foxn1
500um
J
Gcm2
K
Gcm2
L
Gcm2
M
Pax1
N
Pax1
O
Pax1
pp3
pp3
pp3
500um

Fig. 2.5

Fig. 2.5. Thymus and parathyroid defects are not rescued by zebrafish HoxA3a.

(**A-F**) Transverse paraffin sections of newborn animals were stained with hematoxylin and eosin. Thymus and parathyroid are absent in *Hoxa3*$^{null/null}$ (-/-) and *Hoxa3*$^{zf/zf}$ (*zf/zf*) mice. th, thymus; pt, parathyroid. Dorsal is up. Scale bar: 200um. (**G-I**) Whole-mount in situ hybridization to analyze Foxn1 expression in E11.5 embryos. Foxn1 is expressed in the 3rd pharyngeal pouch in the wild-type embryos. But Foxn1 expression in the pouch is absent in *Hoxa3*$^{null/null}$ (-/-) and *Hoxa3*$^{zf/zf}$ (*zf/zf*) embryos. Crainial is up. (**J-L**) Gcm2 expression at E10.5 is detected at eh 3rd pouch in control embryo, but is missing in Hoxa3null/null and Hoxa3zf/zf embryos. (**M-O**) At E10.5, Pax1 expression at the 3rd pouch is reduced in *Hoxa3*$^{null/null}$ (-/-) embryo, but the expression at the other pouches remains unchanged. *Hoxa3*$^{zf/zf}$ (*zf/zf*) shows the same Pax1 expression pattern as *Hoxa3*$^{null/null}$ (-/-). pp, pharyngeal pouch; pa, pharyngeal arch. Scale bar: 500um, applies to (G)-(O).

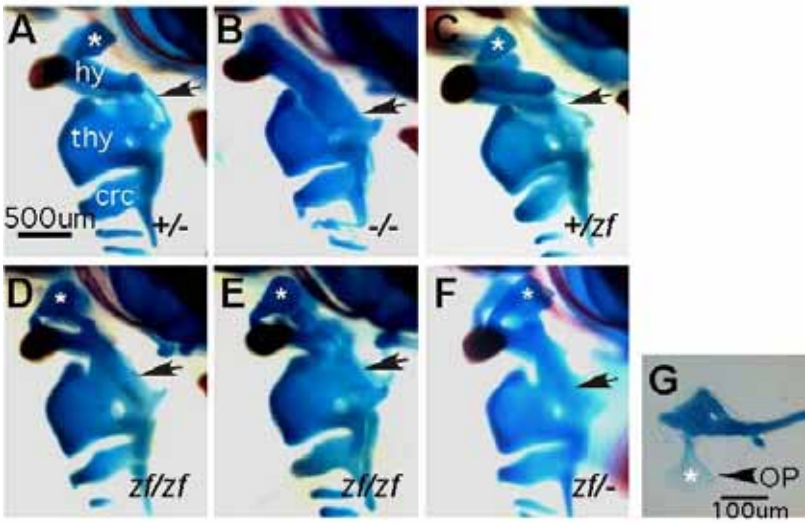

Fig. 2.6

Fig. 2.6. Novel hyoid bone morphology in *Hoxa3*$^{zf/zf}$ (*zf/zf*) and *Hoxa3*$^{zf/null}$ (*zf*/-) mice. (**A-F**) Lateral views of the throat cartilages in cleared newborn skeletal preparations. Anterior is up, dorsal is to the right. Scale bar: 1mm. (**A**) *Hoxa3*$^{+/null}$ (+/-) control. *, lesser horn of hyoid bone; hy, greater horn of hyoid bone; thy, thyroid cartilage; crc, cricoid cartilage. (**B**) *Hoxa3*$^{+/zf}$ (*+/zf*) mice have normal throat cartilages. (**C**) In *Hoxa3*$^{null/null}$ (-/-) animal, lesser horn of hyoid bone is greatly reduced or deleted, and the greater horn is malformed and fused to thyroid cartilage. The arrow shows the fusion between greater horn and thyroid cartilage. (**D-E**) In *Hoxa3*$^{zf/zf}$ (*zf/zf*) mouse, the greater horn is malformed and fused to thyroid cartilage, but the lesser horn is restored. The restored lesser horn is in an abnormal morphology, different from either control or *Hoxa3*$^{null/null}$ (-/-) mutant. (**F**) *Hoxa3*$^{zf/null}$ (*zf*/-) shows a similar throat cartilage phenotype as *Hoxa3*$^{zf/zf}$ (*zf/zf*). (**G**) Opercular bone (OP) and cartilage of 6dpf zebrafish embryo. The OP (*) is in a similar shape as the lesser horn in *Hoxa3*$^{zf/zf}$ (*zf/zf*) mouse.

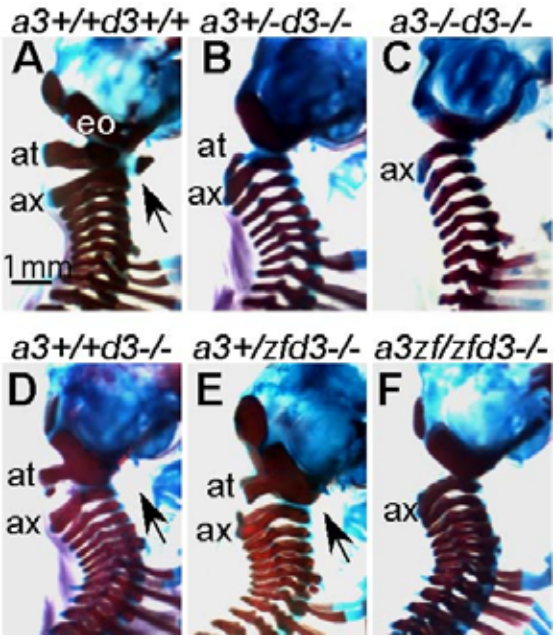
a3+/+d3+/+
a3+/-d3-/-
a3-/-d3-/-
A
B
C
eo
at
ax
1mm
at
ax
ax
a3+/+d3-/-
a3+/zfd3-/-
a3zf/zfd3-/-
D
E
F
at
ax
at
ax
ax

Fig. 2.7

Fig. 2.7. Cervical vertebrae phenotype of compound Hoxa3 and Hoxd3 mutants.

Lateral views of the cervical region in cleared skeleton preparations of the implicated genotypes at newborn. Anterior is up, dorsal is to the left. Scale bar: 1mm. (**A)** Wild-type control, exoccipital (eo) bone, atlas (at), axis (ax) and anterior arch of atlas (arrow) are indicated. (**B**) Hoxd3 homozygous mutant. The anterior arch of atlas is deleted. The ventral part of atlas is fused to the basioccipital bone at the base of the skull. (**C**) When there is only one copy of Hoxa3, *Hoxd3*$^{-/-}$ mutant phenotype is exacerbated. The atlas is almost completely deleted, with only a small piece remained. (**D**) *Hoxa3*$^{+/zf}$*;Hoxd3*$^{-/-}$ shows a phenotype similar to *Hoxa3*$^{+/+}$*;Hoxd3*$^{-/-}$, with the anterior arch of atlas deleted and the ventral part of atlas fused to the basioccipital bone. (**E**) In *Hoxa3*$^{-/-}$*;Hoxd3*$^{-/-}$ double mutant, the cervical vertebrae phenotype is further affected, with the atlas entirely deleted. (**F**) *Hoxa3*$^{zf/zf}$*;Hoxd3*$^{-/-}$ mimics *Hoxa3*$^{-/-}$*;Hoxd3*$^{-/-}$ in the cervical vertebrae defect.

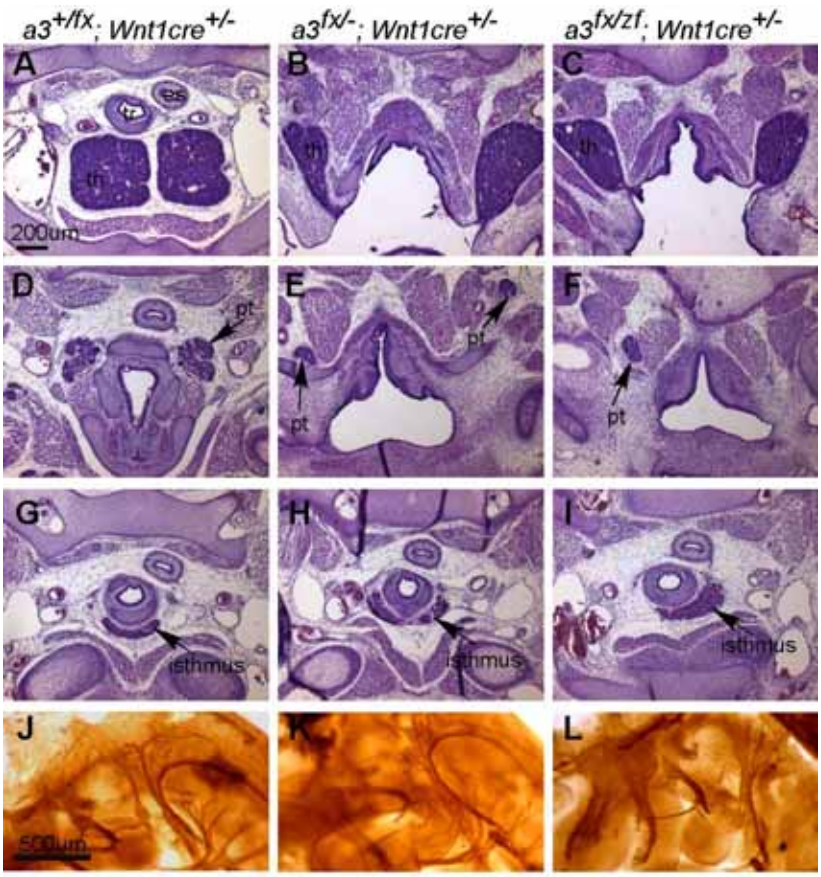
a3+/fx; Wnt1cre+/-
a3fx/-; Wnt1cre+/-
a3fx/zf; Wnt1cre+/-
A
B
C
D
E
F
G
H
I
J
K
L
es
tr
th
200um
pt
isthmus
500um

Fig. 2.8

Fig. 2.8. *Hoxa3*^{zf} allele plays null function in neural crest cells. (**A-I**) Transverse paraffin section of E15.5 embryos. Dorsal is up, scale bar: 200 μm. (**A**) In the control embryo, the two thymus lobes are located in the chest. (**B**) In *Hoxa3*$^{fx/-}$*;Wnt1cre*$^{+/-}$ embryo the thymus lobes are still attached to the pharynx, and located more anterior than the normal position. (**C**) *Hoxa3*$^{fx/zf}$*;Wnt1cre*$^{+/-}$ embryo has ectopic thymus as (B). (**D-F**) In the control embryo, parathyroid (pt) is embedded in the thyroid organ, but in *Hoxa3*$^{fx/-}$*;Wnt1cre*$^{+/-}$ (E) and *Hoxa3*$^{fx/zf}$*;Wnt1cre*$^{+/-}$ (F), parathyroid is positioned more anteriorly due to the failure of migration. (**G-I**) Thyroid isthmus is formed and normally positioned in the embryos of all three genotypes. (**J-L**) Whole mount neurofilament staining with E10.5 and E11.5 embryos. The IX cranial nerve in *Hoxa3*$^{fx/-}$*;Wnt1cre*$^{+/-}$ (K) and *Hoxa3*$^{fx/zf}$*;Wnt1cre*$^{+/-}$ (L) is not connected to the hindbrain. Scale bar: 500 μm.

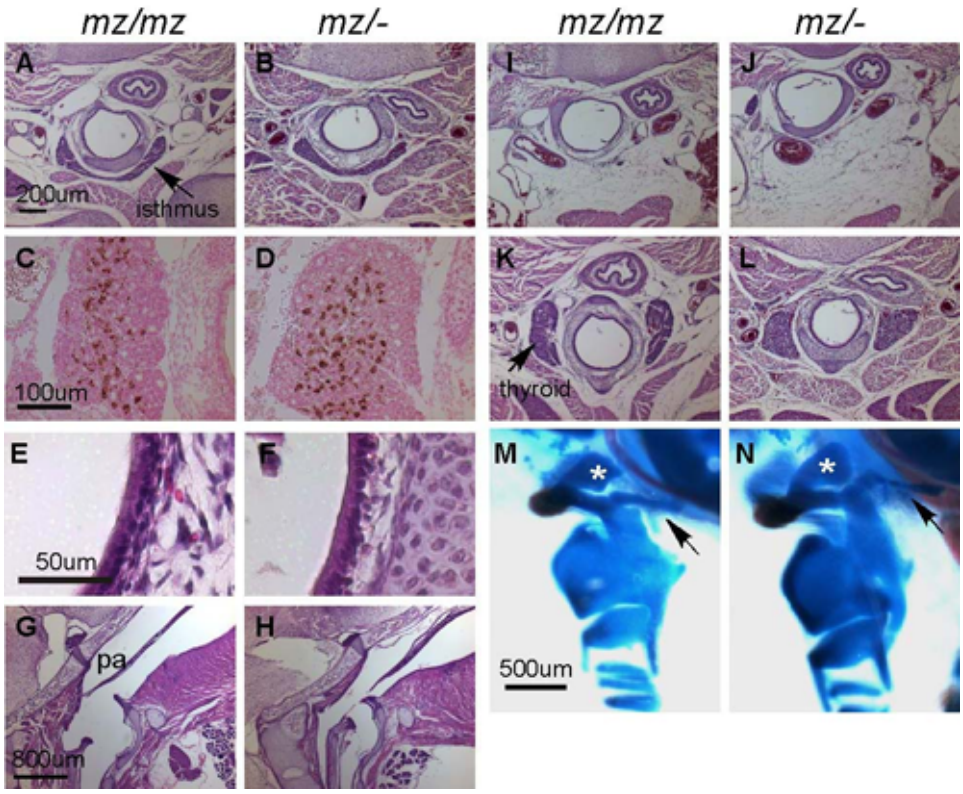
mz/mz
mz/-
mz/mz
mz/-
A
B
I
J
200um
isthmus
C
D
K
L
100um
thyroid
E
F
M
N
50um
*
*
G
H
pa
500um
800um

Fig. 2.9

Fig. 2.9. Chimera protein expressed from *Hoxa3*^{mz} allele functions virtually equivalently to zebrafish HoxA3a protein. (**A-B**) H&E staining of transverse paraffin sections of newborn animals showing that thyroid isthmus is normal in both *Hoxa3*$^{mz/mz}$ (*mz/mz*) and *Hoxa3*$^{mz/null}$ (*mz/-*). Scale bar: 200 μm, applies to (A-B, I-L). (**C-D**) Transverse sections of newborn mice were stained with anti-calcitonin antibody. Calcitonin-positive cells are shown in brown. In both *mz/mz* and *mz/-* newborn mice, calcitonin-positive cells are embedded within the thyroid lobe normally. Scale bar: 100 μm. (**E-F**) H&E staining of transverse paraffin sections showing the organized lining of trachea epithelial cells in both *mz/mz* and *mz/-* newborn animals. (**G-H**) H&E staining of sagital paraffin sections of newborn mice. The soft palate is in a normal length in both *mz/mz* and *mz/-*. Scale bar: 800 μm. (**I-L**) Transverse sections of newborn animals were stained with H&E showing the absence of thymus (I-J) and parathyroid (K-L). (**M-N**) Lateral views of the throat cartilages in newborn skeletal preparations. Anterior is up, dorsal is to the right. *, lesser horn of hyoid bone; arrows point to an extra cartilage structure connecting throat cartilage with the skull, which is not seen in +/+, -/- or *zf/zf* (Fig 2.6). Scale bar: 1mm.

SUPPLEMENTARY METHODS AND MATERIALS

Generation of mice and genotyping

The following primers were used to clone zebrafish *Hoxa3a* protein coding exon1, exon2 and mouse *Hoxa3* intron with PCR:

zfExon1f: 5'-ATGCAAAAGGCAACCTACTGCG-3'

zfExon1r: 5'-cagCTGAAATGATACTACAGG-3'

zfExon2f: 5'-tacgTAGAGAGCTGCGCTGGAGAC-3'

zfExon2r: 5'-ctaagcgtaatctggaacatcgtatgggtaTAAATGCGTCAGTTTGGGTG-3'

msIntronf: 5'-GTAAATGAATGCCTTTAGGAGG-3'

msIntronr: 5'-TGCCAGGACACAGAGAGGAAG-3'

Letters in upper case indicate the sequence of either exon or intron, lower case indicate introduced sequence of either enzyme sites or HA tag.

zfExon1 and zfExon2 were subcloned into T-easy vector (Promega) respectively, and then the Exon2 was excised from the vector and inserted into Exon1-Teasy vector to generate Exon1&2-T easy plasmid. msIntron was then amplified from BL6 mouse genomic DNA using pfu DNA polymerase and subcloned into Exon1&2-Teasy, which was linearized with PvuII and SnaBI, to generate zfExon1 + msIntron + zfExon2 in one plasmid, keeping exon-intron junctions unchanged. A loxP-flanked neomycin^r (Neo^r) gene and an FRT-flanked kanamycin^r (Kan^r) gene were inserted to the 3' of the stop codon. Then the following primers were used to add 50 base pairs of homologous arms (for BAC recombination) flanking the zfexon1-msintron-zfexon2-Neo^r-Kan^r fragment with PCR:

Forward:5’-ccttacgggtgtcaagcccttgtcagagagtgtgatcacgatcgtgaaacatcgcgATGCAAAAGGCAACCTACTG-3’

Reverse:5’-ctaaccaaagaaggtcgggtgggcaactctcctggctcacagccctgggcccatcaGAAGTTCCTATTCTCTAGAAAG-3’

Lower case indicates the sequence of mouse *Hoxa3* 5’-UTR or 3’-UTR, and upper case indicates sequence of zebrafish *Hoxa3a* exon or FRT site.

BAC DNA (RP23-253E11, Cam^+, GenBank) was transformed into EL250 E.coli line which expresses a inducable FLP gene. Then the 5.5 Kb PCR product was transformed into EL250 containing the BAC. $Cam^+/Kan^+/Amp^-$ clones were selected and checked for the occurrence of recombination, which resulted in the replacement of mouse *Hoxa3* protein coding exons with zebrafish *Hoxa3a* protein coding exons, and the introduction of Neo and Kan genes into the BAC. The FRT-flanked Kan^r cassette was then flipped out by adding 0.1 g/ml L-arabinose into the culture, which induced the expression of FLP.

We then extracted the modified BAC DNA and digested it with NotI. The two NotI sites flanking a 12 Kb mouse *Hoxa3* genomic DNA enabled us to subclone the modified Hoxa3 genomic DNA into a plasmid vector containing two TK genes to generate the final targeting vector.

The targeting vector was linearized with XhoI and electroporated into BL6 ES cell line and subjected to positive-negative selection. Southern blot with flanking probes was used to screen the targeted ES cell clones and targeted mice. The targeted ES cells were then injected into

blastocysts to generate chimeras and then targeted mice. The Neo^r selection marker gene was deleted by crossing to a ubiquitous cre-expressing mouse colony.

The following primers were used for genotyping of this Hoxa3-zfki mouse colony with PCR (~500bps wild-type band and ~400 bps targeted band):

msE2in: 5'-CTATGTGGAGCCCATGAGCAA-3'

HA: 5'-CCATACGATGTTCCTGATTACG-3'

3'UTR: 5'-AGGAAAAGGATGCAGGGCCAG-3'

Southern Blot analysis

Two micro-grams of genomic DNA extracted from the ES cell clones were digested with restriction endonucleases PmeI&SpeI or BamHI in 25-µl reactions and separated on 0.7% agarose gels in 1x TBE overnight at 60V. The gels were then denatured in 0.5M NaOH, 1.5M NaCl for 30 minutes followed by neutralized in 0.5M Tris PH7.5, 1.5M NaCl for 30 minutes. The DNA was then blotted onto Hybond N+ membranes (Amersham) by upward capillary transfer in 10x SSPE for overnight. The nylon membranes were then UV-crosslinked and baked at 80º C for 2 hours. The membranes can then be stored at 4º C until use. The membrane was prehybridized in 4xSSPE, 0.1% Sodium Pyrophosphate, 0.1% SDS, 0.2% BSA, 0.2% ficoll 400, 0.2% polyvinylpyrrolidone and 100ng/ml Salmon Sperm DNA at 55º C for 1h, and hybridized with radioactive DNA probes in a fresh solution at 55º C overnight. The probes were labeled with [α-32P]dCTP using the Klenow enzyme (New England BioLab). The hybridized membranes were washed twice in 2x SSC, 0.1% SDS at RT for 15 min; once in 0.2x SSC, 0.1%

SDS at 60º C for 10-15 min. An X-ray film was placed over the membrane in a developing cassette for overnight at -80º C to detect the signal.

Immunofluorecence (anti-HA staining)

Paraffin sections of E10.5 mouse embryos were de-waxed and rehydrated with gradient ethanol/PBS. Antigen retrieval was performed by incubating in 10mM citrate buffer in a boiling water bath for 20 minutes. The sections were then cooled down and rinsed with water before treated with 3% H_2O_2 in PBST (0.3% tritonX-100 in PBS). The sections were blocked in TNB [0.5% bloking reagent (PerkinElmer, Inc) in TNT (0.1 M Tris-HCl, PH7.5, 0.15 M NaCl)] and then incubated with anti-HA (Roche) 1:50 diluted in TNB overnight at 4℃. After wash in TNT, the sections were incubated with 1:100 anti Rat IgG-Biotin (Jackson Laboratory, Inc) in TNB for 1 hour at room temperature followed by wash and incubation with SA-HRP (PerkinElmer, Inc) for 30 minutes. Biotinyl Tyramide (TSA Biotin system Kit from PerkinElmer) was applied followed by incubation in 1:100 SAV-Texas Red (Jaskson laboratory, Inc) for 30 minutes. The sections were then stained with DAPI and mounted with aqueous mounting medium. Imaging was done on a Zeiss Axioplan 2 microsope with the AxioCam HRm camera.

RT-PCR and sequencing

E10.5 mouse embryos were homogenized in trizol (Invitrogen) and total RNA was extracted according to the manual coming with trizol reagent. The total RNA was then incubated with DNaseI (Roche) at 37℃ for 20 minutes to remove any DNA from the RNA samples. First-strand cDNA was reverse transcribed with superscript III (Invitrogen) and random primers (Invitrogen), incubated at 42℃ for 90 minutes and then at 70℃ for 15 minutes. RNaseH and RNaseA

(Promega) were used to remove RNA from the transcribed first-strand cDNA. PCR was then carried out with the cDNA and multiple pairs of primers and the PCR products were subcloned into T-easy vector (Promega) for sequencing purpose.

Absolute quantification qRT-PCR

Absolute quantitative PCR was performed on an ABI 7500 real time PCR system with SYBR green PCR master mix (Applied Biosystems) and the following primers designed with Primer Express3.0 software:

Mouse Hoxa3 Pair#1: Forward 5'-CAGCCAATGGGTTCGCTTA-3'

Reverse 5'-GCGGACGGCGCGTAT-3'

Mouse Hoxa3 Pair#3: Forward 5'-CCCGGTGCAGGAGGCTAT-3'

Reverse 5'-GGCTCATATGGGACACTGTTGA-3'

Zebrafish Hoxa3a Pair#3: Forward 5'-GATTCCGCCGCCAAGAA-3'

Reverse 5'-AAATGTGTTTCCTTGTGGATGGT-3'

Zebrafish Hoxa3a Pair#7: Forward 5'-GCCAAGAATCCAGTCCACGTA-3'

Reverse 5'-TCATCCAAGGGAAAATGTGTTTC-3'

Two plasmids containing full length cDNA of either mouse Hoxa3 gene or zebrafish Hoxa3a gene were used to generate standard curves for absolute quantification. The PCR condition is as the following: 50℃, 2min; 95℃, 10min; 40 cycles of 95℃ for 15sec and 60℃ for 1min, followed by dissociation steps. Absolute copy number was determined using 7500 SDS software (Applied Biosystems).

CHAPTER 3

FOXN1 IS REQUIRED TO MAINTAIN THE POSTNATAL THYMIC MICROENVIRONMENT IN A DOSAGE-SENSITIVE MANNER

[1]Lizhen Chen, Shiyun Xiao, and Nancy R. Manley 2008. *Blood.* In press

Reprinted here with permission of publisher.

ABSTRACT

The postnatal thymus is the primary source of T cells in vertebrates, and many if not all stages of thymocyte development require interactions with thymic epithelial cells (TECs). The *Foxn1* gene is a key regulator of TEC differentiation, and is required for multiple aspects of fetal TEC differentiation. *Foxn1* is also expressed in the postnatal thymus, but its function after birth is unknown. We generated a *Foxn1* allele with normal fetal expression and thymus development, but decreased expression in the postnatal thymus. This down-regulation causes rapid thymic compartment degeneration and reduced T cell production. TEC subsets that express higher *Foxn1* levels are most sensitive to its down-regulation, in particular $MHCII^{hi}UEA\text{-}1^{hi}$ medullary TECs. The requirement for Foxn1 is extremely dosage-sensitive, with small changes in *Foxn1* levels having large effects on thymus phenotypes. Our results provide the first evidence that *Foxn1* is required to maintain the postnatal thymus. Furthermore, the similarities of this phenotype to accelerated aging-related thymic involution support the possibility that changes in Foxn1 expression in TECs during aging contribute to the mechanism of involution.

INTRODUCTION

The postnatal thymus consists of a complex cellular and extracellular environment through which developing thymocytes migrate in a stereotypical manner during their differentiation to self-restricted, self-tolerant T cells (Anderson et al., 2006; Petrie, 2002). The principal thymic stromal cell types are thymic epithelial cells (TECs), which are broadly divided into cortical and medullary classes, and have specific functions to promote all stages of thymocyte development (Laufer et al., 1999; Prockop and Petrie, 2000). The normal postnatal thymus displays dramatic shifts in size and phenotype over the life of the animal due to the influence of external and internal changes. In the early postnatal stage the thymus undergoes rapid logarithmic expansion in size and T cell production, and the stroma becomes organized and expanded. At about 1-2 weeks (in mice), the thymus enters a period of relative homeostasis and high thymic output that continues until early adulthood. This period result in the generation of a normal complement of peripheral T cells with a diverse repertoire. After this point, the thymus gradually undergoes a process known as age-associated involution. The fully involuted thymus has significantly reduced thymopoiesis. The thymic architecture is changed, as TEC numbers decrease and the cortical and medullary compartments break down (Taub and Longo, 2005). Besides a dramatic decrease in the production of naïve T cells, the percentage of the most immature (DN1) thymocyte subpopulation is increased in aged mice (Phillips et al., 2004; Thoman, 1995), although the number of early thymic progenitors (ETPs) is decreased (Min et al., 2004; Zhu et al., 2007).

Both the initial development and the maintenance of thymic compartment organization and T cell production require ongoing productive interactions between thymocytes and thymic stromal cells (Gray et al., 2005). Failure to maintain the postnatal thymus results in dramatically

reduced T cell production, and thus thymic involution is a critical component of aging related immunodeficiency (Zediak and Bhandoola, 2005). Thus, while the identification of the cellular target(s) responsible for involution is central for understanding the mechanisms that maintain the postnatal thymus, this goal is complicated by the interdependence of the different cell populations in the thymus. Indeed, recent evidence has implicated both TEC and HSC-intrinsic defects in involution (Gui et al., 2007; Min et al., 2004; Montecino-Rodriquez et al., 2005; Zediak et al., 2007). Thus, the identity of the cell type(s) responsible for maintaining the steady-state postnatal thymus, and the mechanism(s) by which initiation and progression of involution occurs remains controversial (Aspinall and Andrew, 2001; Geiger and Van Zant, 2002; Morrison et al., 1996; Sudo et al., 2000; Yu et al., 1997; Zhu et al., 2007).

The best-known regulator of fetal thymus development is the forkhead transcription factor Foxn1 (Nehls et al., 1994). *Foxn1* is expressed in all TECs during initial thymus organogenesis and broadly during fetal stages (Gordon et al., 2001; Itoi et al., 2007; Nehls et al., 1996). In the fetal thymus, Foxn1 is required cell-autonomously for initial TEC differentiation (Blackburn et al., 1996), is sufficient to induce both cortical and medullary differentiation (Bleul et al., 2006), and has been implicated in mediating crosstalk-dependent differentiation of TECs (Su et al., 2003). Foxn1 is also expressed broadly in postnatal TECs (Nehls et al., 1996), although one report has suggested that the presence of Foxn1 protein may be differentially regulated in TECs postnatally (Itoi et al., 2007; Nehls et al., 1996). Although the *Foxn1* gene has been studied for over a decade, previous functional studies have been restricted to fetal differentiation stages, and its postnatal function in the steady-state thymus remains to be investigated.

We have generated a novel *Foxn1* allele, $Foxn1^{lacZ}$, which we have previously reported has normal Foxn1 expression and function through the newborn stage (Gordon et al.). We now

show that this allele has a reduction in *Foxn1* expression beginning at about 1 week postnatally. Using this novel allele of *Foxn1*, we showed that down-regulation of *Foxn1* below 50% of normal mRNA expression levels caused thymic compartment degeneration, loss of specific TEC subsets, and reduced T cell production, in a highly dosage-dependent manner. Our results provide the first functional evidence that Foxn1 is required to maintain the postnatal thymus. We also showed that those TEC subsets that normally express higher *Foxn1* levels were most sensitive to its down-regulation, resulting in specific changes to the postnatal thymic microenvironment. These phenotypes are strikingly similar to aging-associated involution, but on a dramatically accelerated time frame, providing evidence that a TEC-intrinsic mechanism can recapitulate all aspects of involution.

MATERIALS AND METHODS

Mice

Foxn1$^{lacZ/lacZ}$ and *Foxn1*$^{cre/cre}$ mice were generated as described previously (Gordon et al., 2007). These strains have been backcrossed onto the C57Bl6/J strain for 3-7 generations, and are on a mixed 129Sv/C57Bl6/J background that is majority C57Bl6/J. *Foxn1*$^{+/nude}$ mice on a C57Bl6/J background were purchased from the Jackson Lab. All analysis was performed on littermate animals generated from *+/lacZ* x *lacZ/nu* crosses whenever possible to control for genetic background variation. All the mice were maintained in SPF facility at University of Georgia; experiments were approved by the UGA IACUC.

Histology and Immunofluorescence

For H&E staining, adult or newborn thymi were fixed with 4%PFA overnight, dehydrated in gradient ethanol solutions, and embedded in paraffin. 10 micrometer (μm) sections were cut and

stained with hematoxylin and eosin. Imaging was done on Leica MZ125 dissection scope with Q imaging digital camera or on a Zeiss Axioplan microscope with an Optronics digital camera.

X-gal staining was performed with frozen thymus sections using a standard protocol. Immunofluorescence was performed on cryosections using the following antibodies: Rabbit anti-mouse K5, Rabbit anti-mouse K14 (Covance), Rat anti-mouse K8 (Troma-1) or with UEA-1-biotin (Vector), Donkey anti-rat IgG-FITC, Donkey anti-rabbit IgG-Texas Red secondary antibodies, Streptavidin-FITC (Jackson Immunoresearch), goat anti-mouse Foxn1 (WHN G-20, Santa Cruz), and Rat anti-mouse MHCII (BD Pharmigen). Imaging was done on a Zeiss Axioplan 2 microsope with a AxioCam HRm digital camera. Detailed protocols for X-gal staining and immunofluoresence can be found in Supplementary Data.

Flow cytometry

1×10^6 freshly isolated suspension thymocytes were used for each sample. Cells were blocked by anti-CD16/32 antibody plus Rat serum before staining. For tracing the kinetic phenotypic profile and counting cell numbers of thymocyte subsets, anti-CD4-APC, anti-CD8-FITC, anti-CD44-PE and anti-CD25-Biotin followed by streptavidin-PerCP were used. For analyzing the profile of T cells in total DN subpopulations, PE conjugated lineage markers (anti-CD3, CD4, CD8, CD11b, CD19, B220, Gr-1, TER-119, NK1.1) combined with anti-CD25 and anti-CD44 antibodies were used. All antibodies were from either BD pharmigen or Biolegend if not indicated.

Thymic stromal cells (TSC) were isolated by digesting thymic lobes with collagenase IV+ I (1mg/ml + 0.25mg/ml) and DNase I (10μg/ml) for 30-60 minutes, and depleting most thymocytes with gradient density centrifugation in 13% Opti-Prep (Greiner Bio-One Longwood, FL) solution at 2000rpm× 20min. Enriched TSCs were incubated with anti-EpCam followed by

anti-rat IgG-Biotin (Jackson Immunoresearch) and Streptavidin-APC and then stained with CD45-PE and Ly51-FITC. Cells were also stained directly with anti-CD45-APC, MHCII-PE and UEA-1-Biotin (Vector, CA) followed by streptavidin-PerCP for FACS analysis.

For PI staining, the enriched TSCs were stained by antiCD45-FITC and then fixed with cold 70% ethanol for 30 minutes. Cells were stained in 50ug/ml PI + 20μg/ml RNAse in PBS (Sigma and Invitrogen) for at least 30 minutes before analysis by flow cytometry. Flow cytometry used FL2-W versus FL2-A for doublet discrimination. All cells were acquired with dual-laser FACS Calibur system and analyzed with CellQuest (BD Biosciences) or Flowjo (Tree Star, Inc) software.

BrdU analysis of TEC subsets.

Mice were injected with 1 mg of 5-bromo-2'-deoxyuridine (BrdU, Sigma) once intraperitoneally and then fed with BrdU-containing water (0.8mg/ml) for 3 days. Thymic lobes were digested, and TSCs were enriched as above. The enriched TSCs were stained with anti-CD45-APC, anti-MHC II-FITC and UEA-1-Biotin (Vector) followed by Streptavidin PerCP mAbs for surface staining and then were fixed and permeablized in PBS containing 1% PFA + 0.01 Tween 20 for24-48 hours at 4°C. The cells were then submitted to the BrdU, DNase detection technique using anti-BrdU-FITC mAb.

RNA preparation and real-time quantitative RT-PCR

TSCs were isolated and enriched as described above, then incubated with anti-mouse CD45-PE followed by incubation with magnetic beads-anti Rat IgG (Dynal biotech, Norway). TSCs were purified by magnetically depleting $CD45^+$ cells. For the purification of different subsets of TSC, the enriched TSCs were stained with anti-CD45-APC and anti-MHCII-PE, or with UEA-1-biotin followed by Streptavidin-APC and anti-CD45-PE. Cells were then sorted on

a MoFlo (Dako, Ft.Collins, CO). Total RNA of TSCs or the sorted cells was extracted using a QIAGEN microRNA purification kit.

For analysis of the lacZ:cre ratio, whole thymi or primarily cultured TSCs from *Foxn1*$^{lacZ/cre}$ mice at different ages were homogenized in trizol (Invitrogen) and total RNA was extracted according to the manufacturer. The reverse transcription was performed with superscript III system (Invitrogen). Quantitative PCR was performed on an ABI 7500 real time PCR system with Taqman universal PCR mix or SYBR green PCR master mix (Applied Biosystems). Please see the Supplements for the details of reverse transcription and real-time PCR.

Primary TEC culture and de-methylation treatment

Enriched TECs were prepared from *Foxn1*$^{lacZ/Cre}$ thymi as described above, cultured and treated with 5μM 5-Aza-dC and 300nM TSA (sigma). Please see Supplemental Data for details.

RESULTS

Foxn1^{lacZ} causes postnatal thymic degeneration

We generated a *Foxn1*^{lacZ} allele with an IRES-lacZ cassette inserted into the 3'UTR, generating a bicistronic message and resulting in *lacZ* expression that faithfully replicates *Foxn1* expression in the fetal thymus (Gordon et al., 2007). While Foxn1 function is normal through the newborn stage, the *Foxn1*$^{lacZ/lacZ}$ adult thymus showed significantly reduced thymus size compared to controls (Fig. 3.1A-B). To determine whether this phenotype was due to an affect on Foxn1 dosage or to the presence of β-galactosidase protein, we crossed the *Foxn1*^{lacZ} allele with the null allele, *nude* (*nu*). *lacZ/nu* mice had more rapid and severe postnatal thymic degeneration than *lacZ/lacZ* mice (Figs. 3.1A-B, and S3.1). In addition, expression of the *lacZ* gene in TECs of *Foxn1*$^{cre/nu}$*;R26R* thymus had no effect on thymic architecture and were similar

to *+/nu* (Fig. 3.1C), showing no evidence for degeneration phenotypes associated with lacZ expression in TECs, nor any interaction between reduced Foxn1 dose and the presence of *β*-galactosidase protein. These data indicated that the thymic degeneration phenotype depended on Foxn1 dosage and was not due to toxicity of β-galactosidase protein, or to a linked second-site mutation in the *lacZ* line. Comparison of the postnatal thymus phenotype of six genotypes, wild-type (+/+), *Foxn1*$^{+/lacZ}$ (*+/lacZ*), *Foxn1*$^{+/nu}$ (*+/nu*), *lacZ/lacZ*, *lacZ/nu* and *Foxn1*$^{nu/nu}$ (*nu/nu*), revealed a close correlation between the Foxn1 dosage and the thymic phenotype both by thymus size (Fig. 3.1A) and as quantified by thymic weight (Fig. S3.1F). Postnatal thymocyte numbers were also reduced relative to controls in a dose-dependent fashion after one week postnatal (Fig. 3.1D; see below). These results further suggested that reduced expression from the *Foxn1*^{lacZ} allele postnatally was responsible for the degenerative phenotype in the postnatal *lacZ/lacZ* and *lacZ/nu* thymus.

Expression from *Foxn1*^{lacZ} allele is down-regulated postnatally

To identify the molecular basis for these phenotypes, we measured expression levels from the *Foxn1*^{lacZ} allele in the postnatal thymus. *Foxn1* expression in T cell -depleted thymic stromal cells (TSCs) was compared between +/+ and *lacZ/lacZ* at different stages. *Foxn1* expression in *lacZ/lacZ* TSCs were comparable to +/+ at the newborn stage, but reduced to 20%-30% of +/+ at 5 weeks (Fig. 3.2A). *Foxn1* is expressed broadly during fetal stages, but may be differentially regulated in postnatal TECs (Itoi et al., 2007; Nehls et al., 1996). The percentage of TECs in postnatal stroma is also dynamic (Gray et al., 2006). Therefore, changes in either the TEC/TSC ratio or TEC composition could confound comparison of *Foxn1* expression in bulk stroma from controls and mutants at stages after phenotypes are apparent. To avoid variability in either stromal composition or the efficiency of TEC isolation associated with phenotypic differences

between control and mutant thymi, we took advantage of the *Foxn1*^{cre} allele, which we generated using the same strategy as the *lacZ* allele (Gordon et al., 2007). Unlike the *lacZ/lacZ* thymus, the *cre/cre* thymus is normal at both fetal and postnatal stages ((Gordon et al., 2007), data not shown). As both alleles produce a bicistronic mRNA, we used *cre* and *lacZ*-specific primers to specifically detect the mRNAs made from each allele (Fig. 3.2B). We measured the *lacZ:cre* mRNA ratio in total thymus cDNA derived from *lacZ/cre* mice. At 1 week, the *lacZ:cre* ratio in most samples was at or below 50% of newborn ratios (Fig. 3.2C), and by 3-4 weeks relative *LacZ* levels dropped to .25-.40. Since the *Foxn1* mRNA level was consistently below 50% (i.e. less than *+/nu* heterozygotes), this degree of down-regulation could be sufficient to cause the observed phenotypes. At later stages, the average ratios rose to the vicinity of .5 and variability decreased, although this change could represent decreased c*re* allele expression, as this time point coincides with a previously reported postnatal decrease in wild-type *Foxn1* expression in thymic stroma (Ortman et al., 2002).

Since insertion of the *lacZ* gene into the 3'-UTR of the *β*-actin gene has been shown to reduce expression via allele-specific methylation of the β-actin promoter (Strathdee et al., 2008), we tested whether down-regulation of *Foxn1*^{lacZ} is caused by hypermethylation. Due to the poor definition of the *Foxn1* promoter and technical difficulties in purifying sufficient TECs for direct analysis of methylation, we chose an indirect assay to test the hypothesis. TSCs from *Foxn1*$^{lacZ/cre}$ mice were isolated and treated with de-methylating agents in primary culture. The majority of the cultured TSCs were TECs (Fig. S3.2), and variability between cultures was internally controlled by the use of the *lacZ/cre* genotype. The *lacZ:cre* mRNA ratio in the cultured TECs was measured with or without de-methylation treatment. If the *Foxn1*^{lacZ} allele were hypermethylated, the suppression of *lacZ* expression after the newborn stage (Fig. 3.2B)

should recover after de-methylation treatment to be equivalent to *Foxn1*^{cre}. Indeed, treated cultures at all postnatal stages had a *lacZ:cre* ratio close to 1 (Fig. 3.2D), indicating that demethyation reversed the down regulation of the *lacZ* allele. We obtained similar results with TECs derived from *Foxn1*$^{lacZ/cre}$*;R26YFP* mice, using YFP as endogenous control for real-time RT-PCR (data not shown). These results are compatible with postnatal hypermethylation of the *Foxn1*^{lacZ} locus underlying the reduced expression from this allele.

Disorganization of thymic compartments and the CMJ

The cortico-medullary junction (CMJ) is the location of the blood vessels where lymphoid progenitor cells (LPCs) enter the postnatal thymus, newly generated T cells exit to the periphery, and is where at least one type of potential TEC progenitor is located (Klug et al., 1998). At 10 weeks, *+/lacZ* and *+/nu* thymi had a normal steady-state size and architecture; in contrast, the *lacZ/lacZ* and *lacZ/nu* thymi were atrophic and CMJ organization had dramatically deteriorated (Fig. 3.1B). We also observed an increased density of blood vessels in the *lacZ/lacZ* and *lacZ/nu* thymi, possibly due to the dramatic decrease in T cell number and the rapid collapse of thymic stroma. The phenotypes of both 10 week *lacZ/lacZ* and 4 week *lacZ/nu* thymi had a striking resemblance to an 18 month wild-type thymus (Fig. 3.1B, S3.1E). The 10 weeks *lacZ/nu* thymus was even more severely affected, with an extremely high vascular density and no discernable compartmental organization (Fig. 3.1B).

Ontogeny of defects in the thymic microenvironment

To determine the ontogeny of these phenotypes and assess them at the cellular level, we assayed TEC subsets, stromal organization, and the CMJ using histological analysis and Keratins (K) and other differentiation markers (Blackburn and Manley, 2004) from the newborn stage. In

the normal thymus, medullary TECs (mTECs) form compact medullary compartments ($K5^+$) surrounded by $K8^+$ cortex. K14 and UEA-1 mark non-overlapping mTEC subsets (Klug et al., 1998; Surh et al., 1992). At the newborn stage, *+/lacZ* and *lacZ/lacZ* thymi were similar, while *+/nu* and *Z/nu* mice were smaller (Fig S3.1A, F). Small, proto-medullary regions ($K5^+$and either $K14^+$ or UEA-1^+) were present and similar in all four genotypes, although *+/nu* and *lacZ/nu* thymi also had some scattered UEA-1^+ cells (Fig. S3.3A-B) indicating a mild TEC organization defect due to haploinsufficiency of the *nu* allele. By 1 week postnatal, all four genotypes showed similar well-defined cortico-medullary organization and epithelial marker expression (Fig. S3.1B; S3.3A-B). By 2 weeks of age, just after expression from the $Foxn1^{lacZ}$ allele decreases, the *lacZ/lacZ* thymi had a noticeable decrease in thymus size and cortical area (FigS3.1C). TEC phenotypes were progressive and dosage-sensitive. The *lacZ/lacZ* thymi first lost CMJ definition at 3 weeks (Fig. 3.3B, S3.1D), and by 6 weeks the *lacZ/lacZ* thymic architecture was disorganized (Fig. 3.3C). In comparison, *lacZ/nu* thymi showed CMJ disorganization as early as 2 weeks (Fig. 3.3A, S3.1C), and by 3 weeks had almost completely lost cortico-medullary organization (Fig. 3.3B). In addition, *lacZ/lacZ* and *lacZ/nu* thymi showed reduced UEA-1^+ mTECs within the $K14^+$ medullary regions (Fig. 3.3E). All of these TEC and stromal organization phenotypes were similar to those seen in the aged wild-type thymus (Aw et al., 2008; Steinmann, 1986) (Fig. 3.3D, F).

Reduced Foxn1 expression causes a loss in specific TEC subsets

Thymic stromal cells (TSCs) were further analyzed by flow cytometry at 3-4 weeks. The mTEC:cTEC ratio of *lacZ/lacZ* thymus was comparable to wild-type at newborn and 2 weeks, but decreased by 4 weeks, similar to aged wild-type thymus (Fig. 3.4A-B) (Gray et al., 2006). The overall percentage of $MHCII^{hi}$ cells in total $CD45^-$ TSCs at 3-4 weeks was decreased in both

lacZ/lacZ and *lacZ/nu* mice compared to *+/lacZ* (Fig. 3.4C-D). MHCII^{hi}UEA-1^{+} mTECs were specifically reduced by about 50%, with a concomitant increase in MHCII^{lo}UEA-1^{+} cells. *lacZ/nu* mice at this stage showed an overall decrease in UEA-1^{+} TECs, with a more than 50% loss of MHCII^{hi}UEA-1^{+} cells; this loss was associated with an increase in MHCII^{lo}UEA-1^{-} cells (Fig. 3.4E-F; R2 and R4). While the total percentage of UEA-1^{+} cells was similar in control and *lacZ/lacZ* TECs (although reduced in *lacZ/nu;* data not shown), the percentage of UEA-1^{hi} cells was significantly decreased in *lacZ/lacZ* TECs, and the decrease in *lacZ/nu* TECs was similar to that seen in the 13-month thymus (Fig. 3.4G, and data not shown). By 6 weeks, the *lacZ/lacZ* phenotype (not shown) was similar to the 4-week *lacZ/nu* phenotype, indicating that both genotypes underwent a similar progression of phenotypes but at different rates.

Strikingly, analysis of *Foxn1* mRNA levels in these same TEC subsets showed a much higher level of expression in the most sensitive subsets, MHCII^{hi} and UEA-1^{hi} TECs (Fig. 3.4H, S3.4). Immunostaining on thymus sections also showed that MHCII^{hi} and UEA-I^{hi} TECs were associated with high levels of Foxn1 protein (Fig. 3.4I; note that Foxn1 is nuclear and MHCII and UEA-1 are cell surface markers). These data suggest that these cell types might require higher Foxn1 expression for their initial differentiation and/or to maintain their phenotype, and therefore might be more sensitive to the loss of Foxn1 expression. As decreases in these same TEC subsets have been recently reported in aged thymus (Gray et al., 2006), we investigated whether the presence of lacZ^{hi} TECs correlated with the presence of these cells. Consistent with this notion, lacZ^{hi} TECs were greatly reduced in aged *+/lacZ* thymus compared to younger ages (Fig. 3.5). Since lacZ^{hi} cells were still present even at 6 weeks in heterozygotes, the loss of these cells in *lacZ/lacZ* homozygotes did not simply reflect decreased expression from the *lacZ* allele, and was consistent with the progressive loss of TECs with highest *Foxn1* levels in aged mice.

Decreased proliferation of TECs in *lacZ/lacZ* mice

Foxn1 has been suggested to regulate TEC proliferation during fetal stages (Itoi et al., 2001). To investigate the cellular mechanism involved in the loss of TEC subsets in postnatal *lacZ/lacZ* thymus, we analyzed proliferation in TECs. Cell cycle analysis of $CD45^-$ stromal cells at 2 weeks showed that the percentage of total proliferating TSCs was decreased by about 40% in the *lacZ/lacZ* mutant at this stage (Fig. 3.6A-B). As this time point is prior to the major changes in CMJ organization and TEC subsets, these data suggest that changes in TEC proliferation contribute to at least some of the observed phenotypes in these mice. To correlate this analysis to changes in TEC populations, we analyzed the same five stromal subsets (R1-R5) defined by MHCII and UEA-1 staining in Figure 4 by BrdU analysis of proliferation at 4 weeks postnatal (Fig. 3.6C, S3.5). Reduced proliferation was restricted to the $MHCII^{lo}$ subsets (corresponding to R3 and R4 in Figure 3.4), while proliferation of $MHCII^{hi}$ cells was unchanged (Fig. 3.6C). These results suggest that Foxn1 regulation of proliferation is TEC subset-specific.

Thymocyte number and differentiation defects in *lacZ/lacZ* mice

The changes in TEC phenotypes resulted in immediate, non-cell autonomous defects in thymocyte development. Newborn thymocyte numbers were similar in *+/lacZ* and *lacZ/lacZ*, and increased logarithmically in the first week postnatal; *lacZ/nu* numbers were lower due to haploinsufficiency for nude, but paralleled the other two genotypes for the first week (Fig. 3.1D). Thymocyte numbers began decreasing in both *lacZ/lacZ* and *lacZ/nu* between 1 and 2 weeks (Fig. 3.1D), immediately after *Foxn1* down-regulation (Fig. 3.2C). A further nearly 10-fold drop in cell number occurred at 5 weeks in *lacZ/lacZ* with similar timing to controls, but this decrease was more severe and precipitous than the normal cell number decrease at this stage (Fig. 3.1D) (Gray et al., 2006). This decrease occurred earlier in *lacZ/nu*, at 4 weeks, indicating that the

timing of this drop may also be influenced by Foxn1 dosage. After this point, cell numbers were relatively stable in all genotypes through at least 3 months of age.

Both *lacZ/lacZ* and *lacZ/nu* mice also showed specific thymocyte development defects. The first change was a reduced frequency of $CD4^+$ SP cells beginning at about 14 days (Fig. 3.7A, C). By 3 weeks the DN cell percentage increased in both *lacZ/lacZ* and *lacZ/nu* mice (Fig. 3.7B-C). Subset analysis of Lin^- DN cells showed decreased DN2 cells at 3 weeks in both *lacZ/lacZ* and *lacZ/nu*, indicating a partial block or delay in the DN1-DN2 transition (Fig. 3.7B), which is also associated with normal aged thymus (Phillips et al., 2004; Thoman, 1995). *lacZ/nu* mice also showed fewer $CD4^+$ cells and a milder DN1-DN2 block at the newborn stage, reflecting haploinsufficiency for nude. Consistent with the expression of *Foxn1* only in TECs, bone marrow cells from adult *lacZ/nu* mice showed normal thymocyte development in a wild-type host (Fig. S3.6), confirming that these thymocyte development phenotypes were due to a TEC-intrinsic mechanism.

DISCUSSION

Our data indicate that *Foxn1* down-regulation in *lacZ/lacZ* mice resulted in collapse of the postnatal steady-state thymus in a gene dosage-sensitive manner. We show that the effects of reduced Foxn1 on TECs are specific and progressive, and include CMJ disorganization, decreased proliferation, and the loss of $MHCII^{hi}$ and UEA-1^{hi} cells, which we demonstrate are also the TECs with highest wild-type Foxn1 levels. The loss of UEA-1^{hi} cells is consistent with our previous work showing that UEA-1^+ TECs never develop in a *Foxn1* constitutive hypomorph, $Foxn1^{\Delta/\Delta}$ (Su et al., 2003). As UEA-1^+ TECs are associated with medullary compartment organization (Naquet et al., 1999), these cells may represent a critical target for Foxn1 function

to maintain the postnatal thymus microenvironment. Our BrdU analysis also shows that TEC proliferation is specifically decreased in the MHCII^{lo} population, but not in the MHCII^{hi} TECs, even though MHCII^{hi} cells are decreased in number and MHCII^{lo} subsets increase in *lacZ* mutants and with age. These results suggest that reduction of *Foxn1* levels affects both differentiation and proliferation, but may affect these two processes in opposite directions and in a subset-specific manner. This apparent contradiction suggests that while Foxn1 may control both TEC differentiation and proliferation in the postnatal thymus, these two functions may be independently regulated, and is clearly an avenue worth further investigation.

Both fetal TEC differentiation and maintenance of the postnatal thymus microenvironment require "crosstalk" interactions between TECs and developing thymocytes (Klug et al., 1998; Klug et al., 2002). Our previous analysis of a *Foxn1* hypomorphic allele implicated Foxn1 in mediating crosstalk-dependent differentiation of TECs in the fetal thymus (Su et al., 2003). Our current data provide the first functional evidence that Foxn1 is also required in the postnatal thymus. Thus our current data suggest that *Foxn1* is required at multiple stages in the thymus. This data is reminiscent of the role of NKX2.1, which is required for thyroid organogenesis and to maintain the differentiated thyroid (Kusakabe et al., 2006). Similar to NKX2.1, Foxn1 is dispensable for initial thymus formation, but is required for both fetal TEC differentiation and functional maintenance of the mature organ. This suggests that the endodermal organs share similar paradigms in the molecular mechanisms linking fetal differentiation and functional regulation.

The timing and progression of phenotypes and the apparently uncoupled effects on TEC differentiation and proliferation suggest that multiple defects contribute to thymic degeneration after loss of Foxn1, and that Foxn1 may be required both to maintain existing TECs and in

progenitors for the generation of new TECs after turnover. Since TECs turn over every 10-14 days in adult mice (Gray et al., 2007; Gray et al., 2006), the appearance of TEC proliferation and thymocyte development phenotypes within one week of *Foxn1* down-regulation suggests that decreased *Foxn1* causes changes in TEC function in real time, causing an immediate loss of thymic function. Other phenotypes appear at or after 3 weeks postnatal, including DN cell defects, decreased UEA-1^{hi} TECs, and degenerative progression of initial phenotypes without further reductions in *Foxn1* expression. These changes may reflect failure to replace TECs after turnover, causing reduced niche availability to promote thymocyte development.

Multiple mechanisms may also underlie the thymocyte development defects seen after Foxn1 down regulation. The most striking finding is the immediate loss of thymocyte generation capacity, well before TEC phenotypes, morphological defects, or specific changes in thymocyte differentiation were detected. The early loss of MHCII expression may directly affect the specific ability of TECs to promote differentiation of $CD4^{+}$ thymocytes, resulting in the selective decrease in these cells. These results show that cell-autonomous changes in thymic organization are associated with reduced thymocyte number and abnormal thymocyte development that were largely consistent with changes previously reported for aging-related involution (Thoman, 1995). The reduced TEC proliferation and subsequent loss of TEC subsets likely cause a progressive decrease in microenvironmental niches capable of supporting thymocyte development, with the loss of compartment organization would be expected to decrease the efficiency of thymocyte differentiation. Thus, both cellular and molecular mechanisms likely contribute to the indirect loss of thymocyte development capacity in the *lacZ/lacZ* thymus, and may operate in the aged thymus as well.

Our data indicate that TECs may have an extreme degree of dosage sensitivity for Foxn1.

It has been known for more than three decades that the *+/nu* thymus has a mild thymus size reduction (Kojima et al., 1984; Scheiff et al., 1978), indicating that Foxn1 dose is critical for thymus development. Our data show that 50% of normal *Foxn1* expression (*+/nu*) caused reduced thymus size and thymocyte production and mild stromal organization and thymocyte development defects. Decreasing to 30-40% of normal levels (*lacZ/lacZ*) affected the maintenance and/or phenotype of MHCII+ TECs. Reduction to 20% or less (*lacZ/nu*) caused more rapid degeneration, as 3 week old *lacZ/nu* thymi bear a striking resemblance to the 10 week *lacZ/lacZ* thymus, as well as the involuted 18-month wild-type thymus. By 10 weeks *lacZ/nu* thymi had degenerated beyond even the normal aged thymus. This *Foxn1* expression level may thus be too low to maintain TECs, while the *lacZ/lacZ* phenotype appears to be a reasonably physiological model for premature involution, and might represent a threshold Foxn1 level for thymic maintenance. These results indicate that TECs are extremely sensitive to changes in *Foxn1* dosage of only 10-20%, reminiscent of a recent report showing similar sensitivity to bicoid protein levels in the early *Drosophila* embryo (Gregor et al., 2007). To our knowledge this is the first demonstration of this level of dosage sensitivity for a transcription factor in vertebrates, particularly for postnatal function.

While our results are compatible with the hypothesis that the down-regulation of the $Foxn1^{lacZ}$ allele is due to lacZ-induced allele-specific methylation, the question of its postnatal specificity remains. A recent study showed that 3'-UTR insertion of lacZ in the β-actin locus changed the methylation of and suppressed expression from the modified allele. Interestingly, this hypermethylation only occurred in differentiated ES cells, but not in undifferentiated cells (Strathdee et al., 2008), suggesting that this methylation might be regulated by differentiation-related signals. This phenomenon suggests that the postnatal-specific down regulation of the

Foxn1^{lacZ} allele may be triggered by differentiation- or temporally controlled cues. Since the effect on *Foxn1* expression is due to insertion of the lacZ gene, the question of whether methylation is normal regulator of *Foxn1* expression during thymic involution remains to be seen.

Disorganization of the thymic stroma and in particular the CMJ is a morphological hallmark of aging-related involution (Takeoka et al., 1996). Although thymic involution is a critical component of aging related immunodeficiency (Zediak and Bhandoola, 2005), the cellular and molecular basis of postnatal thymic homeostasis and involution is not well understood. Both fetal TEC differentiation and maintenance of the postnatal thymus microenvironment require crosstalk interactions between TECs and developing thymocytes (Klug et al., 1998; Klug et al., 2002), cell-autonomous defects in either compartment could result in the failure of crosstalk and contribute to normal thymic aging phenotypes. However, the cellular target responsible for involution is controversial, with evidence implicating both TEC and HSC-intrinsic defects in involution(Gui et al., 2007; Min et al., 2004; Montecino-Rodriquez et al., 2005; Zediak et al., 2007).

Our results provide the first functional evidence that Foxn1 is required for maintenance of the postnatal thymic epithelium and adult thymic homeostasis. Our data show that a change in the expression level of a single critical transcription factor in TECs is sufficient to mimic accelerated involution, causing aging-associated phenotypes that have been previously reported in both TECs (Gray et al., 2006) and thymocytes (Thoman, 1995). Furthermore, *Foxn1* expression has been reported to be progressively down-regulated in wild-type TECs with aging (Ortman et al., 2002). While our data do not prove that down regulation of Foxn1 is a proximal cause of involution, the close similarity between the *Foxn1lacZ*-associated phenotypes and normal aging-related phenotypes raise the possibility that loss of *Foxn1*may contribute to normal

aging-related involution, and furthermore provide evidence that a TEC-intrinsic mechanism can recapitulate both the TEC and thymocyte-based phenotypic aspects of aging-related involution.

The increased susceptibility to infection, autoimmune diseases and cancer in aged individuals is due, at least in part, to the aging of the immune system. As TEC maintenance and function and HSC differentiation in the thymus are intricately linked, the identification of Foxn1 as a central factor in postnatal TEC maintenance is critical for understanding the molecular nature of this cellular interdependence. Whether changes in *Foxn1* expression in the wild-type thymus are the cause of or a downstream effect of the normal mechanisms underlying involution, investigation of the mechanisms by which *Foxn1* is regulated in TECs during normal aging could provide an avenue for understanding the molecular control of thymic homeostasis, and therefore potential therapeutic targets to maintain postnatal T cell production.

ACKNOWLEDGEMENTS

We thank Dong-ming Su for performing the initial experiments indicating thymic degeneration associated with the Foxn1^{lacZ} allele while he was a member of the Manley lab. We thank C. Blackburn, E. Richie, and B. Condie for critical discussions, reading of the manuscript, and for sharing data prior to publication; A. Farr for the TSC isolation protocol, Z. Liu for advice and technical help, and J. Nelson in the Center for Tropical and Emerging Global Diseases Flow Cytometry Facility at the University of Georgia for technical support for flow cytometry and cell sorting. Supported by a grant to NRM from NIAID/NIH.

REFERENCES

Anderson, G., Jenkinson, W. E., Jones, T., Parnell, S. M., Kinsella, F. A., White, A. J., Pongrac'z, J. E., Rossi, S. W. and Jenkinson, E. J. (2006). Establishment and functioning of intrathymic microenvironments. *Immunol Rev* **209**, 10-27.

Aspinall, R. and Andrew, D. (2001). Age-associated thymic atrophy is not associated with a deficiency in the CD44(+)CD25(-)CD3(-)CD4(-)CD8(-) thymocyte population. *Cell Immunol* **212**, 150-7.

Aw, D., Silva, A. B., Maddick, M., von Zglinicki, T. and Palmer, D. B. (2008). Architectural changes in the thymus of aging mice. *Aging Cell* **7**, 158-67.

Blackburn, C. C., Augustine, C. L., Li, R., Harvey, R. P., Malin, M. A., Boyd, R. L., Miller, J. F. and Morahan, G. (1996). The nu gene acts cell-autonomously and is required for differentiation of thymic epithelial progenitors. *Proc Natl Acad Sci U S A* **93**, 5742-6.

Blackburn, C. C. and Manley, N. R. (2004). Developing a new paradigm for thymus organogenesis. *Nat Rev Immunol* **4**, 278-89.

Bleul, C. C., Corbeaux, T., Reuter, A., Fisch, P., Monting, J. S. and Boehm, T. (2006). Formation of a functional thymus initiated by a postnatal epithelial progenitor cell. *Nature* **441**, 992-6.

Geiger, H. and Van Zant, G. (2002). The aging of lympho-hematopoietic stem cells. *Nat Immunol* **3**, 329-33.

Gordon, J., Bennett, A. R., Blackburn, C. C. and Manley, N. R. (2001). Gcm2 and Foxn1 mark early parathyroid- and thymus-specific domains in the developing third pharyngeal pouch. *Mech Dev* **103**, 141-3.

Gordon, J., Xiao, S., Hughes, B., 3rd, Su, D. M., Navarre, S. P., Condie, B. G. and Manley, N. R. (2007). Specific expression of lacZ and cre recombinase in fetal thymic epithelial cells by multiplex gene targeting at the Foxn1 locus. *BMC Dev Biol* **7**, 69.

Gray, D., Abramson, J., Benoist, C. and Mathis, D. (2007). Proliferative arrest and rapid turnover of thymic epithelial cells expressing Aire. *J Exp Med* **204**, 2521-8.

Gray, D. H., Seach, N., Ueno, T., Milton, M. K., Liston, A., Lew, A. M., Goodnow, C. C. and Boyd, R. L. (2006). Developmental kinetics, turnover, and stimulatory capacity of thymic epithelial cells. *Blood* **108**, 3777-85.

Gray, D. H., Ueno, T., Chidgey, A. P., Malin, M., Goldberg, G. L., Takahama, Y. and Boyd, R. L. (2005). Controlling the thymic microenvironment. *Curr Opin Immunol* **17**, 137-43.

Gregor, T., Tank, D. W., Wieschaus, E. F. and Bialek, W. (2007). Probing the limits to positional information. *Cell* **130**, 153-64.

Gui, J., Zhu, X., Dohkan, J., Cheng, L., Barnes, P. F. and Su, D. M. (2007). The aged thymus shows normal recruitment of lymphohematopoietic progenitors but has defects in thymic epithelial cells. *Int Immunol* **19**, 1201-11.

Itoi, M., Kawamoto, H., Katsura, Y. and Amagai, T. (2001). Two distinct steps of immigration of hematopoietic progenitors into the early thymus anlage. *Int Immunol* **13**, 1203-11.

Itoi, M., Tsukamoto, N. and Amagai, T. (2007). Expression of Dll4 and CCL25 in Foxn1-negative epithelial cells in the post-natal thymus. *Int Immunol* **19**, 127-32.

Klug, D. B., Carter, C., Crouch, E., Roop, D., Conti, C. J. and Richie, E. R. (1998). Interdependence of cortical thymic epithelial cell differentiation and T-lineage commitment. *Proc Natl Acad Sci U S A* **95**, 11822-7.

Klug, D. B., Carter, C., Gimenez-Conti, I. B. and Richie, E. R. (2002). Cutting edge: thymocyte-independent and thymocyte-dependent phases of epithelial patterning in the fetal thymus. *J Immunol* **169**, 2842-5.
Kojima, A., Saito, M., Hioki, K., Shimanura, K. and Habu, S. (1984). NFS/N-nu/ + mice can macroscopically be distinguished from NFS/N- +/+ littermates by their thymic size and shape. *Exp Cell Biol* **52**, 107-10.
Kusakabe, T., Kawaguchi, A., Hoshi, N., Kawaguchi, R., Hoshi, S. and Kimura, S. (2006). Thyroid-specific enhancer-binding protein/NKX2.1 is required for the maintenance of ordered architecture and function of the differentiated thyroid. *Mol Endocrinol* **20**, 1796-809.
Laufer, T. M., Glimcher, L. H. and Lo, D. (1999). Using thymus anatomy to dissect T cell repertoire selection. *Semin Immunol* **11**, 65-70.
Min, H., Montecino-Rodriguez, E. and Dorshkind, K. (2004). Reduction in the developmental potential of intrathymic T cell progenitors with age. *J Immunol* **173**, 245-50.
Montecino-Rodriquez, E., Min, H. and Dorshkind, K. (2005). Reevaluating current models of thymic involution. *Semin Immunol* **17**, 356-61.
Morrison, S. J., Wandycz, A. M., Akashi, K., Globerson, A. and Weissman, I. L. (1996). The aging of hematopoietic stem cells. *Nat Med* **2**, 1011-6.
Naquet, P., Naspetti, M. and Boyd, R. (1999). Development, organization and function of the thymic medulla in normal, immunodeficient or autoimmune mice. *Semin Immunol* **11**, 47-55.
Nehls, M., Kyewski, B., Messerle, M., Waldschutz, R., Schuddekopf, K., Smith, A. J. and Boehm, T. (1996). Two genetically separable steps in the differentiation of thymic epithelium. *Science* **272**, 886-9.
Nehls, M., Pfeifer, D., Schorpp, M., Hedrich, H. and Boehm, T. (1994). New member of the winged-helix protein family disrupted in mouse and rat nude mutations. *Nature* **372**, 103-7.
Ortman, C. L., Dittmar, K. A., Witte, P. L. and Le, P. T. (2002). Molecular characterization of the mouse involuted thymus: aberrations in expression of transcription regulators in thymocyte and epithelial compartments. *Int Immunol* **14**, 813-22.
Petrie, H. T. (2002). Role of thymic organ structure and stromal composition in steady-state postnatal T-cell production. *Immunol Rev* **189**, 8-19.
Phillips, J. A., Brondstetter, T. I., English, C. A., Lee, H. E., Virts, E. L. and Thoman, M. L. (2004). IL-7 gene therapy in aging restores early thymopoiesis without reversing involution. *J Immunol* **173**, 4867-74.
Prockop, S. and Petrie, H. T. (2000). Cell migration and the anatomic control of thymocyte precursor differentiation. *Semin Immunol* **12**, 435-44.
Scheiff, J. M., Cordier, A. C. and Haumont, S. (1978). The thymus of Nu/+ mice. *Anat Embryol (Berl)* **153**, 115-22.
Steinmann, G. G. (1986). Changes in the human thymus during aging. *Curr Top Pathol* **75**, 43-88.
Strathdee, D., Whitelaw, C. B. and Clark, A. J. (2008). Distal transgene insertion affects CpG island maintenance during differentiation. *J Biol Chem* **283**, 11509-15.
Su, D. M., Navarre, S., Oh, W. J., Condie, B. G. and Manley, N. R. (2003). A domain of Foxn1 required for crosstalk-dependent thymic epithelial cell differentiation. *Nat Immunol* **4**, 1128-35.
Sudo, K., Ema, H., Morita, Y. and Nakauchi, H. (2000). Age-associated characteristics of murine hematopoietic stem cells. *J Exp Med* **192**, 1273-80.

Surh, C. D., Gao, E. K., Kosaka, H., Lo, D., Ahn, C., Murphy, D. B., Karlsson, L., Peterson, P. and Sprent, J. (1992). Two subsets of epithelial cells in the thymic medulla. *J Exp Med* **176**, 495-505.
Takeoka, Y., Chen, S. Y., Yago, H., Boyd, R., Suehiro, S., Shultz, L. D., Ansari, A. A. and Gershwin, M. E. (1996). The murine thymic microenvironment: changes with age. *Int Arch Allergy Immunol* **111**, 5-12.
Taub, D. D. and Longo, D. L. (2005). Insights into thymic aging and regeneration. *Immunol Rev* **205**, 72-93.
Thoman, M. L. (1995). The pattern of T lymphocyte differentiation is altered during thymic involution. *Mech Ageing Dev* **82**, 155-70.
Yu, S., Abel, L. and Globerson, A. (1997). Thymocyte progenitors and T cell development in aging. *Mech Ageing Dev* **94**, 103-11.
Zediak, V. P. and Bhandoola, A. (2005). Aging and T cell development: interplay between progenitors and their environment. *Semin Immunol* **17**, 337-46.
Zediak, V. P., Maillard, I. and Bhandoola, A. (2007). Multiple prethymic defects underlie age-related loss of T progenitor competence. *Blood* **110**, 1161-7.
Zhu, X., Gui, J., Dohkan, J., Cheng, L., Barnes, P. F. and Su, D. M. (2007). Lymphohematopoietic progenitors do not have a synchronized defect with age-related thymic involution. *Aging Cell* **6**, 663-72.

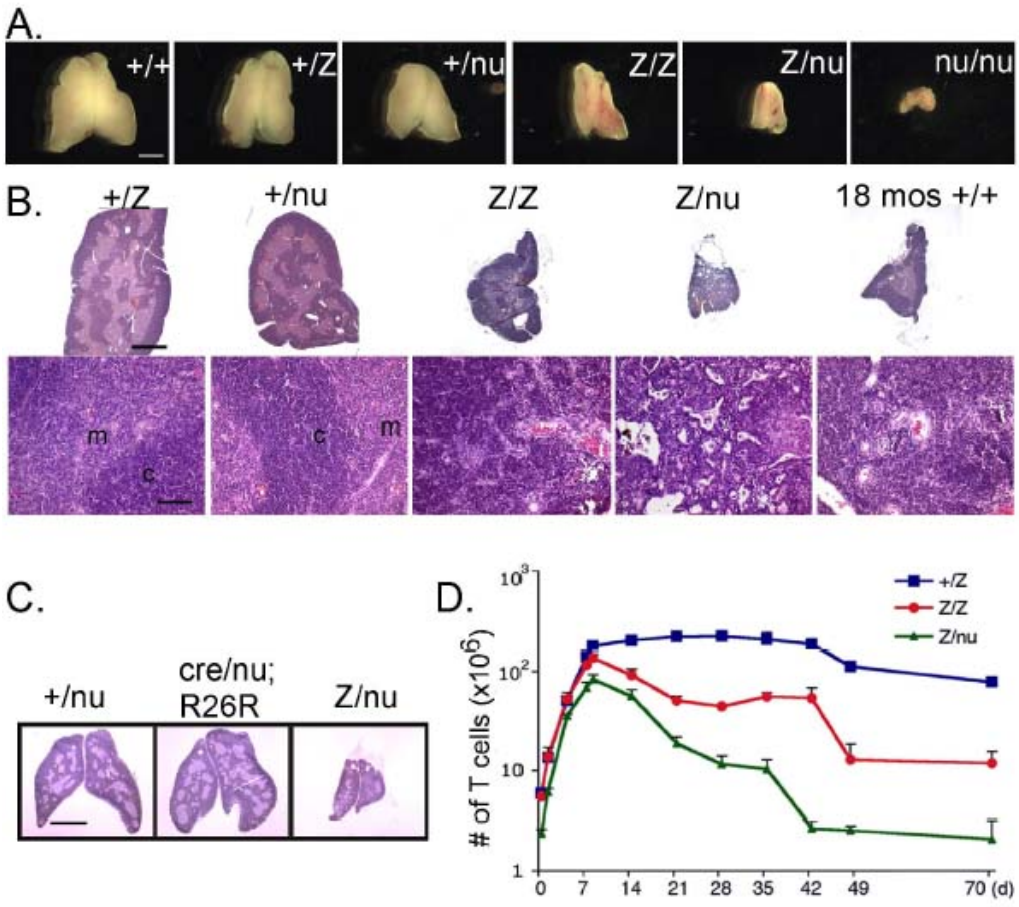
A.
+/+
+/Z
+/nu
Z/Z
Z/nu
nu/nu
B.
+/Z
+/nu
Z/Z
Z/nu
18 mos +/+
m
c
c
m
C.
+/nu
cre/nu;
R26R
Z/nu
D.
# of T cells (x10^6)
10^3
10^2
10
1
0
7
14
21
28
35
42
49
70 (d)
+/Z
Z/Z
Z/nu

Fig. 3.1

Fig. 3.1. The *Foxn1*^{lacZ} allele causes postnatal thymic atrophy. The *lacZ* allele is indicated in all figures as "Z". (**A**) Thymi from 5 week-old +/+, *+/lacZ, +/nu, lacZ/lacZ, lacZ/nu* and *nu/nu*. Foxn1 dosage is closely correlated with postnatal thymus phenotype. Scale bar: 2mm, applies to all panels in (A). (**B**) Hematoxylin and eosin stained paraffin sections of thymi from *+/lacZ, +/nu*, *lacZ/lacZ* and *lacZ/nu* mice at 10 weeks. Thymus size was greatly reduced, and cortico-medullary architecture was dramatically disorganized in *lacZ/lacZ* and *lacZ/nu* thymus. An 18 months-old wild-type thymus is shown as an involuted thymus control. Scale bar in the upper panel and lower panel: 1 mm and 100um respectively, applies to all upper panels and lower panels in (B). m, medulla; c, cortex. (**C**) Hematoxylin and eosin stained sections of 3 weeks old *Foxn1*$^{+/nude}$, *Foxn1*$^{cre/nude}$;*R26R* and *Foxn1*$^{lacZ/nude}$ thymi. Scale bar: 2mm. *Foxn1*$^{cre/nude}$;*R26R* thymus showed a phenotype similar to *Foxn1*$^{+/nude}$, indicating that the presence of β-gal protein in TECs does not cause the phenotype associated with the *Foxn1*^{lacZ} allele. (**D**) Total thymocyte numbers in *+/lacZ, lacZ/lacZ* and *lacZ/nu* thymi from newborn through 70 days postnatal. Newborn thymocyte numbers were similar in *+/lacZ* and *lacZ/lacZ*, and increased logarithmically in the first week postnatal; thymocyte number in *lacZ/nu* thymi was smaller due to haploinsufficiency of the *nude* allele, but paralleled the other two genotypes for the first week.

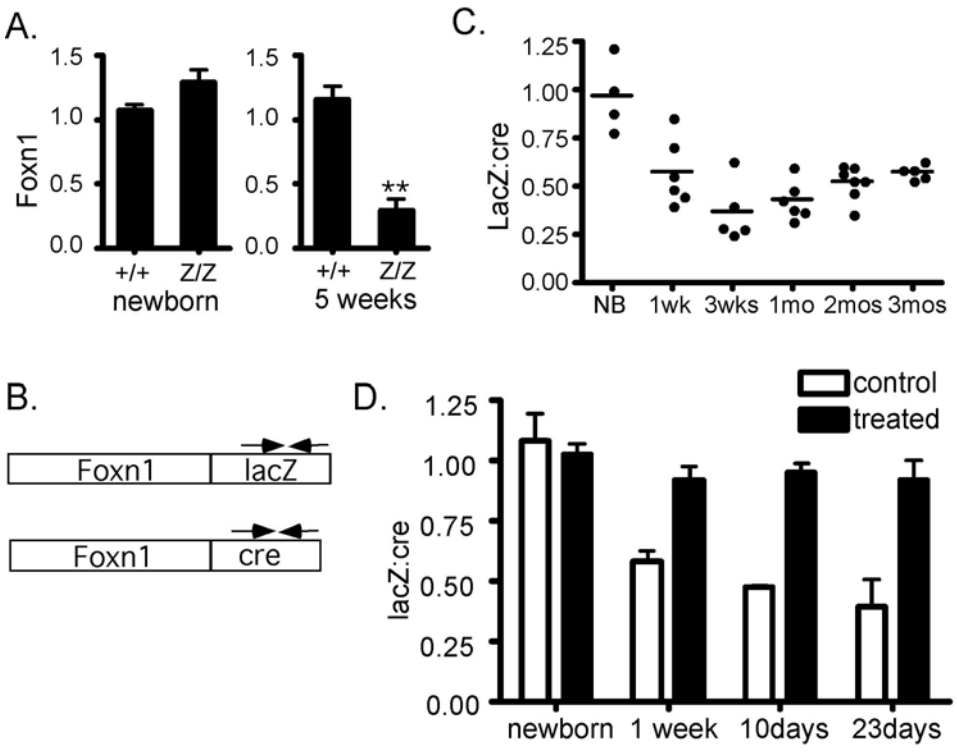
A.
Foxn1
1.5
1.0
0.5
0.0
+/+
Z/Z
newborn
**
5 weeks
C.
LacZ:cre
1.25
1.00
0.75
0.50
0.25
0.00
NB
1wk
3wks
1mo
2mos
3mos
B.
Foxn1
lacZ
Foxn1
cre
D.
control
treated
lacZ:cre
newborn
1 week
10days
23days

Fig. 3.2

Fig. 3.2. *Foxn1* mRNA expression from the $Foxn1^{lacZ}$ allele is down-regulated postnatally. (**A**) Relative quantity of Foxn1 expression in $CD45^-$ total thymic stromal cells (TSCs) of +/+ and *lacZ/lacZ* mice at newborn and 5 weeks. At newborn stage, Z/Z and +/+ showed similar Foxn1 expression levels in TSCs. At 5 weeks, Foxn1 expression level in *lacZ/lacZ* thymi was reduced to about 30% of that of +/+ thymi. (**B**) Schematic representation of *Foxn1-lacZ* and *Foxn1-cre* bicistronic message RNA. Allele specific primers (arrows) were used for quantitative RT-PCR. (**C**) Comparison of *Foxn1* transcript levels from $Foxn1^{lacZ}$ and $Foxn1^{cre}$ allele. The *lacZ:cre* ratio decreased at postnatal stages, suggesting that the expression of Foxn1 from the $Foxn1^{lacZ}$ was reduced postnatally compared to that from $Foxn1^{cre}$ allele. $P<0.001$. (**D**) *lacZ* and *cre* mRNA expression were measured with relative quantitative real-time PCR in primary culture thymic stromal cells from $Foxn1^{lacZ/cre}$ mice at different postnatal ages with or without de-methylating drug treatment.

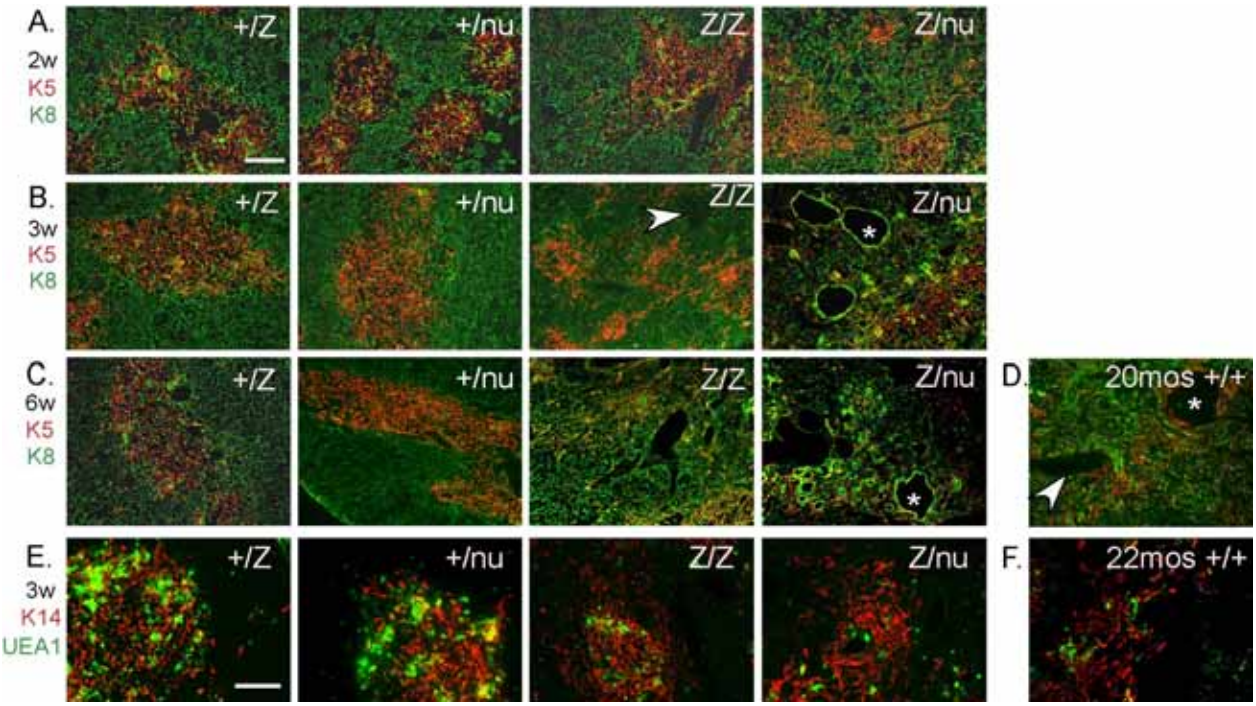
A.
2w
K5
K8
+/Z
+/nu
Z/Z
Z/nu
B.
3w
K5
K8
+/Z
+/nu
Z/Z
Z/nu
C.
6w
K5
K8
+/Z
+/nu
Z/Z
Z/nu
D.
20mos +/+
E.
3w
K14
UEA1
+/Z
+/nu
Z/Z
Z/nu
F.
22mos +/+

Fig. 3.3

Fig. 3.3. Progressive thymic epithelium phenotypes in *Foxn1*^{lacZ} mutants. (**A-D**) Cryosections were stained for Keratin 8 (green) and Keratin 5 (red), Scale bar: 200 μm. Arrow head, perivascular space. *, cystic structure. (**A**) 2 week *+/lacZ*, *+/nu* and *lacZ/lacZ* thymi showed organized cortico-medullary architecture; lac*Z/nu* thymus also show a breakdown of the cortico-medullary junction (CMJ). (**B**) At 3 weeks *lacZ/lacZ* thymus shows CMJ degeneration, and there was a more severe phenotype in *lacZ/nu* thymus, with no organized cortical or medullary regions. (**C**) 6 weeks *lacZ/lacZ* and *lacZ/nu* thymi had an even more severe defect compared to 3 weeks. (**D**) A 20 month-old +/+ thymus is shown as a normal involution control. (**E-F**) Frozen thymus sections stained with anti-Keratin 14 (red) and UEA-1 (green). Scale bar: 200 μm. Both 3 week *lacZ/lacZ* and *lacZ/nu* (**E**) and 22 month +/+ thymus (**F**) have fewer UEA-1^{+} mTECs within K14^{+} medullary regions.

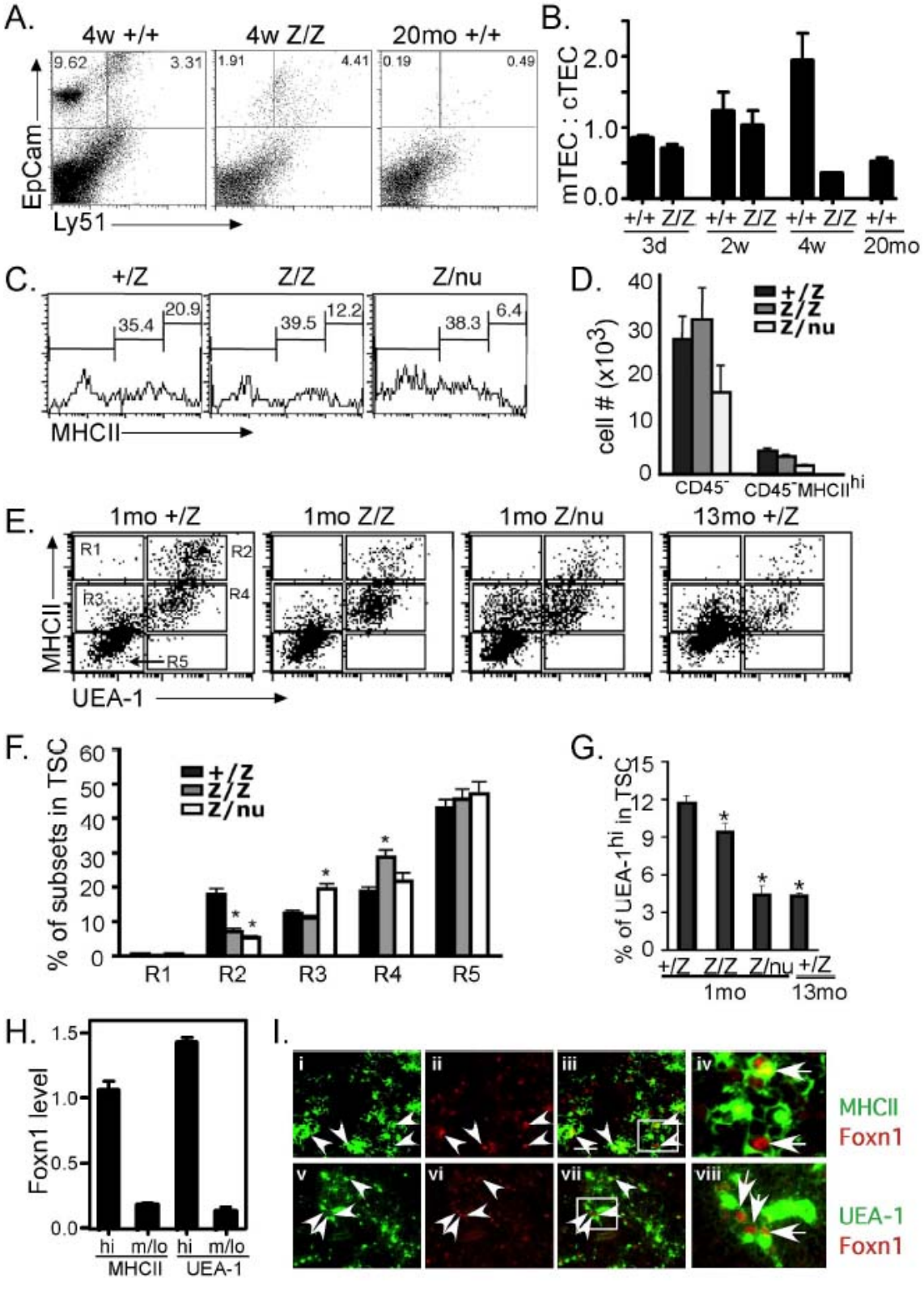
A.
4w +/+
4w Z/Z
20mo +/+
9.62
3.31
1.91
4.41
0.19
0.49
EpCam
Ly51
B.
mTEC : cTEC
2.0
1.0
0.0
+/+ Z/Z +/+ Z/Z +/+ Z/Z +/+
3d
2w
4w
20mo
C.
+/Z
Z/Z
Z/nu
35.4
20.9
39.5
12.2
38.3
6.4
MHCII
D.
cell # (x10^3)
40
30
20
10
0
+/Z
Z/Z
Z/nu
CD45-
CD45-MHCIIhi
E.
1mo +/Z
1mo Z/Z
1mo Z/nu
13mo +/Z
R1
R2
R3
R4
R5
MHCII
UEA-1
F.
% of subsets in TSC
60
50
40
30
20
10
0
+/Z
Z/Z
Z/nu
R1
R2
R3
R4
R5
G.
% of UEA-1hi in TSC
15
12
9
6
3
0
+/Z Z/Z Z/nu +/Z
1mo
13mo
H.
Foxn1 level
1.5
1.0
0.5
0.0
hi m/lo hi m/lo
MHCII
UEA-1
I.
i
ii
iii
iv
v
vi
vii
viii
MHCII
Foxn1
UEA-1
Foxn1

Fig. 3.4

Fig. 3.4. Specific TEC subsets are more sensitive to the loss of Foxn1. (**A**) Gated $CD45^-$ stromal cells from 4 weeks thymi were stained for EpCam and Ly51 expression. The percentage of the $Ly51^-EpCam^+$ group was greatly reduced in *lacZ/lacZ* thymus compared to +/+. (**B**) Quantitative summary of mTEC:cTEC ratio at different stages. mTEC:cTEC ratio was reduced in *lacZ/lacZ* thymus at 4 weeks, similar to +/+ thymus at 20 months. (**C**) Gated $CD45^-$ TSCs from 5 week old thymi analyzed for the MHCII expression. The percentage of $MHCII^{hi}$ cells was greatly reduced in *lacZ/lacZ* and Z/nu thymi. (**D**) Quantitative summary of the total $CD45^-$ TSCs and MHC II^{hi} cell number. (**E**) Gated $CD45^-$ stromal cells from *+/lacZ, lacZ/lacZ* and *laccZ/nu* thymi at 1 month and *+/lacZ* thymus at 13 months analyzed for MHCII and UEA-1 by flow cytometry. R1-R5 gates are indicated with boxes. (**F**) Summary of the percentages of cells in each gate for each genotype; significant changes relative to +/*lacZ* controls are indicated (*; $p<0.05$). (**G**) Summary of the percentage of $UEA\text{-}1^{hi}$ cells in 1 month thymus of each genotype and 13 months *+/lacZ* thymus (*; $p<0.05$). (**H**) $MHCII^{hi}$ and $UEA\text{-}1^{hi}$ TEC subsets express higher levels of *Foxn1*. Quantitative real-time PCR was performed with cDNA from sorted TEC subsets from 4 week old wild-type thymus (see Fig. S4 for sorting gates). $p<0.001$, $n = 3$. (**I**) Cryostat sections of 4 week old wild-type thymus stained for Foxn1 and either MHCII (i-iv), or UEA-1 (v-viii). $MHCII^{hi}$ and $UEA\text{-}1^{hi}$ cells were associated with bright Foxn1 signals (arrow heads). Scale bar in (iii): 50μm, applies to (i) - (iii) and (v) - (vii). **(iv, viii)** Higher magnification views of the boxes in (iii) and (vii) showing co-localization of Foxn1 (nuclear) and MHCII or UEA-1.

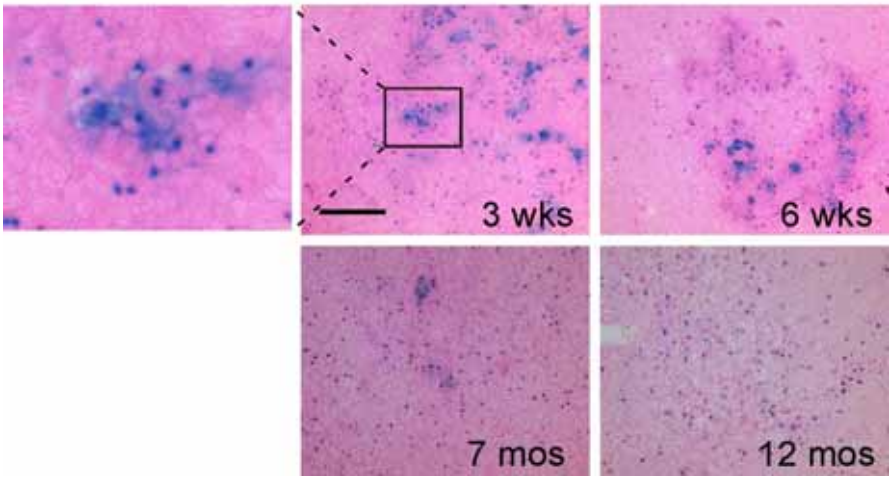

Fig. 3.5

Fig. 3.5. Loss of Foxn1^{hi} (lacZ^{hi}) TECs in aged thymus. X-gal staining on frozen sections of *Foxn1*$^{+/lacZ}$ thymi at 3weeks, 6 weeks, 7 months and 12 months. Eosin counterstaining (pink) is lighter in aged thymus due to lower T cell density.

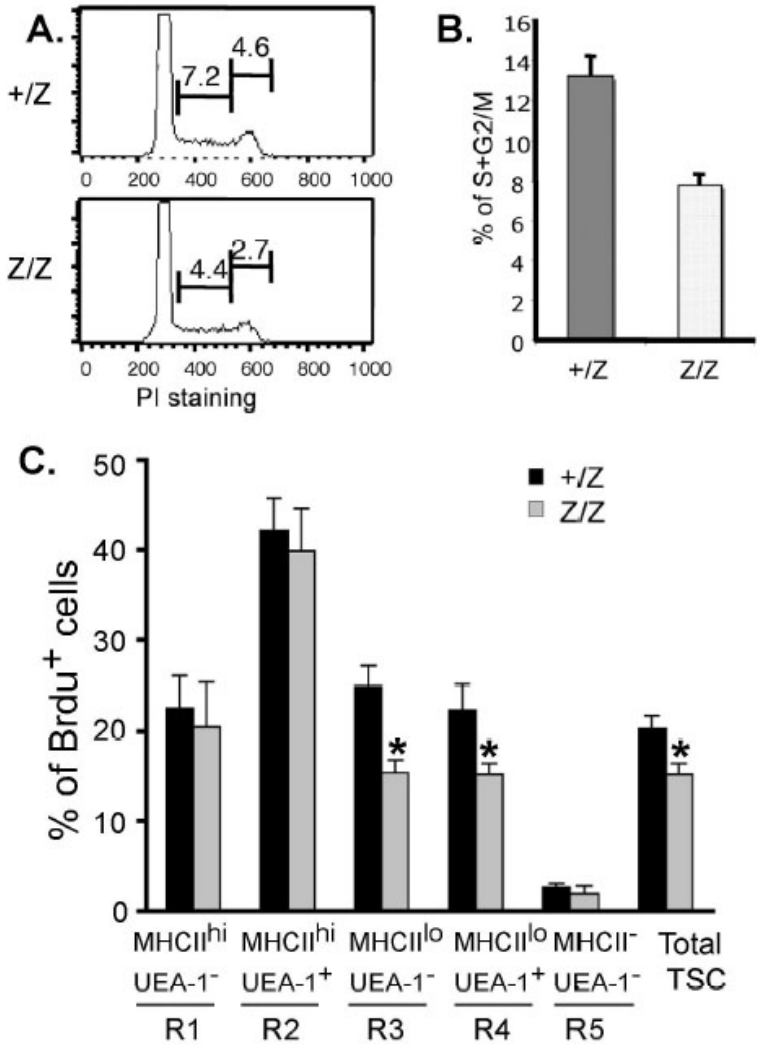
A.
+/Z
7.2
4.6
0 200 400 600 800 1000
Z/Z
4.4
2.7
0 200 400 600 800 1000
PI staining
B.
% of S+G2/M
16
14
12
10
8
6
4
2
0
+/Z
Z/Z
C.
% of Brdu+ cells
50
40
30
20
10
0
+/Z
Z/Z
*
*
*
MHCII^hi UEA-1^- R1
MHCII^hi UEA-1^+ R2
MHCII^lo UEA-1^- R3
MHCII^lo UEA-1^+ R4
MHCII^- UEA-1^- R5
Total TSC

Fig. 3.6

Fig. 3.6. Reduced proliferation of CD45$^-$ TSCs in Foxn1^{lacZ} mutant mice. (**A**) CD45$^-$ TSCs from 2 weeks *+/lacZ* and *lacZ/lacZ* thymi stained for propidium iodide and analyzed for cell cycle. The percentage of the populations at S and G2/M phases was reduced in *lacZ/lacZ* thymus. (**B**) Quantitative summary of CD45$^-$ TSCs at S and G2/M phases. N=3, $P<0.05$, standard error is indicated. (**C**) Brdu analysis of proliferation on different thymic stromal subsets of *+/lacZ*, *lacZ/lacZ* and *lacZ/nu* at 1 month (See Fig. 4E for the gates and Fig. S5 for the histogram of Brdu$^+$ cells).

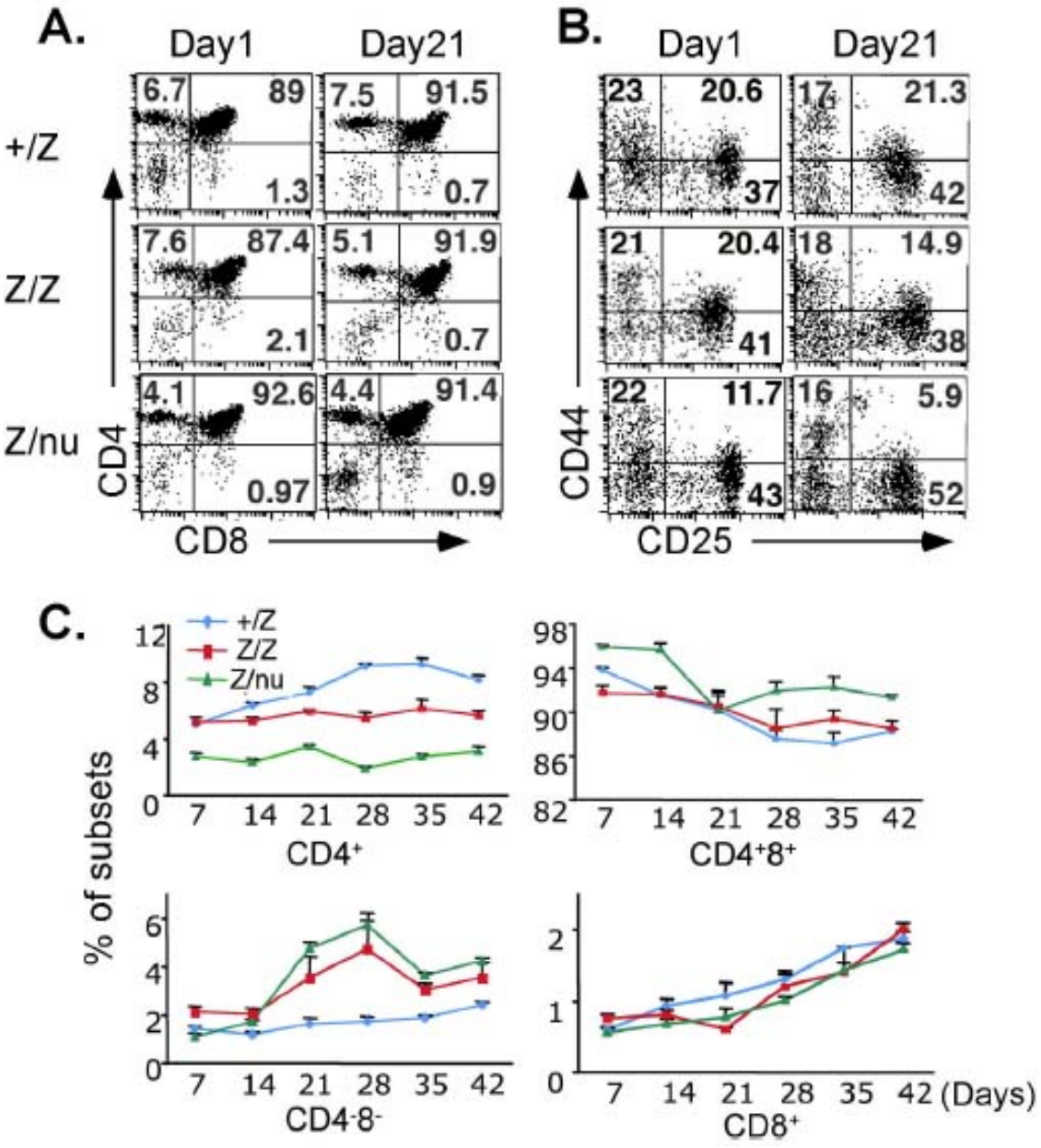
A.
Day1
Day21
+/Z
Z/Z
Z/nu
6.7
89
1.3
7.5
91.5
0.7
7.6
87.4
2.1
5.1
91.9
0.7
4.1
92.6
0.97
4.4
91.4
0.9
CD4
CD8
B.
Day1
Day21
23
20.6
37
17
21.3
42
21
20.4
41
18
14.9
38
22
11.7
43
16
5.9
52
CD44
CD25
C.
+/Z
Z/Z
Z/nu
% of subsets
CD4+
CD4+8+
CD4-8-
CD8+
(Days)

Fig. 3.7

Fig. 3.7. T cell development was affected in mutant thymi. (**A**) Thymocytes from *+/lacZ, lacZ/lacZ* and *lacZ/nu* thymi at newborn and 3 weeks were analyzed for CD4 and CD8 expression with flow cytometry. Numbers of DN, $CD4^+$ SP, $CD8^+$ SP and DP cells are indicated as percent. (**B**) Gated $CD4^-CD8^-$ DN populations at newborn and 3 weeks were analyzed for CD44 and CD25 expression. Numbers of DN1 ($CD44^+CD25^-$), DN2 ($CD44^+CD25^{hi}$), DN3 ($CD44^-CD25^{hi/lo}$) and DN4 ($CD44^-CD25^-$) cells are indicated as percent. (**C**) Summary of each subpopulation at multiple time points. Each time point represents at least 3 individuals.

SUPPLEMENTARY DATA AND METHODS FOR

"*FOXN1* IS REQUIRED TO MAINTAIN THE POSTNATAL THYMIC MICROENVIRONMENT IN A DOSAGE-SENSITIVE MANNER"

Supplementary Methods:

Immunofluorescence

Thymi were embedded with OCT, "flash frozen" in liquid nitrogen, and cut at 10 μm. Cryosections were fixed in acetone, rinsed in TBST (0.1% Tween20), blocked in TBS with 0.5% Tween20 and 10% serum, and incubated with the following primary antibodies: Rabbit anti-mouse K5 (Covance), Rabbit anti-mouse K14 (Covance), Rat anti-mouse K8 (Troma-1) or with UEA-1-biotin (Vector) at RT for 2 hours or at 4°C overnight, followed by Donkey anti-rat IgG-FITC or Donkey anti-rabbit IgG-Texas Red secondary antibodies, or Streptavidin-FITC (Jackson Immunoresearch) at RT for 30 minutes. Foxn1 staining was performed with a polyclonal antibody to Foxn1 (WHN G-20, Santa Cruz) in combination with either UEA-1 or anti-MHCII-FITC (BD Pharmigen). Imaging was done on a Zeiss Axioplan 2 microsope with a AxioCam HRm digital camera.

X-gal staining

Frozen thymus sections were rinsed with PBS and fixed with 4%PFA for 5 minutes at 4°C, then washed with PBS and incubated with detergent rinse solution (0.1M PO_4, pH7.4, 2mM $MgCl_2$, 0.01% sodium deoxycholate, 0.02% Igepal) for 10 minutes at RT, followed by incubating with staining buffer [0.1M PO_4, pH7.4, 2mM $MgCl_2$, 0.01% sodium deoxycholate,

0.02% Igepal, 5mM $K_3Fe(CN)_6$, 5mM $K_4Fe(CN)_6$] at 37°C for overnight. The sections were then washed with PBS and re-fixed in acetone and counter-stained with eosin.

Quantitative RT-PCR

Total RNA was extracted with trizol (Invitrogen) or micro RNA purification Kit (Qiagen). First-strand cDNA was reverse transcribed with superscript III (Invitrogen) and random primers (Invitrogen), incubated at 42°C for 90 minutes and then at 70°C for 15 minutes. RNaseH and RNaseA (Promega) were used to remove RNA from the transcribed first-strand cDNA. Quantitative PCR was performed on an ABI 7500 real time PCR system with Taqman universal PCR mix (Applied Biosystems) and the following primers purchased from Applied Biosystems: 18S rRNA VIC/TAMRA primer-probe (4310893E), and Foxn1 FAM primer-probe (Forward primer: 5'-CCTCCCTTGCAACATATGTACTGT-3', Reverse primer: 5'-GGTAGGGCACAGGGTAGCT-3' , Reporter: 5'-CCTTCCATCAGTACTCCC-3', Dye: FAM).

Alternatively, PCR was performed with SYBR green PCR master mix and the following primers designed with Primer Express3.0 software (Applied Biosystems): 5'-CGATGCCCTGAGGCTCTTT-3' and 5'-TGGATGCCACATGATTCCA-3' for Actin as endogenous control; 5'-TTGCAGTGCACGGCAGATAC-3' and 5'-ACGCGTGAGCGGTCGTAA-3' for LacZ; 5'-GCCGCGCGAGATATGG-3' and 5'-AGCTTGCATGATCTCCGGTATT-3' for Cre. The PCR condition is as follows: 50°C, 2min; 95°C, 10min; 40 cycles of 95°C for 15sec and 60°C for 1min. Relative quantity of the gene expression was determined using 7500 SDS software (Applied Biosystems).

Primary TEC culture and de-methylation treatment

Enriched TECs were prepared from *Foxn1*$^{lacZ/Cre}$ thymi as described above and resuspended in culture medium [RPMI 1640 with 2mM L-Glutamine, 10% Fetal Bovine Serum, 100 IU/ml penicillin, 100 mg/ml streptomycin (Gibco)]. The cells were plated onto 100mm cell culture dishes pre-coated with 0.1% gelatin and cultured at 37 °C with 5% CO_2. The medium was changed every other day to wash off non-adherent cells. After 5 days' culture, half of the cultures were treated with 5μM 5-Aza-dC (Sigma) for 48 hours (medium was changed every 24 hours) and followed by 5μM 5-Aza-dC and 300nM TSA (sigma) for 24 hours. Cells were then collected for RNA extraction and FACS analysis.

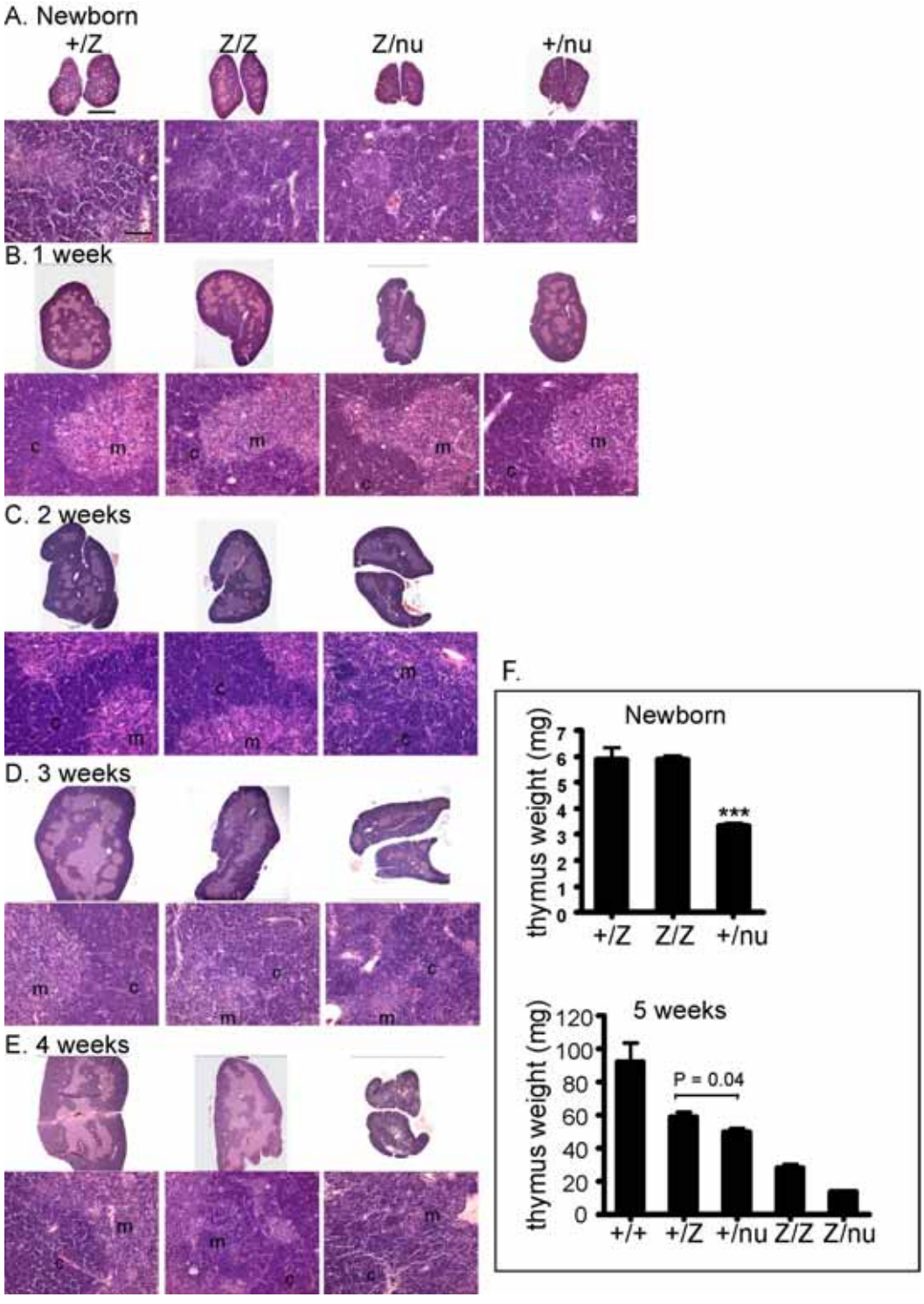
A. Newborn
+/Z
Z/Z
Z/nu
+/nu
B. 1 week
C. 2 weeks
D. 3 weeks
E. 4 weeks
c
m
F.
Newborn
thymus weight (mg)
0
1
2
3
4
5
6
7
***
+/Z
Z/Z
+/nu
5 weeks
thymus weight (mg)
0
20
40
60
80
100
120
P = 0.04
+/+
+/Z
+/nu
Z/Z
Z/nu

Fig. S3.1

The lacZ allele is indicated as "Z" in all figures.

Fig. S3.1. Gradual loss of cortical-medullary architecture and reduced thymus size in *Foxn1*^{lacZ} mutants. (**A**)-(**F**), Hematoxylin and eosin stained paraffin sections of thymi from *+/lacZ,lacZlac/Z, lacZ/nu* and *+/nu* at newborn (A), 1 week (B), 2 weeks (C), 3 weeks (D) and 4 weeks (E). The normal postnatal thymus displays dramatic shifts in size and phenotype over the life of the animal. (**A**) Newborn *+/lacZ* and *lacZ/lacZ* thymi were similar, while thymi from newborn *+/nu* and *lacZ/nu* mice were smaller and less well-organized, showing that even a 50% reduction in *Foxn1* dosage influenced thymus development. **(B)** At 1 week, all genotypes showed normal cortico-medullary junction (CMJ) organization. **(C)** By 2 weeks, *lacZ/lacZ* and *lacZ/nu* thymi had a noticeable decrease in cortical area, and *lacZ/nu* also showed initial CMJ disorganization. **(D)** CMJ disorganization began at 3 weeks in *lacZ/lacZ*, while *lacZ/nu* degeneration progressed further. **(E)** All phenotypes were progressive at 4 weeks. Scale bar in the upper panel of (A): 1 mm, applies to all upper panels. Scale bar in the lower panel of (A): 100 μm, applies to all lower panels. (**F**) Thymus weights of different genotypes at newborn and 5 weeks. Newborn +/+ and *lacZ/lacZ* have similar thymus weight, but thymus weight of +/nu is significantly lower ($p<0.05$). At 5 weeks, there is a gradient of thymus weight correlated to the dosage of Foxn1. Thymus weights are significantly different between any two genotypes; p value for the most similar measurements is shown on the graph.

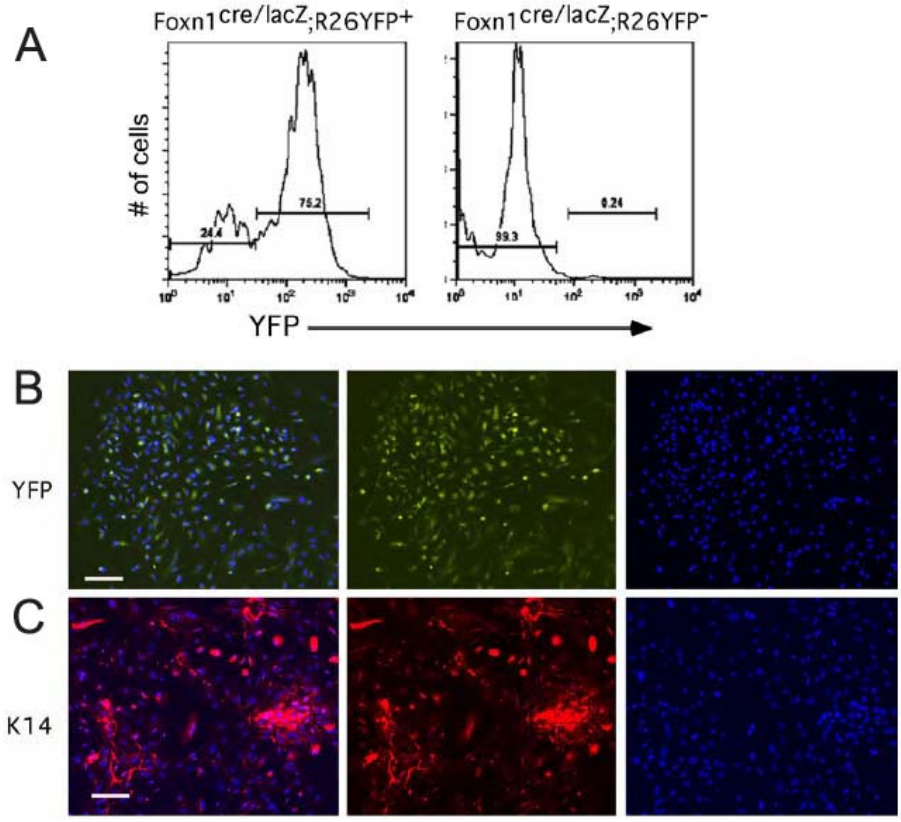
A
Foxn1cre/lacZ;R26YFP+
Foxn1cre/lacZ;R26YFP-
# of cells
75.2
24.4
99.3
0.24
YFP
B
YFP
C
K14

Fig. S3.2

Fig. S3.2. Primary cultures of thymic stromal cells (TSCs) contain mostly thymic epithelial cells (TECs). (**A**) Cultured TSCs derived from *Foxn1cre/lacZ;R26YFP* mice were analyzed for YFP with flow cytometry. More than 70% of the total cultured TSCs are YFP^+ cells, which are TEC lineage cells. (**B**) Most of the cultured TSCs of *Foxn1cre/lacZ;R26YFP* mice are YFP^+. (**C**) Cultured TSCs stained for the expression of Keratin 14, a marker for medullary TECs. The majority of the cells are $K14^+$.

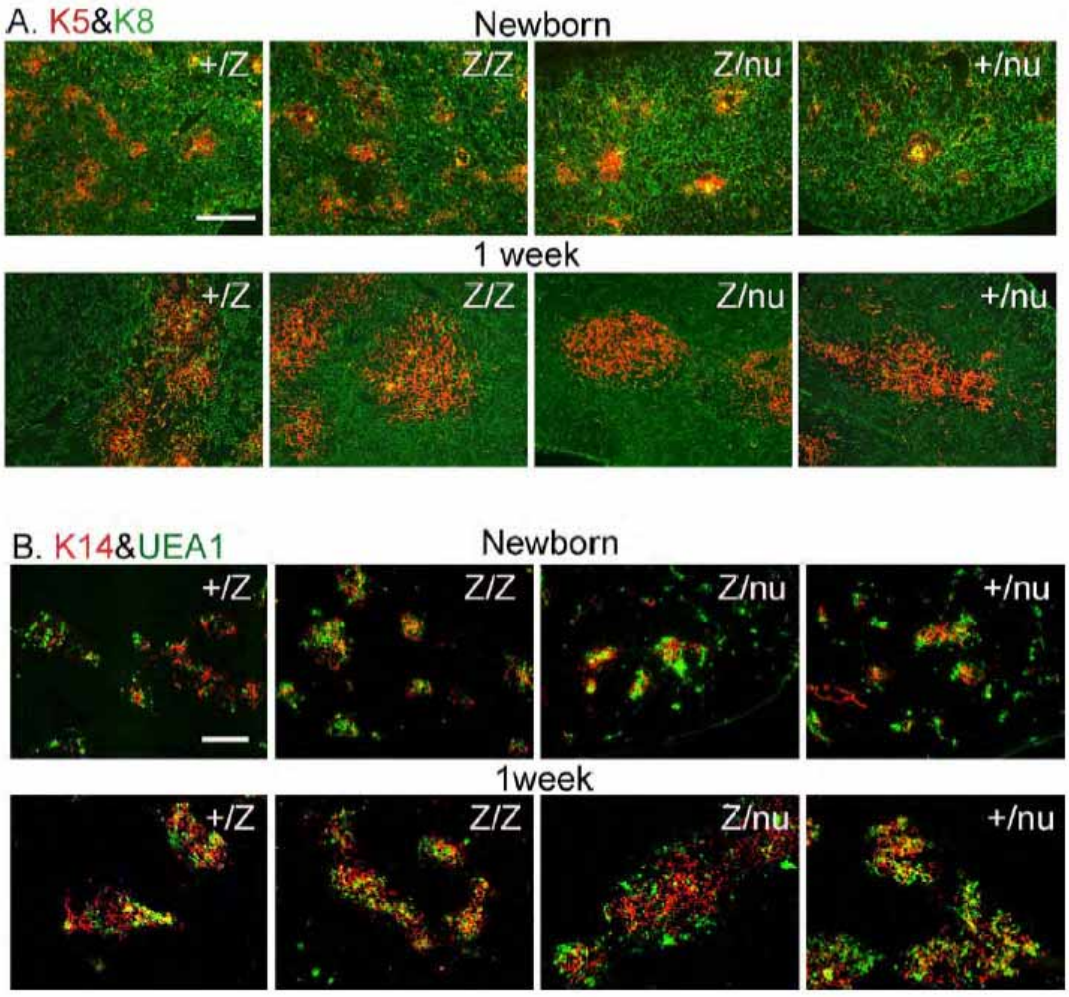
A. K5&K8
Newborn
+/Z
Z/Z
Z/nu
+/nu
1 week
+/Z
Z/Z
Z/nu
+/nu
B. K14&UEA1
Newborn
+/Z
Z/Z
Z/nu
+/nu
1week
+/Z
Z/Z
Z/nu
+/nu

Fig. S3.3

Fig. S3.3. The epithelial architecture in *Foxn1*^{lacZ} thymus is relatively normal at newborn and 1 week. Cryosections of *+/lacZ, lacZ/lacZ, lacZ/nu* and *+/nu* thymi at newborn and 1week were stained with anti-Keratin8 (green) and anti-Keratin5 (red) (**A**) or with anti-Keratin 14 (red) and UEA-1 (green) (**B**). Small, proto-medullary regions were seen at newborn, and clearly defined organized medullary compartments were formed at 1 week in all four genotypes. Note scattered UEA-1^{+} cells in newborn *+/nu* and *lacZ/nu* thymi due to the haploinsufficiency of the *nu* allele. Scale bar: 200 μm, applies to all panels.

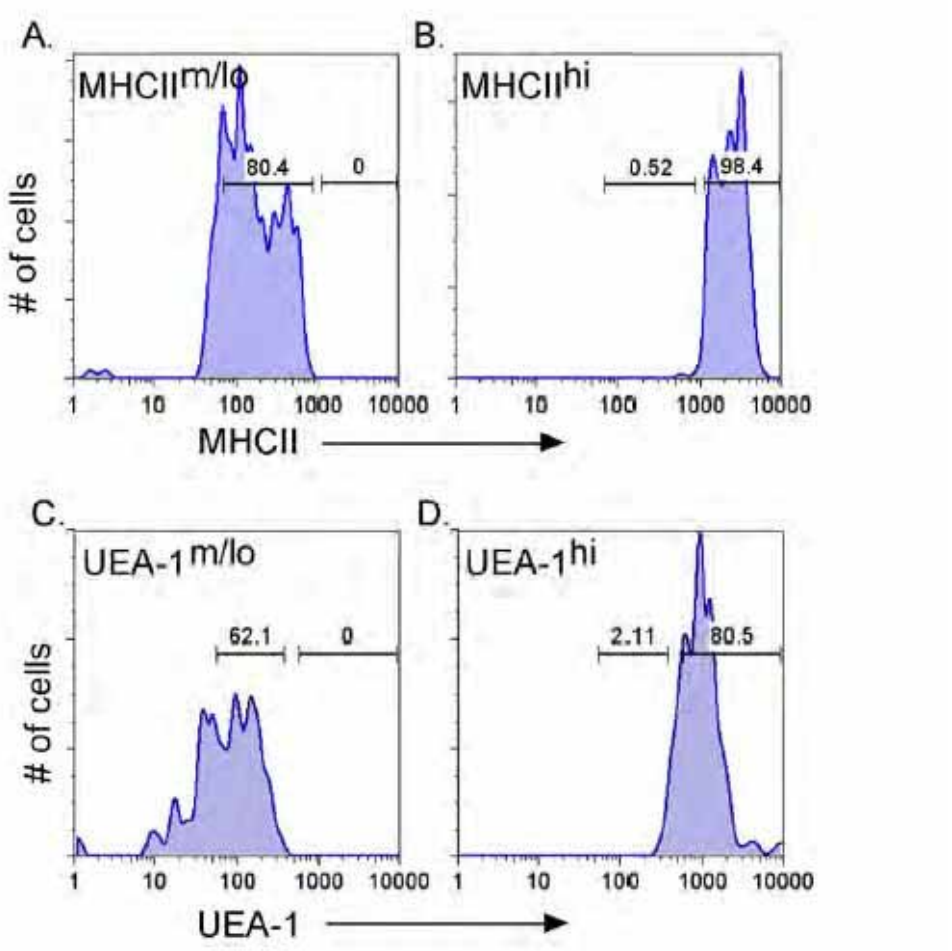
A.
MHCII m/lo
80.4
0
# of cells
1
10
100
1000
10000
MHCII
B.
MHCII hi
0.52
98.4
C.
UEA-1 m/lo
62.1
0
UEA-1
D.
UEA-1 hi
2.11
80.5

Fig. S3.4

Fig. S3.4. Sorting gates of TEC subsets shown in Figure 2D. Gated CD45- thymic stromal cells from 4 weeks old +/+ mice were sorted with flow cytometry for MHCII^{high} versus MHCII$^{middle/low}$ and for UEA-1^{high} versus UEA-1$^{middle/low}$. Sorted cells were checked for purity: MHCII$^{middle/low}$ (**A**), MHCII^{high} (**B**), UEA-1$^{middle/low}$ (**C**) and UEA-1^{high} (**D**).

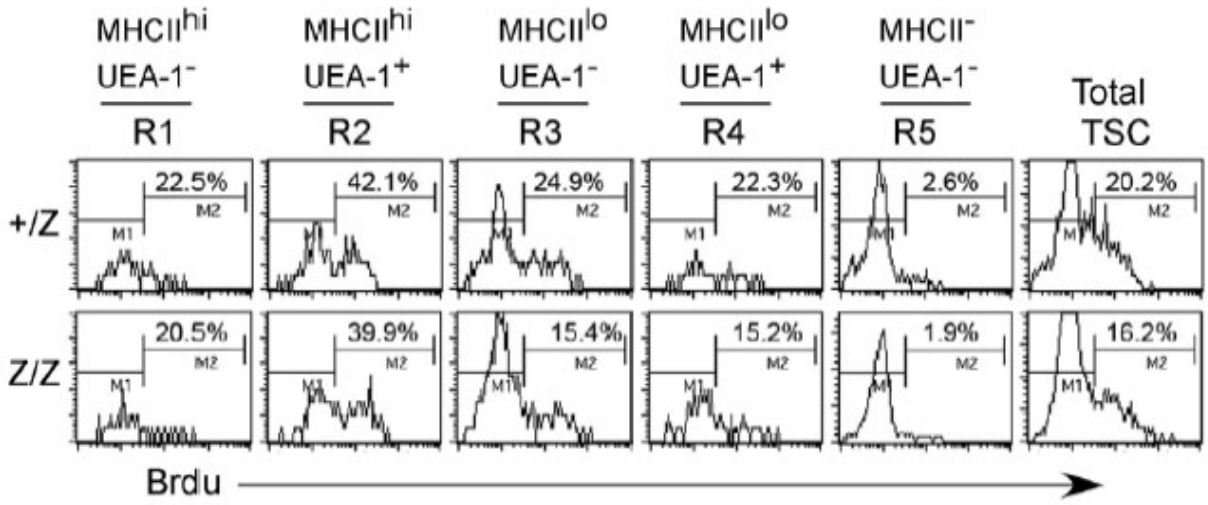
MHCII^hi UEA-1^- R1
MHCII^hi UEA-1^+ R2
MHCII^lo UEA-1^- R3
MHCII^lo UEA-1^+ R4
MHCII^- UEA-1^- R5
Total TSC
+/Z
Z/Z
22.5%
42.1%
24.9%
22.3%
2.6%
20.2%
20.5%
39.9%
15.4%
15.2%
1.9%
16.2%
M1
M2
Brdu

Fig. S3.5

Fig. S3.5. BrdU analysis of TSC from 1 month old *+/lacZ* and *lacZ/lacZ* thymus. $CD45^-$ cells were gated and stained for UEA-1 and MHCII expression. Total TSC and specific subsets as shown in Figure 4E were analyzed for the percentage of $BrdU^+$ cells. A summary of these data is shown in Figure 4F.

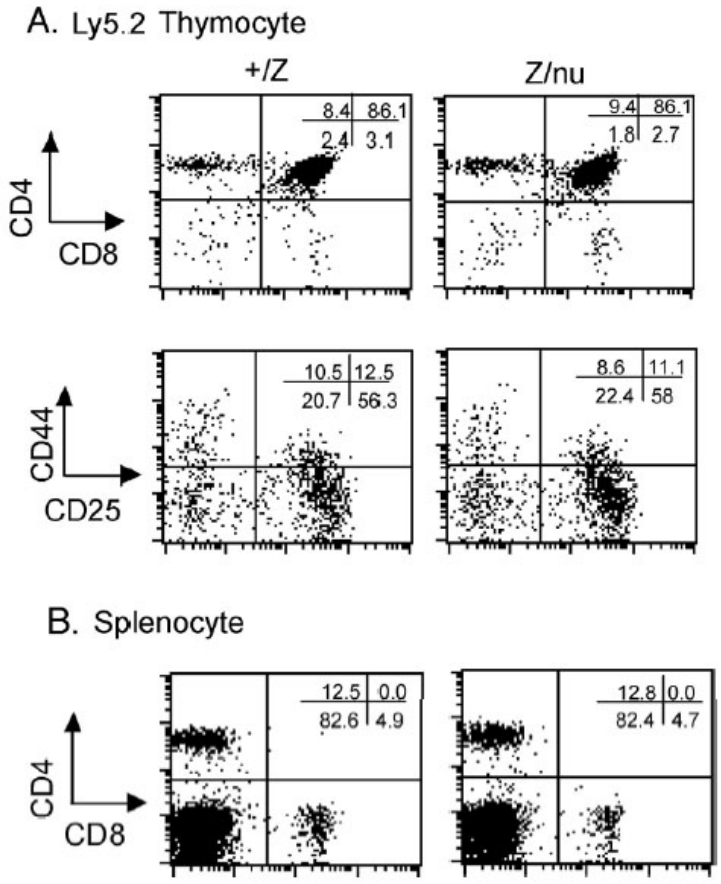
A. Ly5.2 Thymocyte
+/Z
Z/nu
8.4
86.1
2.4
3.1
9.4
86.1
1.8
2.7
CD4
CD8
10.5
12.5
20.7
56.3
8.6
11.1
22.4
58
CD44
CD25
B. Splenocyte
12.5
0.0
82.6
4.9
12.8
0.0
82.4
4.7
CD4
CD8

Fig. S3.6

Fig. S3.6. The hemopoietic cells in *Foxn1*^{lacZ} mutant are not affected. Bone marrow of adult *+/lacZ* and *lacZ/nu* mice were transferred into irradiated BL6Ly5.1 mice. (**A**) Ly5.2^{+} thymocytes were analyzed 4 weeks after reconstitution for CD4 and CD8 expression, and gated CD4^{-}CD8^{-} cells were analyzed for CD44 and CD25 expression. (**B**) Splenocytes were also analyzed as controls.

CHAPTER 4

CONCLUSIONS AND DISCUSSION

Developmental biologists seek to understand how body shape and pattern can be affected by changes in gene expression and function. Evolutionary biologists are interested in understanding how modulations in gene expression pattern and function contribute to morphological changes during evolution. During my Ph.D studies, I have been fortunate to have an opportunity to study the development of mouse pharyngeal organs, including the organogenesis and maintenance of the differentiated organs. In the process, I have been exposed to the evolutionary aspects of these organs and the genes involved. The first section of this thesis study focused on testing the conservation of Hoxa3 gene function in the development of pharyngeal pouches and arches derived organs and tissues, and revealed non-equivalent protein function between zebrafish and mouse HoxA3 proteins. The second section focused on the function of Foxn1 in the postnatal thymus and demonstrated that Foxn1 is required for the maintenance of postnatal thymus structure and function in a dosage-sensitive manner.

How conserved is the function of Hoxa3 gene during evolution?

Hox genes play conserved function cross phyla in patterning the body plan during embryogenesis. In all bilaterian animals, Hox genes are responsible for defining positional

identity along the A-P axis and paraxis (McGinnis and Krumlauf, 1992; Wagner et al., 2003). Numerous genetic complementary studies cross species have shown the functional conservation between orthologous Hox proteins. However, the majority of these studies were done by expressing a vertebrate Hox gene in Drosophila, and in most cases, the vertebrate Hox genes function equivalently to their homologs in Drosophila. To our knowledge, this is the first time that a Hox gene from an evolutionarily "lower" organism is expressed in a "higher" organism by precise gene swapping.

Our results show that the mouse HoxA3 protein and zebrafish HoxA3a protein share conserved functions, but they also possess diverged functions. This suggests that mouse Hox gene might have acquired novel functions onto the more ancestral protein function, or zebrafish Hox gene might have lost some of the ancestral function since the divergence of mouse and zebrafish. The genome wide duplication that occurred in the teleost fish lineage generated Hoxaa and Hoxab clusters. Subsequently, Hoxa3 function could be subfunctionalized into Hoxa3a and Hoxa3b genes, followed by the loss of Hoxa3b gene. It is also possible that part of the ancestral Hoxa3 function could be acquired by other paralogous Hox3 genes in zebrafish. Our data also suggest that the functional difference between mouse and zebrafish HoxA3 proteins resides mainly in the C-terminal domain.

The functional non-equivalence between orthologous Hox proteins revealed in this study provides additional evidence of functional evolution of Hox proteins during vertebrate evolution. Although there is a large body of evidence supporting the prevailing model that changes in gene regulation is the predominant driving force of morphological evolution (Carroll et al., 2005;

Gellon and McGinnis, 1998; Lynch and Wagner, 2008; Pearson et al., 2005; Wray, 2007), more evidence, including this thesis study, is emerging to show the importance of the evolution of the protein function (Galant and Carroll, 2002; Lynch and Wagner, 2008; Ronshaugen et al., 2002; Vervoort, 2002), challenging the prevailing notion.

We have also studied the conservation of the expression patterns between mouse and zebrafish Hoxa3 genes (Appendix). Like mouse Hoxa3, zebrafish Hoxa3a is expressed in both the pharyngeal arch mesenchyme and pouch endoderm. Interestingly, Hoxa3 expression in pouch endoderm seems to be correlated with the existence of thymus in higher vertebrates. In lamprey, a jawless vertebrate, Hox3 gene expression is only observed in pharyngeal arches, but not in the pouches (unpublished data of Manley Lab). This is compatible with the hypothesis that acquisition of Hoxa3 expression in pharyngeal pouch endoderm might be involved in the evolution of pharyngeal organs.

It immediately becomes very important to know what the function of Hoxa3a gene is in zebrafish development. Is it required for thymus formation like mouse Hoxa3? The most direct way to answer this question is to check whether thymus development is affected in the animals with deficient Hoxa3a function. Since my data demonstrates that morpholino knockdown is not a useful approach to study gene function at late stage of embryogenesis (appendix), a genetic approach is needed. Two *Hoxa3a* mutant transgenic zebrafish lines with insertions into Hoxa3a exons have recently become available at Znomics Inc. We will soon be able to test whether Hoxa3a is required for the development of pharyngeal apparatus in zebrafish, and whether the Hoxa3 gene has conserved function in thymus formation during vertebrate evolution.

In this thesis study, we have demonstrated that mouse and zebrafish HoxA3 proteins possess conserved and diverged functions. It will be very informative to extend this study to a broader scope. Using the backbone of the targeting vector that I have generated, we can replace mouse Hoxa3 gene with orthologs from different species, such as lobe fin fishes and invertebrates. I actually have generated a targeting vector for the replacement with amphioxus Hox3 gene. We will then be able to compare the function of Hox proteins from different species, when expressed from the same biological context. This will shed light on our understanding of the functional evolution of Hox proteins.

One interesting common feature of Hox3 proteins is the large C-terminal domain, which is not found in other Hox groups except for Hox2. Our data from the chimeric protein indicate that the functional difference between mouse and zebrafish HoxA3 proteins largely lies in the C-terminal domain. It will be of great interest to test the function of the other chimeric protein consists of zebrafish N-terminal and mouse C-terminal domains. So far, little is known about the biological function of the large C-terminal domain of group3 Hox proteins. Alignment of HoxA3 protein sequences of different species will aid us in identifying the evolutionarily conserved sequence and motifs. Combination of biochemistry assays and mutation analyses will provide valuable information to determine the function of the C-terminal domain.

Foxn1 function in thymus maintenance and involution

Despite the critical roles that thymus plays in the immune system, thymus function deteriorates with progressive aging. In addition to aging, many other physiological and pathological alterations affect thymus structure and function. For instance, puberty, pregnancy,

inflammation, exercise, bacterial and viral infections, and stress have all been reported to affect thymus size and thymocyte number (Taub and Longo, 2005). Although the expression level of many genes have been found altered in the involuted thymus, the molecular mechanism of the maintenance and involution of a differentiated thymus remains poorly understood.

Foxn1, the gene mutated in the nude mice (Nehls et al., 1996), has been studied for over a decade. Analyses on the null and hypomorphic *Foxn1* mutants have shown that the function of *Foxn1* is required for the initiation of TEC differentiation in a cell-autonomous manner, hence it is required for thymus organogenesis (Blackburn et al., 1996; Su et al., 2003). However, due to the lack of a conditional knock-out allele, the function of Foxn1 in the differentiated thymus has not been studied.

In this study, a novel *Foxn1* mutant allele, $Foxn1^{lacZ}$ was used to dissect the postnatal Foxn1 function in thymus. Foxn1 expression and thymus development is normal in the $Foxn1^{lacZ/lacZ}$ mice at fetal and newborn stages (Gordon et al., 2007). However expression from $Foxn1^{lacZ}$ allele is gradually reduced, making this allele a useful tool to test Foxn1 function in postnatal thymus. We showed that down-regulation of *Foxn1* below 50% of normal mRNA expression levels caused thymic compartment degeneration, loss of specific TEC subsets, and reduced T cell production. Thus, our results provide the first functional evidence that Foxn1 is required to maintain the postnatal thymus.

We have compared the postnatal thymus phenotype of the following six genotypes: +/+, *+/lacZ*, *+/nu*, *lacZ/lacZ*, *lacZ/nu* and *nu/nu*, we found a close correlation between the Foxn1 dosage and the thymic phenotype. *+/lacZ* and *+/nu*, in which the Foxn1 expression level is over

50% of the +/+, have a very mild thymic defect. With a Foxn1 expression level as about 30-40% of wild-type, *lacZ/lacZ* mutant shows a quite severe thymic phenotype. When the Foxn1 expression drops to around 15-20% of wild-type, we see the most severe phenotype in the *lacZ/nu* thymi. This suggests that TECs are extremely sensitive to the change of Foxn1 dosage, especially when the dosage is lower than a certain amount that could be regarded as a threshold.

It has been reported previously that Foxn1 is expressed in most, if not all, of the TEC subsets at both fetal and adult stages (Gordon et al., 2007; Liston et al., 2007; Nehls et al., 1996). However, another study with Foxn1 antibody has suggested that Foxn1 is only expressed in 20% of adult TECs (Itoi et al., 2007). These controversial results then raise the possibilities that different subsets might have different expression levels of Foxn1, and that low level of Foxn1 expression might not be detectable by Foxn1 antibody. Our data has showed that MHCII^{hi} and UEA-1^{hi} TEC subsets express higher level of Foxn1 than the other TEC subsets, supporting the notion that Foxn1 expression is not uniform in all TECs, and the expression level might be dynamic during thymus development.

As different TEC subsets express Foxn1 at different levels, and play different functions in T cell development (Blackburn and Manley, 2004), it will be interesting to test whether different TEC subsets react distinctly to the loss of Foxn1. A conditional *Foxn1* allele will be very useful to address this question. By crossing to specific Cre lines, Foxn1 can be knocked out in specific TEC subgroups in order to determine the function of Foxn1 in those TECs. In addition, by using

Cre lines with temporal control (e.g. tamoxifen-Cre), we will be able to study Foxn1 function at specific stages.

In this study we have shown that loss of Foxn1 in the differentiated thymus leads to thymus degeneration resembling premature thymus aging. On the other hand, reduced Foxn1 expression has been reported in aged thymic stroma (Ortman et al., 2002). It then raises the questions: is Foxn1 involved in the regulation of aging-associated thymic involution? Can loss of Foxn1 trigger thymic involution? A gain-of-function study is needed to confirm the function of Foxn1 in maintenance of postnatal thymus structure and function. It will also be important to test whether over-expression of Foxn1 could delay, prevent or even reverse thymic involution. If diminished Foxn1 expression contributes to aging-related thymic involution, what is the mechanism by which Foxn1 is down-regulated? Our data suggest that altered methylation might be involved in regulating the expression from *Foxn1*^{lacZ} allele. But whether methylation is involved in normal Foxn1 regulation requires additional study.

REFERENCES

Blackburn, C. C., Augustine, C. L., Li, R., Harvey, R. P., Malin, M. A., Boyd, R. L., Miller, J. F. and Morahan, G. (1996). The nu gene acts cell-autonomously and is required for differentiation of thymic epithelial progenitors. *Proc Natl Acad Sci U S A* **93**, 5742-6.

Blackburn, C. C. and Manley, N. R. (2004). Developing a new paradigm for thymus organogenesis. *Nat Rev Immunol* **4**, 278-89.

Carroll, S. B., Grenier, J. K. and Weatherbee, S. D. (2005). From DNA To Diversity. In *Blackwell Science*, (ed., pp. 1-258.

Galant, R. and Carroll, S. B. (2002). Evolution of a transcriptional repression domain in an insect Hox protein. *Nature* **415**, 910-3.

Gellon, G. and McGinnis, W. (1998). Shaping animal body plans in development and evolution by modulation of Hox expression patterns. *Bioessays* **20**, 116-25.

Gordon, J., Xiao, S., Hughes, B., 3rd, Su, D. M., Navarre, S. P., Condie, B. G. and Manley, N. R. (2007). Specific expression of lacZ and cre recombinase in fetal thymic epithelial cells by multiplex gene targeting at the Foxn1 locus. *BMC Dev Biol* **7**, 69.

Itoi, M., Tsukamoto, N. and Amagai, T. (2007). Expression of Dll4 and CCL25 in Foxn1-negative epithelial cells in the post-natal thymus. *Int Immunol* **19**, 127-32.

Liston, A., Farr, A. G., Chen, Z., Benoist, C., Mathis, D., Manley, N. R. and Rudensky, A. Y. (2007). Lack of Foxp3 function and expression in the thymic epithelium. *J Exp Med* **204**, 475-80.

Lynch, V. J. and Wagner, G. P. (2008). Resurrecting the role of transcription factor change in developmental evolution. *Evolution* **62**, 2131-54.

McGinnis, W. and Krumlauf, R. (1992). Homeobox genes and axial patterning. *Cell* **68**, 283-302.

Nehls, M., Kyewski, B., Messerle, M., Waldschutz, R., Schuddekopf, K., Smith, A. J. and Boehm, T. (1996). Two genetically separable steps in the differentiation of thymic epithelium. *Science* **272**, 886-9.

Ortman, C. L., Dittmar, K. A., Witte, P. L. and Le, P. T. (2002). Molecular characterization of the mouse involuted thymus: aberrations in expression of transcription regulators in thymocyte and epithelial compartments. *Int Immunol* **14**, 813-22.

Pearson, J. C., Lemons, D. and McGinnis, W. (2005). Modulating Hox gene functions during animal body patterning. *Nat Rev Genet* **6**, 893-904.

Ronshaugen, M., McGinnis, N. and McGinnis, W. (2002). Hox protein mutation and macroevolution of the insect body plan. *Nature* **415**, 914-7.

Su, D. M., Navarre, S., Oh, W. J., Condie, B. G. and Manley, N. R. (2003). A domain of Foxn1 required for crosstalk-dependent thymic epithelial cell differentiation. *Nat Immunol* **4**, 1128-35.

Taub, D. D. and Longo, D. L. (2005). Insights into thymic aging and regeneration. *Immunol Rev* **205**, 72-93.

Vervoort, M. (2002). Functional evolution of Hox proteins in arthropods. *Bioessays* **24**, 775-9.

Wagner, G. P., Amemiya, C. and Ruddle, F. (2003). Hox cluster duplications and the opportunity for evolutionary novelties. *Proc Natl Acad Sci U S A* **100**, 14603-6.

Wray, G. A. (2007). The evolutionary significance of cis-regulatory mutations. *Nat Rev Genet* **8**, 206-16.

APPENDIX

EXPRESSION AND FUNCTIONAL ANALYSIS OF *HOX* GROUP 3 GENES IN ZEBRAFISH PHARYNGEAL DEVELOPMENT

ABSTRACT

Hox genes play conserved functions in patterning the anterior-posterior axis during embryogenesis. They are expressed in both the axial and paraxial tissues with a highly conserved expression pattern cross phyla. Mouse *Hox* Group 3 genes have been shown to regulate the development of many organs derived from pharyngeal pouches, including thymus, thyroid and parathyroid. All three paralogous group 3 *Hox* genes are expressed in the pharyngeal arch mesenchyme, but only *Hoxa3* is expressed in the pouch endoderm. Hoxa3 deficient mouse lacks thymus and parathyroid, which are derived from pharyngeal pouch endoderm. Zebrafish and mouse share similar pharyngeal structures and several conserved molecular regulators expressed in these structures. However the expression pattern and the function of zebrafish *Hox3* genes in zebrafish pharyngeal development remain to be characterized. In this study, in situ hybridization was used to study the expression pattern. And we found the expression patterns of *Hoxa3a*, *Hoxb3a* and *Hoxd3a* are very similar. We then used morpholino mediated knockdown approach to investigate whether zebrafish *Hoxa3a* plays evolutionarily conserved function in thymus development. Co-injection of morpholinos specific to Hoxa3a and Hoxb3a had no phenotypic consequence on thymus organogenesis. Further analysis revealed that the morpholino was able to suppress Hox3 gene expression effectively by 24hpf, but not at 48hpf or later. Therefore, morpholino knock-down is not an effective approach to study thymus development, which initiates at about 48hpf.

INTRODUCTION

PG3 Hox genes in mouse are expressed in the developing hindbrain with the cranial limit of rhombomere 4/5, and also expressed in the neural crest emanating from r6 and posterior (Manley and Capecchi, 1995; Sham et al., 1992). All three PG3 *Hox* genes in mouse are expressed in the third and fourth pharyngeal arch mesenchyme, but only *Hoxa3* is expressed in the pharyngeal pouch endoderm (Manley and Capecchi, 1995). *Hoxa3* mutant mouse shows a spectrum of defects in the pharyngeal apparatus, including deletion of thymus and parathyroid, deletion and malformation of the throat cartilages and disorganization of the throat musculature and trachea epithelium (Chisaka and Capecchi, 1991; Manley and Capecchi, 1995).

In mouse, thymus derives from the ventral and posterior part of the third pharyngeal pouch endoderm (Gordon et al., 2001; Gordon et al., 2004). The interaction between pouch endoderm and arch mesenchyme is required for the formation of thymus premordium (Manley, 2000). At E10.5, the third pouch starts to bud out and forms a thymic rudiment, which consists of epithelial cells and is surrounded by neural crest-derived capsule. Around E11-E11.5, T-lymphocyte precursors originated from bone marrow start to invade the thymic rudiment. And at E12.5, the T cell-dependent differentiation of thymic epithelial cell initiates. At least part of the function of Hoxa3 in thymus development may be via its regulation of Pax1 and Pax9 in the third pouch endoderm. In *Hoxa3* mutants, the expression of Pax1 and Pax9 at the third pouch is down-regulated (Manley and Capecchi, 1995). Mutations of *Pax1* and *Pax9* show defects in thymus development (Peters et al., 1998; Su and Manley, 2000; Wallin et al., 1996). *Pax1/9* are evolutionarily conserved molecular markers expressed throughout the pharyngeal pouch

endoderm (Hetzer-Egger et al., 2002; Holland et al., 1995; Nornes et al., 1996; Ogasawara et al., 2000; Ogasawara et al., 1999). *Foxn1* is one of the best known genes that are involved in thymus development. *Foxn1* marks the thymus primordium during organogenesis in mouse (Gordon et al., 2001). It is expressed in thymic epithelial cells (TECs) and required cell-autonomously for differentiation of TECs (Blackburn et al., 1996). Another marker gene of thymus development is the recombination activating genes, including *Rag-1* and *Rag-2*, which are expressed in T cells and required for the variable diverted junction (VDJ) recombination of T cell receptor.

The process of thymus development and the molecular regulators involved in thymus development in zebrafish and mouse are overall conserved (Lam et al., 2002; Trede et al., 2004). Ectodermal and endodermal cells are indispensable for thymus organogenesis in zebrafish (Trede et al., 2001). For instance, mutation in an endoderm-expressing gene, *gata5*, results in severe defect in thymus formation (Reiter et al., 2001). Expression of *ikaros*, a transcription factor required for lymphoid development, is detected in zebrafish thymus by 72hpf (Willett et al., 2001). Zebrafish thymic development initiates at about 48hpf, but the first morphologically visible sign of thymic development is the formation of an alymphoid thymic primordium in the third pharyngeal pouch at about 60 hpf (Willett et al., 1999; Willett et al., 1997). T cell precursors start to invade the thymic rediment at 68hpf. From 72hpf, expression of Rag-1 and Rag-2 can be detected in the thymus (Jessen et al., 2001; Jessen et al., 1999). Zebrafish *Foxn1* orthologous gene was also found to be expressed in the presumptive thymic primordium in the third brachial pouch as early as 72hpf (Schorpp et al., 2002).

Although the function of Hoxa3 gene in mouse thymus formation is well characterized, the function of its orthologue in zebrafish thymus development was not known. In this study, we show that PG3 Hox genes are expressed in similar patterns in zebrafish. *Hoxa3a* and *Hoxb3a* are both expressed in the pharyngeal pouch endoderm, conserved with *Hoxa3* in mouse. To investigate the function of *Hoxa3a* and *Hoxb3a* in thymic formation, we knocked-down the expression of both genes with morpholino. However, co-injection of the splicing-suppressing morpholinos had no affect on thymus formation. Further analysis showed that the morpholinos were not able to suppress the target gene expression after 48hpf. Thus, morpholino knock-down is not an effective approach to study thymus organogenesis in zebrafish, which initiates at about 48hpf.

RESULT

Hoxa3a is expressed in pharyngeal pouch endoderm

We first investigated the expression pattern of *Hoxa3a* in zebrafish embryo. In both mouse and zebrafish, the thymus organ develops from the pharyngeal pouch endoderm. *Hoxa3* is expressed in the pouch endoderm and required for thymus formation in mouse (Chisaka and Capecchi, 1991; Manley and Capecchi, 1995). Therefore to understand the role of the *Hoxa3* orthologoues gene in zebrafish thymus organogenesis, it is important to examine whether it is expressed in pouch endoderm. Previous study has shown that zebrafish Hoxa3a is expressed broadly throughout the pharyngeal region, including ectoderm and mesenchyme, at 24 hpf to 48 hpf (Hogan et al., 2004). To extend the study to pouch endoderm and to later stages, fish embryos of different stages were analyzed. At 60hpf, Hoxa3a is expressed in the hindbrain with the anterior

expression boundary at rhombomere4 and 5 (Fig. 1A), which is conserved with mouse *Hoxa3*. In addition, it's also strongly expressed in the pharyngeal region. Sagital sections showed the expression in the pharyngeal arch 3 and posterior, in both of the pouch endoderm and arch mesenchyme (Fig. 1B). At 72hpf, the expression pattern remained similar to 60 hpf, in both pouch endoderm and arch mesenchyme (Fig. 1C, 1D).

Paralogous Group3 *Hox* genes are expressed in similar patterns

As a result of genome-wide duplication and gene loss, zebrafish has four of PG3 *Hox* genes, *Hoxa3a, Hoxb3a, Hoxc3a* and *Hoxd3a* (Amores et al., 2004). Functional redundancy of the *Hox* genes in the same paralogous group is another consequence of duplication. We then examined the expression patterns of the other PG3 *Hox* genes. *Hoxb3a* is expressed in the hindbrain with a more anterior rhombomere boundary compared to *Hoxa3a* (Fig. 2B), which is consistent with previous studies on zebrafish (Hogan et al., 2004) and fugu (Amores et al., 2004). Like *Hoxa3a, Hoxb3a* is expressed in the third and more posterior pharyngeal arch mesenchyme and pouch endoderm (Fig. 2D, 2E). The expression patterns of Hoxd3a were also checked. Hoxd3a showed a similar pattern as Hoxa3a in the hindbrain and pharyngeal region (Fig. 2C). Overall, the PG3 *Hox* genes in zebrafish share highly overlapping expression patterns.

Injection of Hoxa3a morpholino has no phenotypic subsequence in thymus formation

Morpholino knock-down approach was used to determine whether PG3 *Hox* genes are required for thymus development in zebrafish. First we designed the morpholino specific to the splicing donor site of *Hoxa3a* gene. 2.5-10 ng of morpholino was injected into the embryo at

the 1-cell stage, the morphants were then analyzed for Rag-1 expression. *Rag-1* is required for T cell development and can mark the thymus organ in the developing zebrafish embryos. We then looked at Rag-1 expression in the Hoxa3a splicing donor morphants to see whether thymus development was affected. Rag-1 expression was detected in *Hoxa3a* morphants and the size of the Rag-1 positive region was similar to controls (Fig. 3A-D).

To further knock-down Hoxa3a expression, a morpholino specific to the splicing acceptor was co-injected into the embryos with the splicing donor morpholino. However co-injection of two morpholinos did not affect Rag-1 expression in the morphants (Fig. 3E, 3F). *Hox* genes of the same paralogous group often function redundantly. For instance, *Hoxa2* and *Hoxb2* are functionally redundant for hyoid arch patterning (Hunter and Prince, 2002). Given that *Hoxb3a* is also expressed in the pouch endoderm, it is very likely that *Hoxb3a* might function redundantly with *Hoxa3a* in thymus development. We then co-injected a morpholino specific to Hoxb3a gene to knock-down both Hoxa3a and Hoxb3a. The *Hoxa3/Hoxb3* morphants showed normal Rag-1 expression (Fig. 3G, 3H), indicating that thymus development was not affected by the injection of Hoxa3a and Hoxb3a morpholinos.

Morpholinos fail to suppress Hox3 expression at 48hpf

Although the *Hoxa3a/Hoxb3a* morphants had a normal Rag-1 expression, it is not sufficient to conclude that Hoxa3a and Hoxb3a are not required for thymus development, because the morpholinos might not be efficient to suppress the expression of target genes. To test this possibility, we assayed for Hoxa3a and Hoxb3a mRNA products before and after splicing (Fig. 4B). In the 24hpf control embryos, the majority Hoxa3a mRNA product was

spliced, and only a small portion of it contained the intron (Fig. 4C). But in the Hoxa3a morphants, most of Hoxa3a mRNA remained un-spliced, with only a small amount of spliced product detected. Therefore, the Hoxa3a morpholino was sufficient to suppress the target gene splicing by 24hpf. Hoxb3a splicing was also analyzed. Like Hoxa3a, the splicing of Hoxb3a was greatly inhibited in the morphants at 24hpf (Fig. 4C).

We then further tested the efficiency of the morpholino at 48hpf. Again RT-PCR was used to analyze the splicing of mRNA products. Strikingly, the Hoxa3a mRNA splicing was dramatically restored in the morphants at 48hpf (Fig. 4D), showing that the morpholino was no longer sufficient to suppress the target gene splicing at 48hpf. Taken together, these data suggest that the morpholino is efficient to knock-down target gene expression at early embryo development, but the morpholino might be gradually saturated during the embryo develops. Given that thymus organogenesis initiates after 48hpf, when the morpholino is not sufficient to suppress target gene expression, morpholino knock-down might not be an efficient approach to study the function of *Hox3* genes in thymus development.

DISCUSSION

Hoxa3 expression pattern and thymus evolution

Thymus organ originates from the pharyngeal pouch, an embryonic structure found in all vertebrates. The morphologic features and the molecular regulators in the development of this structure are evolutionarily conserved. The pharyngeal pouches are bilateral diverticula of the foregut endoderm and will develop into different structures in different organisms, such as gills, thyroid, parathyroid and thymus. Group I Pax genes (Pax1 and Pax9) are found expressed in the

pharyngeal pouches in all chordates tested, and have been identified as molecular markers for gill formations. In gnathostom vertebrates *Hox* genes are expressed in the neural crest cells that migrate from the mid or hindbrain into pharyngeal arches to form the arch mesenchyme. Besides the expression in the pharyngeal arch, mouse *Hoxa3* is also expressed in the pharyngeal pouch endoderm, which gives rise to the thymus organ. But the other two mouse PG3 *Hox* genes are not expressed in the pouch endoderm (Manley and Capecchi, 1995). Mouse *Hoxa3* is required for thymus organogenesis, whereas *Hoxb3* and *Hoxd3* are dispensable for thymus development (Condie and Capecchi, 1993; Manley and Capecchi, 1997). It has been reported that PG3 *Hox* genes are not expressed in the pharyngeal pouches of lamprey, an organism that has no thymus organ. Our result in this study showed that zebrafish *Hoxa3a* and *Hoxb3a* are both expressed in the pharyngeal pouch endoderm. Therefore, the expression of Hoxa3 gene in pharyngeal pouch seems to correlate with the development of thymus in different organisms. Modulation of Hox gene expression has been identified to correlate with evolution of novel body plans. For instance, the loss of Hox gene expression in the mandibular arch is believed to drive the evolution of jaw (Kuratani, 2004). Taken together, expression of Hoxa3 gene in the pharyngeal pouch endoderm might play an important role in the evolution of the thymus organ.

Functional study of *Hox3* genes in zebrafish thymus organogenesis

In this study we have used morpholino knock-down approach to study the function of PG3 *Hox* genes in zebrafish thymus organogenesis. We used splicing suppressing morpholinos to knock-down Hoxa3a and Hoxb3a expression. In deed, the morpholinos suppressed the splicing effectively by 24hpf. However, the morpholinos might be gradually saturated by the newly

synthesized mRNA, resulting in a failure of splicing suppressing at 48hpf. In zebrafish, thymus organogenesis initiates later than 48hpf, when the morpholino was not able to knock-down the target genes effectively. Therefore, morpholino knock-down is not an effective approach to study thymus organogenesis, despite of that it's a broadly used method to study gene function in early zebrafish embryogenesis. Mutagenesis is another wildly used approach to study gene function. Recently there are *Hoxa3a* mutant fish lines available from mutagenesis screening. In this mutants, part of the encoding exons are deleted. Therefore, these mutants would be better tools to dissect the function of *Hoxa3a* gene in thymus development.

MATERIALS AND METHODS

Zebrafish

Wild-type zebrafish stocks were held in University of Georgia using standard husbandry techniques. Collected embryos were incubated at 28°C in egg water [for some experiments, 0.003% 1-phenyl-2-thiourea (PTU) was added into the egg water from 12 h post-fertilisation (hpf).]

In situ hybridization and sections

In situ hybridization was performed as described previously [C. Thisse 1993]. Embryos were fixed 24 hours in 4% paraformaldehyde and dehydrated overnight in methanol at –20°C. Then the embryos were rehydrated stepwise in methanol/PBS and finally put back in 100% PBT (1 x PBS 0.1% Tween 20). Embryos were then treated with proteinase K (10 μg/ml in PBT) for 25 minutes (48hpf) or 30 minutes (72 hpf). The digestion was stopped by rinsing in glycine (2

mg/ml in PBT). Embryos were postfixed in 4% paraformaldehyde 1× PBS for 20 minutes and then washed in PBT 5 times for 5 minutes each. The embryos were prehybridized at least 1 hour before hybridization at 70°C overnight in hybridization buffer [50% formamide, 5× SSC, 50 μg/ml heparin, 500 μg/ml tRNA, 0.1% Tween 20, 9 mM citric acid]. Then the embryos were washed at 70°C for 15 minutes in [75% hybridization buffer, 25% 2× SSC], 15 minutes in [50% hybridization buffer, 50% 2× SSC], 10 minutes in [25% hybridization mix, 75% 2× SSC], 15 minutes in 2× SSC, 2 times 15 minutes in 0.2× SSC. Further washes were performed at room temperature for 10 minutes in [75% 0.2× SSC, 25% PBT], 10 minutes in [50% 0.2× SSC, 50% PBT], 5 minutes in [25% 0.2× SSC, 75% PBT], 10 minutes in PBT, and then 2 hours in [PBT with 2 mg/ml BSA, 2% sheep serum]. Then the embryos were incubated overnight at 4°C with the preabsorbed alkalinephosphatase-labelled anti-digoxigenin antiserum (Roche) at a 1/5000 dilution in a PBT buffer containing 2 mg/ml BSA, 2% sheep serum. The embryos were then washed 6 times for 15 minutes each in PBT at room temperature, followed by washing in staining buffer [100mM Tris HCl pH9.5, 50mM MgCl2, 100mM NaCl, 0.1% tween 20] 3 times for 5 minutes each. Color reaction was performed in BM purple AP substrate (Roche). When the color was developed, the reaction was stopped in 1× PBS/5mM EDTA. The whole-mount images were performed with a Leica MZ125 dissection scope and a Q imaging digital camera. The embryos were then embedded with 7.5% gelatin solution [7.5% gelatin, 15% sucrose in PBS] and sectioned into 10 um sections with cryostat. Imaging was done on a Zeiss microscope with Optronics digital camera.

Morpholino injection

Splicing-suppressing morpholinos were designed by Gene Tools LLC to complement the sequence around the splicing junction. The sequence of the morpholino (MO) is the following, the slash line represents the exon-intron junction.

Hoxa3a:

Splicing donor: 5'-GTGGTTGATGTAATCAC/CTGAAATG-3'

Splicing acceptor: 5'- GCGCAGCTCTCTA/CTGTATGAGTAC-3'

Hoxb3a:

Splicing donor: 5'-TTGGCAAACACAC/CATTAGCTGAGC-3'

The morpholinos, MOhoxa3a, MOhoxb3a and control morpholino, were microinjected (approximately 1 nl) at concentrations ranging from 2.5 to 10 mg/ml in phenol red buffer (0.25% Phenol Red, 120 mM KCl, 20mM Hepes-NaOH, pH 7.5)

RT-PCR

Morpholino-injected or control embryos at different stages were homogenized in trizol (Invitrogen) and total RNA was extracted according to the manual coming with trizol reagent. The total RNA was then incubated with DNaseI (Roche) at 37℃ for 20 minutes to remove any DNA from the RNA samples. The same amount of RNA from each sample was used for reverse transcription. First-strand cDNA was reverse transcribed with superscript III (Invitrogen) and random primers (Invitrogen), incubated at 42℃ for 90 minutes and then at 70℃ for 15 minutes. RNaseH and RNaseA (Promega) were used to remove RNA from the transcribed first-strand cDNA. Primers used in semi-quantitative PCR are as follow:

Hoxa3a exon fP: 5'- TACTGCCCCTTCTGGACCATC-3'

Hoxa3a exon rP: 5’- CATTCCAAGCCCCTTCTGGTC-3’

Hoxa3a intron rP: 5’- CAGACAACATATGACTGCGC-3’

Hoxb3a exon fP: 5’- CTATGGCCACAAACCCAACT-3’

Hoxb3a exon rP: 5’- ATCTTGATCTGCCGCTCACT-3’

ACKNOWLEDGEMENT

I wish to acknowledge Dr. James Lauderdale for letting me use the micro-injector in his lab. I am also grateful to Dr. Jorn Lakowski and Dr. Anirban Majumder for assistance on micro-injection.

REFERENCES

Amores, A., Force, A., Yan, Y. L., Joly, L., Amemiya, C., Fritz, A., Ho, R. K., Langeland, J., Prince, V., Wang, Y. L. et al. (1998). Zebrafish hox clusters and vertebrate genome evolution. *Science* **282**, 1711-4.

Amores, A., Suzuki, T., Yan, Y. L., Pomeroy, J., Singer, A., Amemiya, C. and Postlethwait, J. H. (2004). Developmental roles of pufferfish Hox clusters and genome evolution in ray-fin fish. *Genome Res* **14**, 1-10.

Blackburn, C. C., Augustine, C. L., Li, R., Harvey, R. P., Malin, M. A., Boyd, R. L., Miller, J. F. and Morahan, G. (1996). The nu gene acts cell-autonomously and is required for differentiation of thymic epithelial progenitors. *Proc Natl Acad Sci U S A* **93**, 5742-6.

Chisaka, O. and Capecchi, M. R. (1991). Regionally restricted developmental defects resulting from targeted disruption of the mouse homeobox gene hox-1.5. *Nature* **350**, 473-9.

Condie, B. G. and Capecchi, M. R. (1993). Mice homozygous for a targeted disruption of Hoxd-3 (Hox-4.1) exhibit anterior transformations of the first and second cervical vertebrae, the atlas and the axis. *Development* **119**, 579-95.

Condie, B. G. and Capecchi, M. R. (1994). Mice with targeted disruptions in the paralogous genes hoxa-3 and hoxd-3 reveal synergistic interactions. *Nature* **370**, 304-7.

Gordon, J., Bennett, A. R., Blackburn, C. C. and Manley, N. R. (2001). Gcm2 and Foxn1 mark early parathyroid- and thymus-specific domains in the developing third pharyngeal pouch. *Mech Dev* **103**, 141-3.

Gordon, J., Wilson, V. A., Blair, N. F., Sheridan, J., Farley, A., Wilson, L., Manley, N. R. and Blackburn, C. C. (2004). Functional evidence for a single endodermal origin for the thymic epithelium. *Nat Immunol* **5**, 546-53.
Hetzer-Egger, C., Schorpp, M., Haas-Assenbaum, A., Balling, R., Peters, H. and Boehm, T. (2002). Thymopoiesis requires Pax9 function in thymic epithelial cells. *Eur J Immunol* **32**, 1175-81.
Hogan, B. M., Hunter, M. P., Oates, A. C., Crowhurst, M. O., Hall, N. E., Heath, J. K., Prince, V. E. and Lieschke, G. J. (2004). Zebrafish gcm2 is required for gill filament budding from pharyngeal ectoderm. *Dev Biol* **276**, 508-22.
Holland, N. D., Holland, L. Z. and Kozmik, Z. (1995). An amphioxus Pax gene, AmphiPax-1, expressed in embryonic endoderm, but not in mesoderm: implications for the evolution of class I paired box genes. *Mol Mar Biol Biotechnol* **4**, 206-14.
Hunter, M. P. and Prince, V. E. (2002). Zebrafish hox paralogue group 2 genes function redundantly as selector genes to pattern the second pharyngeal arch. *Dev Biol* **247**, 367-89.
Jessen, J. R., Jessen, T. N., Vogel, S. S. and Lin, S. (2001). Concurrent expression of recombination activating genes 1 and 2 in zebrafish olfactory sensory neurons. *Genesis* **29**, 156-62.
Jessen, J. R., Willett, C. E. and Lin, S. (1999). Artificial chromosome transgenesis reveals long-distance negative regulation of rag1 in zebrafish. *Nat Genet* **23**, 15-6.
Kuratani, S. (2004). Evolution of the vertebrate jaw: comparative embryology and molecular developmental biology reveal the factors behind evolutionary novelty. *J Anat* **205**, 335-47.
Lam, S. H., Chua, H. L., Gong, Z., Wen, Z., Lam, T. J. and Sin, Y. M. (2002). Morphologic transformation of the thymus in developing zebrafish. *Dev Dyn* **225**, 87-94.
Manley, N. R. (2000). Thymus organogenesis and molecular mechanisms of thymic epithelial cell differentiation. *Semin Immunol* **12**, 421-8.
Manley, N. R. and Capecchi, M. R. (1995). The role of Hoxa-3 in mouse thymus and thyroid development. *Development* **121**, 1989-2003.
Manley, N. R. and Capecchi, M. R. (1997). Hox group 3 paralogous genes act synergistically in the formation of somitic and neural crest-derived structures. *Dev Biol* **192**, 274-88.
McNulty, C. L., Peres, J. N., Bardine, N., van den Akker, W. M. and Durston, A. J. (2005). Knockdown of the complete Hox paralogous group 1 leads to dramatic hindbrain and neural crest defects. *Development* **132**, 2861-71.
Nornes, S., Mikkola, I., Krauss, S., Delghandi, M., Perander, M. and Johansen, T. (1996). Zebrafish Pax9 encodes two proteins with distinct C-terminal transactivating domains of different potency negatively regulated by adjacent N-terminal sequences. *J Biol Chem* **271**, 26914-23.
Ogasawara, M., Shigetani, Y., Hirano, S., Satoh, N. and Kuratani, S. (2000). Pax1/Pax9-Related genes in an agnathan vertebrate, Lampetra japonica: expression pattern of LjPax9 implies sequential evolutionary events toward the gnathostome body plan. *Dev Biol* **223**, 399-410.

Ogasawara, M., Wada, H., Peters, H. and Satoh, N. (1999). Developmental expression of Pax1/9 genes in urochordate and hemichordate gills: insight into function and evolution of the pharyngeal epithelium. *Development* **126**, 2539-50.
Peters, H., Neubuser, A., Kratochwil, K. and Balling, R. (1998). Pax9-deficient mice lack pharyngeal pouch derivatives and teeth and exhibit craniofacial and limb abnormalities. *Genes Dev* **12**, 2735-47.
Prince, V. E., Joly, L., Ekker, M. and Ho, R. K. (1998a). Zebrafish hox genes: genomic organization and modified colinear expression patterns in the trunk. *Development* **125**, 407-20.
Prince, V. E., Moens, C. B., Kimmel, C. B. and Ho, R. K. (1998b). Zebrafish hox genes: expression in the hindbrain region of wild-type and mutants of the segmentation gene, valentino. *Development* **125**, 393-406.
Reiter, J. F., Kikuchi, Y. and Stainier, D. Y. (2001). Multiple roles for Gata5 in zebrafish endoderm formation. *Development* **128**, 125-35.
Schilling, T. F. (1997). Genetic analysis of craniofacial development in the vertebrate embryo. *Bioessays* **19**, 459-68.
Schorpp, M., Leicht, M., Nold, E., Hammerschmidt, M., Haas-Assenbaum, A., Wiest, W. and Boehm, T. (2002). A zebrafish orthologue (whnb) of the mouse nude gene is expressed in the epithelial compartment of the embryonic thymic rudiment. *Mech Dev* **118**, 179-85.
Sham, M. H., Hunt, P., Nonchev, S., Papalopulu, N., Graham, A., Boncinelli, E. and Krumlauf, R. (1992). Analysis of the murine Hox-2.7 gene: conserved alternative transcripts with differential distributions in the nervous system and the potential for shared regulatory regions. *EMBO J* **11**, 1825-36.
Su, D. M. and Manley, N. R. (2000). Hoxa3 and pax1 transcription factors regulate the ability of fetal thymic epithelial cells to promote thymocyte development. *J Immunol* **164**, 5753-60.
Trede, N. S., Langenau, D. M., Traver, D., Look, A. T. and Zon, L. I. (2004). The use of zebrafish to understand immunity. *Immunity* **20**, 367-79.
Trede, N. S., Zapata, A. and Zon, L. I. (2001). Fishing for lymphoid genes. *Trends Immunol* **22**, 302-7.
Wallin, J., Eibel, H., Neubuser, A., Wilting, J., Koseki, H. and Balling, R. (1996). Pax1 is expressed during development of the thymus epithelium and is required for normal T-cell maturation. *Development* **122**, 23-30.
Willett, C. E., Cortes, A., Zuasti, A. and Zapata, A. G. (1999). Early hematopoiesis and developing lymphoid organs in the zebrafish. *Dev Dyn* **214**, 323-36.
Willett, C. E., Kawasaki, H., Amemiya, C. T., Lin, S. and Steiner, L. A. (2001). Ikaros expression as a marker for lymphoid progenitors during zebrafish development. *Dev Dyn* **222**, 694-8.
Willett, C. E., Zapata, A. G., Hopkins, N. and Steiner, L. A. (1997). Expression of zebrafish rag genes during early development identifies the thymus. *Dev Biol* **182**, 331-41.

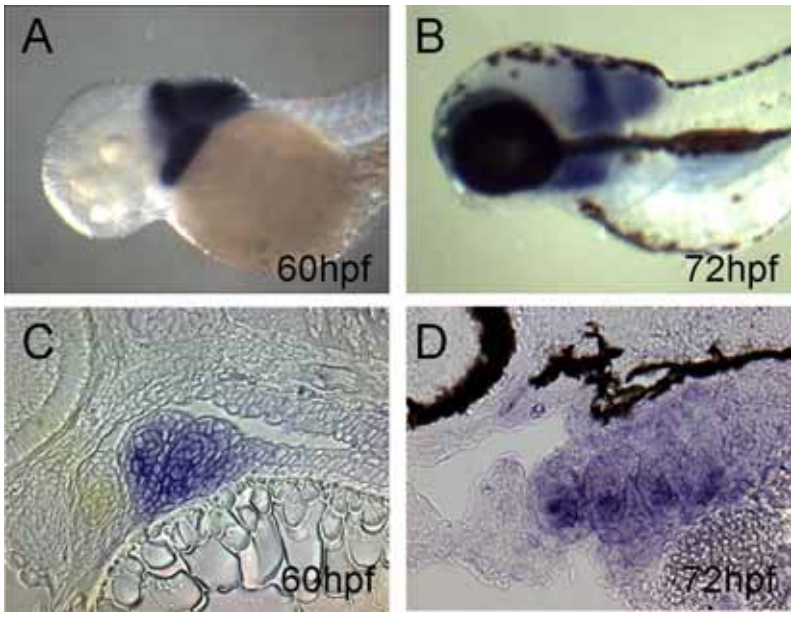

Appendix Fig.1

Appendix Fig. 1. In situ hybridization analysis of zebrafish Hoxa3a gene expression. (**A**) Lateral view of whole-mount Hoxa3a expression at 60hpf. Hoxa3a was expressed in the hindbrain and in pharyngeal region. (**B**)Lateral view of Hoxa3a expression at 72hpf. (**C**-**D**) Section of the 60hpf (C) and 72hpf (D) whole-mount embryos to see the detail expression pattern at pharyngeal arches. Hoxa3a was expressed in the third and more posterior pharyngeal arch mesenchyme and pouch endoderm. Anterior is to the left, dorsal is up.

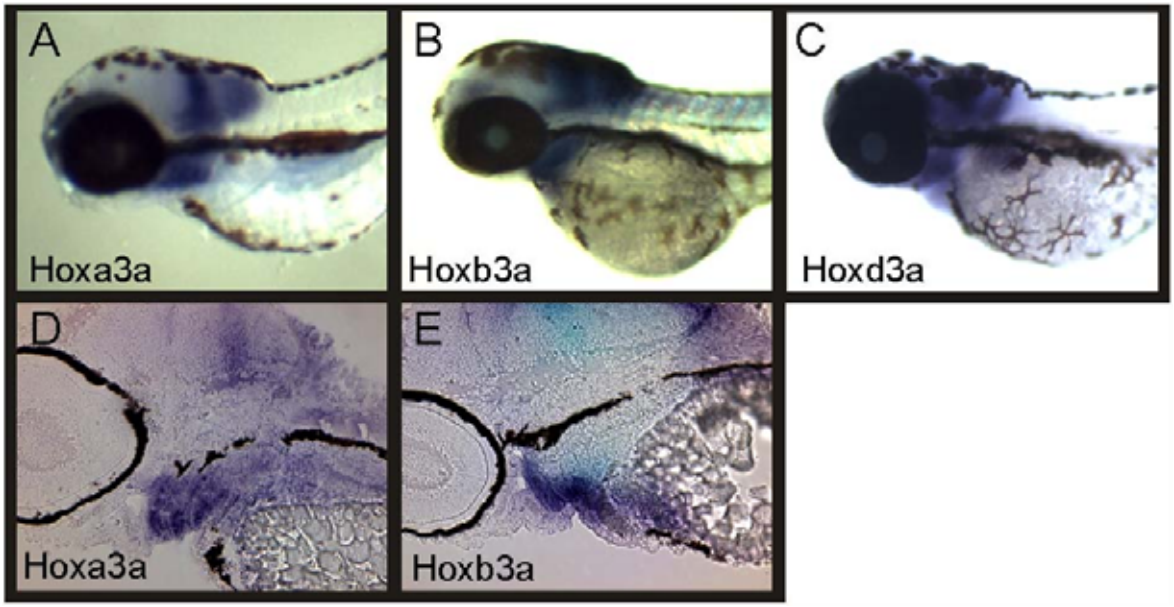

Appendix Fig. 2

Appendix Fig. 2. Expression of PG3 Hox genes in 72 hpf zebrafish embryos. (**A-C**) Whole-mount in situ hybridization with 72hpf embryos showing the expression patterns of Hoxa3a (A), Hoxb3a (B) and Hoxd3a (C). These three PG3 Hox genes were expressed in similar patterns. Hoxb3a had a more anterior expression boundary at hindbrain. (**D-E**) Section of Hoxa3a (D) and Hoxb3a (E) whole-mount in situ hybridization embryos. Hoxa3a and Hoxb3a were both detected to be expressed in the pharyngeal arch mesenchyme and pouch endoderm. Anterior is to the left, dorsal is up.

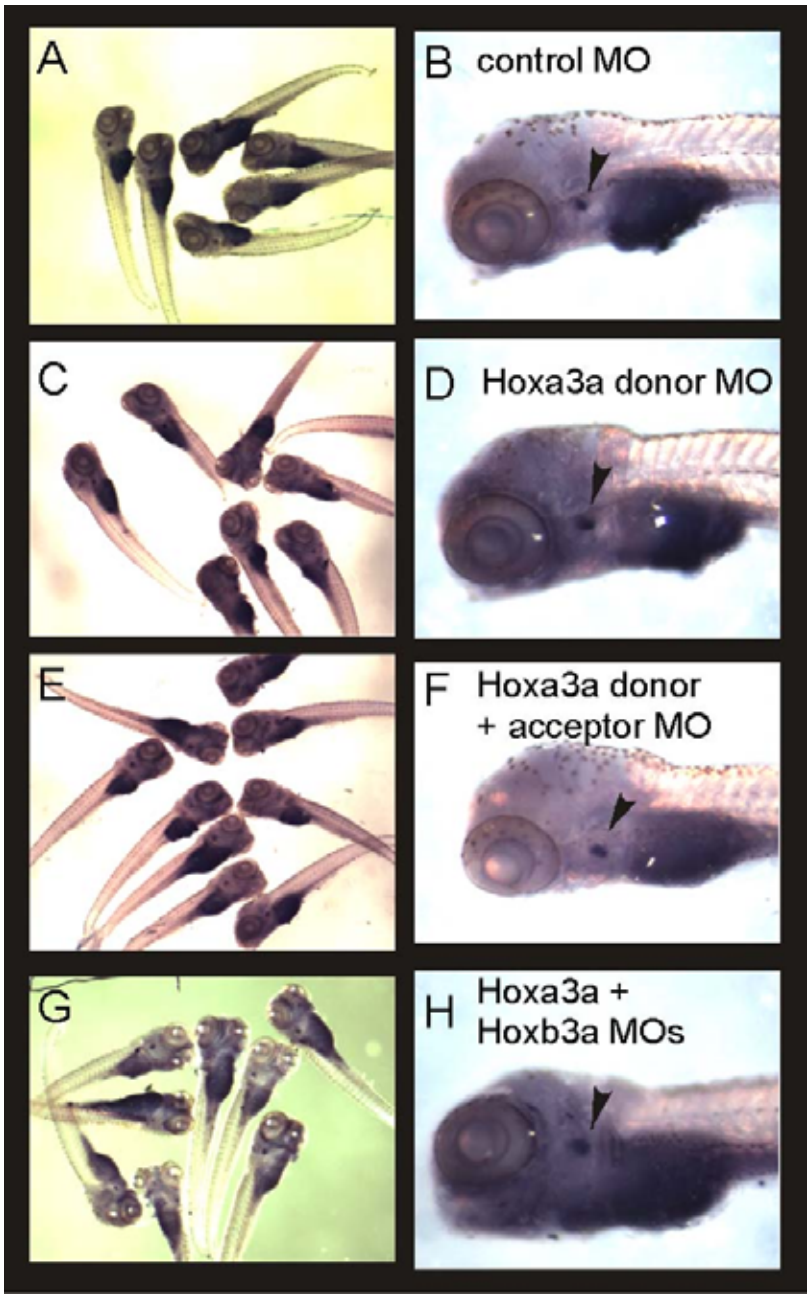

Appendix Fig. 3

Appendix Fig. 3. Whole-mount in situ hybridization analysis on Rag-1 expression in the Hoxa3a/Hoxb3a morphants at 1 week. (**A-B**) Rag-1 expression was detected in the embryos injected with mis-matched morpholino. (**C-D**) Embryos injected with 5ng/embryo of Hoxa3 MO specific to splicing donor site showed normal Rag-1 expression. (**E-F**) 5ng of MOs that were specific to Hoxa3a splicing donor site and acceptor site were co-injected into the embryos. Rag-1 expression in these embryos was not changed. (**G-H**) 3.3 ng/embryos of Hoxb3a MO (splicing donor site) was co-injected with Hoxa3a MOs. Rag-1 expression in these morphants was normal compared to the control. Arrowheads in (B), (D), (F) and (H) indicate Rag-1 expressing cells.

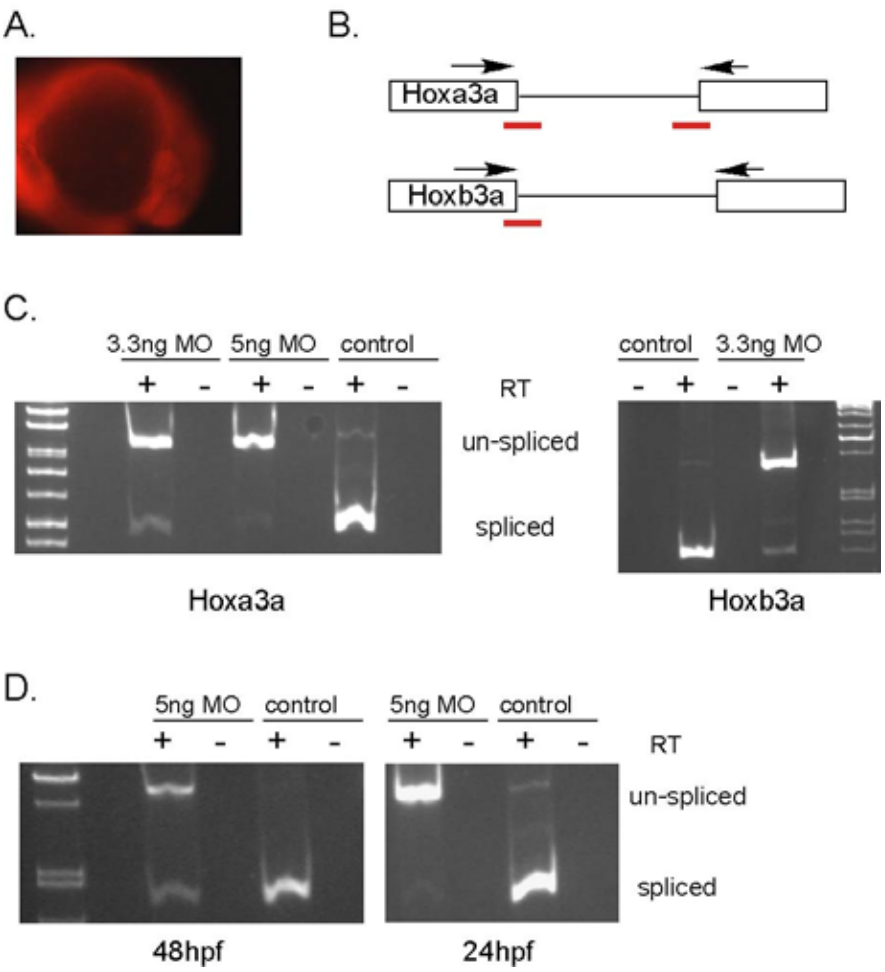

Appendix Fig. 4

Appendix Fig. 4. The efficiency of morpholinos was tested with RT-PCR. (**A**) A 24hpf embryo injected with MOs showing the distribution of the MOs. The MOs were tagged with red-fluorescence. (**B**) Scheme of pre-spliced mRNA of Hoxa3a and Hoxb3a. The red bars indicate the MO specific to the splicing donor or acceptor site. The arrows represent the primers used in RT-PCR. (**C**) RT-PCR products were run on a 1.0% agarose gel. 3.3ng/embryo or 5ng/embryo of Hoxa3a MOs (donor and receptor) or mis-matched MO were injected into 1-cell stage embryos. At 24hpf, the embryos were collected and analyzed for mRNA splicing. On the gel, the lower bands showed the RT-PCR product of post-spliced mRNA and the higher bands showed the product of pre-spliced mRNA. In the MO injected embryos, most of the mRNA was pre-spliced, indicating that the MOs suppressed splicing of target genes effectively. Left panel: Hoxa3a; right panel: Hoxb3a. RT +, PCR with first-strand cDNA; RT -, PCR with non-RT control. (**D**) RNA splicing in 24hpf and 48hpf morphants were analyzed. At 24hpf, there was no post-spliced mRNA product in the morphants, but at 48hpf, the post-spliced mRNA product was restored.